PROBABILISTIC CALIBRATION OF A DISCRETE PARTICLE MODEL

A Thesis

by

YANBEI ZHANG

Submitted to the Office of Graduate Studies of
Texas A&M University
in partial fulfillment of the requirements for the degree of

MASTER OF SCIENCE

August 2010

Major Subject: Civil Engineering

PROBABILISTIC CALIBRATION OF A DISCRETE PARTICLE MODEL

A Thesis

by

YANBEI ZHANG

Submitted to the Office of Graduate Studies of
Texas A&M University
in partial fulfillment of the requirements for the degree of

MASTER OF SCIENCE

Approved by:

Chair of Committee,	Zenon Medina-Cetina
Committee Members,	Charles P. Aubeny
	Raymundo Arroyave
Head of Department,	John Niedzwecki

August 2010

Major Subject: Civil Engineering

ABSTRACT

Probabilistic Calibration of a Discrete Particle Model. (August 2010)

Yanbei Zhang, B.A., Hohai University

Chair of Advisory Committee: Dr. Zenon Medina-Cetina

A discrete element model (DEM) capable of reproducing the mechanistic behavior of a triaxial compressive test performed on a Vosges sandstone specimen is presented considering similar experimental testing conditions and densely packed spherical elements with low lock-in stress. The main aim of this paper is to illustrate the calibration process of the model's micro-parameters when obtained from the experimental meso-parameters measured in the lab. For this purpose, a probabilistic inverse method is introduced to fully define the micro-parameters of the particle models through a joint probability density function, which is conditioned on the experimental observations obtained during a series of tests performed at the L3S-R France. The DEM captures successfully some of the rock mechanical behavior features, including the global stress-strain and failure mechanisms. Results include a detailed parametric analysis consisting of varying each DEM parameter at the time and measuring the model response on the strain-stress domain. First order statistics on probabilistic results show the adequacy of the model to capture the experimental data, including a measure of the DEM performance for different parameter combinations. Also, joint probability density functions and cross-correlations among the micro-parameters are presented.

DEDICATION

To my loving wife

Xialing Wang

Loves make wonders happen!

ACKNOWLEDGEMENTS

I wish to express my gratitude to some of those who have had the most profound impact in making this work possible.

First, I would like to express my sincere gratitude and appreciation to my advisor, Dr. Zenon Medina-Cetina, for his guidance and support throughout the work leading to this thesis. His constant encouragement and willingness to improve my work influenced me throughout my studies at Texas A&M University. I thank him for all he has taught me and all the innovative options he asked me to explore.

I also thank my committee members, Dr. Charles P. Aubeny and Dr. Raymundo Arroyave, for their wise suggestions and insightful helps. I would also like to thank Dr. Pierre Besuelle for authorization to use the experimental results.

I am grateful for the excellent faculty here at Texas A&M University, who model a high level of excellence in both their research and teaching, and have enthusiastically shown a willingness to be accessible to me as a student.

Finally I thank my parents and parents-in-law for their support and encouragement. Especially I thank my father, who has taught me so much about life and has instilled many qualities that have enabled me to be strong and cope with the challenges in my life. Of all people, I am most thankful to my wife, Xialing Wang, who has been by far the greatest blessing in my life. Without her love and companionship, I don’t see how I could have accomplished this goal.

TABLE OF CONTENTS

LIST OF FIGURES

Page

Page

Page

LIST OF TABLES

CHAPTER I

INTRODUCTION

1.1 Problem Statement

Soils are multi-phase particulate systems consisting of soil particles, water and air. However, these are typically modeled as continuum media by using well-established techniques such as the Finite Element Methods or the Finite Difference Methods. Since soil can develop significant local deformations due to its particulate nature, continuum-based methods cannot account for localization effects without an incremental approach involving non-linear elasto-plasticity based constitutive relations.

The discrete element method (DEM) is a collection of numerical techniques for simulating granular materials such as soils, rock, and other discontinua at the particle scale. This method was first introduced by Cundall (1971) [7] for the analysis of rock mechanics problems and then applied to soils by Cundall and Strack (1979) [11]. A state of the art describing the theoretical principles of DEM is given by Cundall (1988) [9] and Hart et al. (1988) [14]. In recent years, DEM has been widely used in geomechanics from soils to intact rocks, and to simulate rock masses as assemblies of blocks. Its applications span many areas, including rock engineering, soil mechanics, mining and petroleum engineering. Previous DEM codes used various types of particles, such as

---

This thesis follows the style of Computers and Geotechnics.

discs, ellipses and polygons, mostly used in two dimensional studies [8, 25, 30]. Three dimensional DEM computer programs have been developed more recently by using balls, ellipsoids and even polytopes as particles [10, 13, 21]. The particle flow code in three dimensions PFC^{3D} [15] is the main tool used to create the discrete particle model in this work.

Since the particle motion is dependent on the physical properties of the granular assembly at each calculation cycle, the interaction of the particles in DEM is a dynamic process. In order to monitor the contact to contact interaction among particles, small time steps and an explicit numerical integration are utilized to trace the motion particle by particle [11]. The use of an explicit numerical scheme makes it possible to simulate the non-linear interaction of large assemblies of particles, which exhibit physical instability without excessive memory requirements.

While the application of DEM is appealing to reproduce more realistic local kinematic phenomena, calibration efforts are strongly dependent on macro- and meso-experimental test, and significant expert judgement [32]. In conventional constitutive modeling, constitutive behavior of geomaterials is often described by complex mathematical representations, many times with synthetic parameters (e.g. elasto-plastic non-associative models with hardening and softening effects). Although the parameterization of these models increase in difficulty with the model complexity, these still can be related to the meso- and macro- mechanistic behavior of the geomaterials. At the micro-scale using an approach DEM, the lack of standardized testing for the calibration of its parameters is a major challenge.

In the calibration process, two main steps need to be performed. The first one is the parameter identification [32], which relates the micro-parameters with the macro-material properties. The other one is called the parameter quantification, which gives the parameters certain values to reproduce the experimental behavior of the testing materials. The parameter identification of bonded particle model is discussed by Potyondy and Cundall (2004) [27], particularly for the parallel bonded material used in PFC^{3D}. The most common and efficient way to conduct parameter identification is through parametric analysis, also called sensitivity analysis, which consists in investigating the effect of one individual parameter (or a combined dimensionless parameter) while keeping the other variables fixed [12, 26, 32].

A major limitation in the use of DEMs is the lack of testing capabilities so as to determine the particle model parameters at the element scale. The selection of the parameters thus is often based on trial and error method by adjusting the simulation results closer to meso-experimental results. Some researchers have tried to use macro-experiment of rods glued together by adhesive to estimate the micro-parameters of particles [18]. However, the behavior of the macro-rods and micro-parameters of particles are not easily comparable. Since material testing at a larger scale cannot be used to parameterize a discrete model with unknown element parameters, this process imposes significant uncertainties. It is not a simple task to determine the exact particle model parameters at the element scale through lab experiment.

Therefore, the parameter quantification of DEMs require a more systematic and comprehensive approach. Only a limited number of researchers have focused on

developing methods for parameter quantification. Most of the papers in DEM directly give the parameters used for the materials without mentioning any calibration process [6, 16, 20, 31,33]. Among these references, it has been found that the trial and error method is commonly adopted with the corresponding limitations. This approach inherently ignores the possibility of multiple combinations of the same DEM parameters that could achieve the same model response (i.e. the calibration process is an ill-posed problem). A typicl optimization approach by the definition of an objective function is an improvement over the calibration process, as it compares the model predictions vs. the experimental data [32], which at the end results in only one optimal set of parameters. Until recently, almost all the methods for parameter calibration used in discrete element analysis were thus deterministic methods.

Medina-Cetina and Khoa (2009) [24] proposed for the first time a probabilistic method to quantify the uncertainty associated to the area selection of the DEM's parameters, which introduces the Bayesian paradigm to form the complete solution to the inverse problem. Herein, an inverse problem is defined as the assessment of model parameters based on available evidence. The main aim is to calibrate the model micro-parameters from the experimental behavior measured in the laboratory by the use of a probabilistic inverse method, joint probability density function defining the variability of the DEM parameters.

The aim of this work is to define a systematic approach for the probabilistic calibration of DEMs. A more comprehensive review on the parameterization of the

DEM is presented, with the objective of improving the understanding of the mechanical behavior of these types of models.

1.2 Literature Review of Parameter Calibration

The discrete element method is a very powerful tool to represent the micro-mechanical behavior of discontinuous materials. However, one of the main problems confronted by most researchers is the determination of the micro-parameters in the discrete particle model. Currently, there is no robust and universal method for determining the parameters of discrete particle models.

The calibration of the micro-parameters serves as the first step to train the discrete particle model, which should reproduce the macro-response of the experimental test. Differences in boundary and loading conditions make the calibration even more complex.

As part of this work's literature review, about one hundred papers on discrete element modeling covering different topical areas were identified. A primary conclusion stemming from this review is that most of the existing papers on discrete element modeling directly present the micro-parameters without any calibration process. Only a few papers focus on the calibration procedures of the micro-parameters, among which most of them reproduce the micro-behaviors by trial-and error method.

Below is a summary of the most valuable papers identified during the literature review in which the parameter calibration is discussed.

Potyondy and Cundall (2004) [27] introduced the concept of bonded particles for modeling rock both in 2D and 3D, which because it presents a way to reproduce cemented-type of materials, is commonly referred by most researchers since. In this work, the calibration reproduces the macro-response of Lac du Bonnet granite by a set of optimal values for each micro-parameter. The macro-response of the materials is represented by the Young's modulus and the Poisson's ratio. The relations between micro-parameters and macro-material behavior have been built for a bonded particle model in PFC^{3D}. The stiffness of the particles is selected to match the Young's modulus, while the ratios of normal to shear stiffness are chosen to match the Poisson's ratio. The parallel normal and shear strength are set equal to one another so as not to exclude mechanisms that may only be activated by micro shear failure, which means both tensile crack and shear crack could be developed under loading. The ratio of standard deviation to mean of the cement strengths is chosen to match the crack initiation stress, and the mean value of the cement strengths is chosen to match the unconfined compressive strength, and the peak strength found in the specimen stress strain curve. The particle friction coefficient appears to affect only post-peak response and it is not clear to what extent its most significant impact is.

Asaf et al. (2007) [1] modeled the soil-implement interaction and introduced an inverse solution technique using the Nelder-Mead algorithm of optimization for calibrating the micro-parameters. In this study, the determination of the parameters was based on in situ field tests. Discrete element models were built in correspondence with the field tests. However, the optimization results of this particular problem were shown

to be sensitive to the initial estimate of the micro-parameters, which means that the initial estimate must be close enough to the proper value of the parameters in order to achieve a unique solution. An energy method and an elastic-plastic rule were developed to determine an initial estimate for the optimization process. The authors addressed the particle friction coefficient and the particle normal spring constant as the two main parameters. Also, the calibration process was limited to calibrate only these two main parameters, while other initial estimated parameters were kept constant.

Wang and Tonon (2009) [32] introduced the concept of equilibrium distance and membrane boundary conditions into the particle model and modeled the triaxial compression of a Lac du Bonnet granite. The authors divided all the micro-parameters into two categories, the deformability parameter and strengths parameters. Deformability parameters include the particle's Young's modulus and the ratio of normal stiffness over shear stiffness at contact. The micro-deformability parameters were calibrated to match the material's macro deformability parameters: Young's modulus, E, and Poisson's ratio, ν, which are determined from lab experiments. The identification of deformability parameters is carried out under non-failure condition by means of modeling uniaxial compressive tests. The authors proved that the specimen's Young's modulus E, is related to both particle's Young's modulus and the ratio K_s/K_n, while the specimen's Poisson's ratio is only related to the ratio K_s/K_n.

The shear or tension failure mechanism of the materials makes the calibration of the strength parameters complicated. The authors identified strength parameters, including the contact tensile strength, T, and c and φ. These strength parameters are calibrated

under different confining pressures to match a failure envelop obtained from experiments. The author used an inverse method to identify a selected set of unknown modeling parameters in DEM to improve the agreement with experimental data. The objective function was used to evaluate the difference between experimental and simulated failure envelopes. The global optimization package SNOBFIT was utilized in the calibration process to find the global optimal parameter point or vector set. In the calibration process, the DEM code and SNOBFIT were repeatedly invoked until the computed failure envelope matched the experimental failure envelope by meeting the tolerance criterion, which was set as 5% in the strength parameters calibration considering the intensive computational effort involved in obtaining the value of objective function.

Belheine et al. (2009) [2] proposed a 3D spherical discrete model for reproducing the behavior of a Labenne sand. Using numerical triaxial tests, the micro-mechanical properties of the numerical material were calibrated in order to match the macroscopic response of the real material. Numerical simulations were carried out under the same conditions as the physical experiments. The pre-peak, peak and post-peak behavior of the numerical material was studied. This paper gave the exact procedure to calibrate the proposed five parameters one by one. The calibration process is to estimate the values of the microscopic parameters $k_n, \alpha = \frac{k_s}{k_n}, \mu, \beta$ and η and subsequently to reproduce, repectively, the macroscopic behavior characterized by Young's modulus E, the Poisson's ratio γ, the dilatancy angle ψ, the peak and the post-peak normal stress σ.

These characteristics are the features of the stress-strain curves deduced from the axisymmetric triaxial tests.

The initial slope of the volumetric strain was used to determine Poisson's ratio γ. The initial slope of the stress-strain diagram is related to Young's modulus E. The slope of the volumetric strain curve in the dilatancy domain is related to the dilatancy angle ψ. The deformation at which the stress is maximum σ_{peak} must also correspond to the maximum dilatancy. During the calibration procedure, the authors first varied the normal contact stiffness k_n and the ratio $\alpha = \frac{k_s}{k_n}$ to match the deformation modulus and Poisson's ratio of the real material while all other parameters of the test were kept constant. Next, the inter-particle friction angle was varied to adjust the dilatancy curve to that of the real material, while all other parameters were kept constant. Finally, by varying the rolling stiffness coefficient it was possible to fit the experimental stress-strain curve.

Cho et al. (2007) [5] proposed a clumped particle model for simulating a rock specimen in two dimensions for both Lac du Bonnet granite and a weak synthetic rock, the particle code calibrated to uniaxial tests using the clumped-particle geometry predicts both the stress-strain behavior and the complete nonlinear failure envelope. The parametric study in this research gave insight into the micro-parameters, friction, contact stiffness, bond strength, particle size and gain shape. However, the calibration method used to determine the whole set of the micro-parameters was not discussed in the paper.

Camusso and Barla (2009) [4] presented a numerical model of Torino subsoils in two dimensions. The model was calibrated to reproduce the experimental response.

Although the paper focused on the micro-parameters calibration, the calibration methodology was not fully addressed.

Fakhimi and Villegas (2007) [12] published the application of dimensional analysis in the calibration of a discrete element model for rock. This calibration method was employed for finding a numerical model for a Pennsylvania blue sandstone. The material model parameters were calibrated by introducing some curves using a dimensional analysis.

In summary, all available calibration methods for DEMs are deterministic. Furthermore, most of the calibration methods and calibration procedures were not fully addressed, limiting the ability to replicate the results. Compared with the deterministic approach, the probabilistic method used in this research provides a new way for solving the parameters here expressed through a joint probability density function.

1.3 Thesis Outline

Chapter II introduces the theoretical framework of the particle flow model in PFC^{3D}, including the contact model, calculation cycle and the physical properties of the model. Also, the sample generation procedure of the discrete particle model is discussed. Chapter III introduces the triaxial lab test of Vosges sandstone performed at the laboratory 'Sols Solides Structures-Risques' at L3S-R in Grenoble, France. Chapter IV presents the experimental localization of the sandstone specimen, followed by the simulation of micro-cracks and discussion on the crack types. Chapter V first introduces the fitting procedure between lab test and simulation, and then the parametric analysis

procedure is conducted to analyze the sensitivity of the micro-parameters. Chapter VI demonstrates the inverse solution of Bayesian theorem, and then discusses the Makov Chain Monte Carlo method for sampling the posterior in the simulation chain and the main parameters in the probabilistic calibration implementation. Chapter VII offers a case study that validates the applicability of the method for the probabilistic calibration of one test with three main micro-parameters. And finally, Chapter VIII provides the conclusions of this work.

CHAPTER II

DISCRETE PARTICLE MODEL

This chapter introduces the discrete particle model for modeling the Vosges sandstone and the supporting algorithms required to build and test the sample in PFC^{3D}. A discussion of the fundamental theory of DEM according to PFC^{3D} is presented [15], including the calculation cycle, the constitutive model, and the contact detection theory.

2.1 Discrete Particle Model for Vosges Sandstone

A series of triaxial compression tests were carried out on cylindrical samples of Vosges sandstone with different height diameter ratios and under various confining pressures to study the onset of localization of deformation, shear band orientation and failure patterning by Besuelle et al. (2000) [3]. The meso-mechanical behavior of the Vosges' sandstone has been selected for calibrating one discrete particle model using PFC^{3D}. The reference experimental data belongs to one test from the Vosges' sandstone cylindrical specimens. The experimental data used in the study corresponds to the triaxial test with a confining pressure of 10MPa.

A synthetic cylindrical model of the rock sample measuring 40mm in diameter and 80mm in height was created to reproduce the experimental triaxial test (Figure 2.1). Due to the fine resolution required to replicate the actual rock specimen and the exploratory nature of this study, it was decided to use a larger grain scale in the DEM model, such that one sphere would approximately represent a small volume of about 6-10 mineral

grains. Therefore, a model was built composing of 1122 particles with a range of artificial radii from 2.0 to 3.3mm uniformly distributed. A process analogous to physical compaction is followed as proposed by Itasca [15] and packed in a way to approach as much as possible to the actual rock characteristics (porosity 0.22 and bulk density 1960 kg/m^3). Note that the average particle size is 2.6mm.

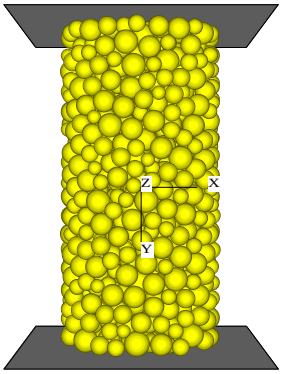

Figure 2.1 PFC^{3D} model of the Vosges sandstone

The testing conditions assumed that the top and bottom platens behave as rigid bodies with zero contact friction. The specimen was loaded in compression at a constant strain rate of $10^{-5}s^{-1}$ by moving both platens at the same velocity. The sleeve walls were controlled by a servo-control mechanism algorithm, used to maintain constant confining pressure on the specimen (notice that the sleeve walls are assumed to be also frictionless). It is further assumed that since the Vosges sandstone is a cemented type material (e.g. when compared with clean sands), it is adequate to introduce a parallel

bond model in addition to the contact bond between spheres, as is suggested by Itasca [15] to simulate synthetic rock. Parallel bonds rely on a sample physical representation of elastic springs with c normal and shear ontact stiffness that is uniformly distributed over a circular disc placed on the contact plane between neighboring spheres (Potyondy and Cundall, 2004). This constitutive contact model is discussed in further detail in section 2.7.

2.2 Sample Generation Procedure

The specimen generation procedure consists of four main steps to produce a cylinder specimen containing a densely packed, parallel bonded particle assembly with low locked-in stresses. The material strength for each contact is picked from a Gaussian distribution specified in terms of a mean value and a standard deviation. The programming language FISH is used to create triaxial test code in PFC^{3D} environment [15].

STEP 1: Generation and initial compaction of particles.

At the beginning of this step, a cylinder specimen consisting of arbitrarily placed particles confined by three walls (top, bottom platens and lateral cylinder wall) is generated by an expansion compaction method (see section 2.3.1). To avoid the particles penetrating the walls, the walls normal stiffnesses are set equal to β times of the average particle normal stiffnesses (see section 5.1). The size distribution of the particles satisfies a uniform distribution characterized by minimum and maximum particle radii. The

porosity is initially set to be 0.22 to calculate the particle number that can be generated in the specified region.

STEP 2: Install specified isotropic stress for the sample.

This step aims at reducing the magnitude of the locked-in stress that will develop after bond installation (STEP 4). The magnitude of the locked-in contact forces caused by the deformation of the particle in the STEP 1will be close to the compressive forces at the time of bond installation. The specified isotropic stress, defined as the mean of the three direct stresses in the principal direction, is achieved by uniformly changing the radii of all the particles at the time. To reduce the influence of the locked-in stress, the specified isotropic stress is typically set to a value relatively low versus the material strength. The current isotropic stress in the assembly is calculated by FISH code.

STEP 3: Reduce the number of floating particles.

A large amount of floating particles with less than three contacts may exist (Figure 2.2), because of the features that non-uniform radius particles are assembly placed randomly and compacted mechanically. All the floating particles should be eliminated to make more realistic and denser network of bond contact in the following bond installation step.

STEP 4: Parallel bond installation

To effectively simulate the behavior of Vosges sandstone, it is supposed to use parallel bond constitutive model for particle contacts. The parallel bonds are installed in all particles that are in physical contact throughout the specimen, and then all particles are assigned a friction coefficient of μ. Now, the sample is ready for testing.

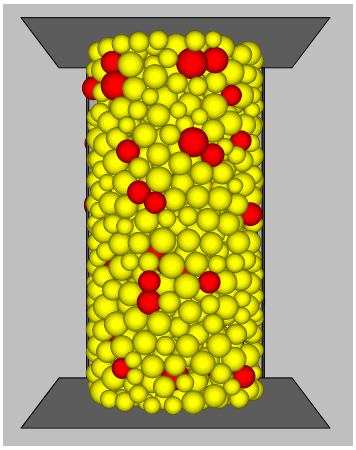

Figure 2.2 Floating particles with less than three contacts

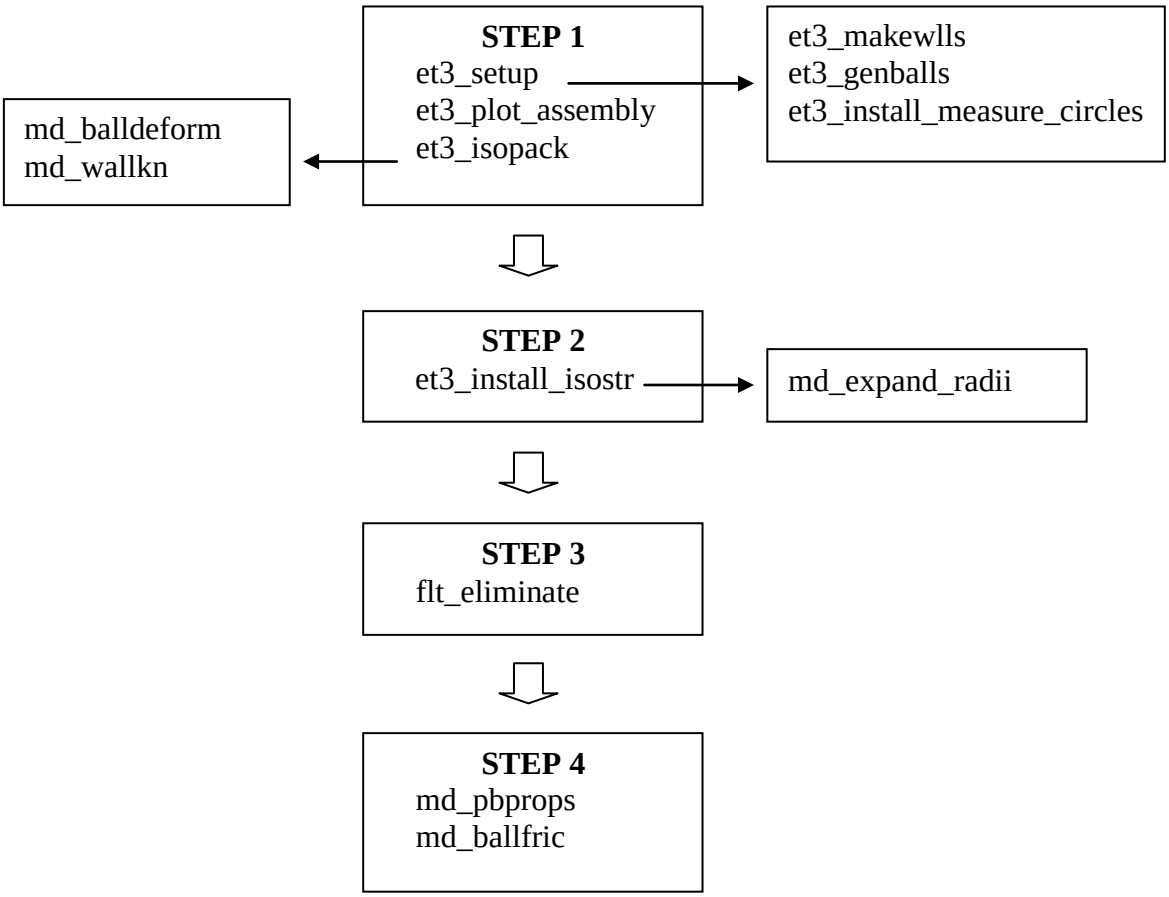

Figure 2.3 Flowchart of FISH functions for sample generation

To better understand the sample generation procedure, please refer to the APPENDIX A and B of this work, where the FISH code for the sample preparation and testing is included. These were partially generated from the sample code developed by Medina-Cetina and Khoa (2009) [24]. An outline of the FISH code for the sample preparation is shown in Figure 2.3.

2.3 Supporting Algorithms

The following presents two main supporting algorithms used in the PFC^{3D} model when programming the implemented codes. The expansion compaction method is designed to achieve the target porosity by expanding the radii of all particles by a specified ratio at the time. The servo-control mechanism is used to maintain constant stress of the lateral wall when the sample is under loading.

2.3.1 Expansion Compaction Method

All particles with reduced radii are randomly generated in a specific area in STEP 1 at the beginning to ensure no overlap and no contact force occurring between any two particles. After all particles are positioned in the specified region, the radii of all particles are restored gradually while the confining pressure is kept constant at the boundaries. The contact force developed between any two particles during the radii growth process allows the particles to move in order to turn the specimen into a dense sample. The rigid boundaries are allowed to move accordingly enabling the stress state to be achieved at equilibrium [17].

A collection of spherical particles with uniform size distribution is generated in a specified volume V at a given porosity n_0 with radii in the range $[R_{min}, R_{max}]$. The number of generated particles N can be computed as:

$$N = \frac{3V(1-n_0)}{4\pi\overline{R}^3}; \text{with } \overline{R} = \frac{R_{min} + R_{max}}{2} \tag{2.1}$$

In the sample generation process, the radii first generated are set to be 0.5 times of the target radii with 2.0 mm to 3.3 mm. The porosity of the initial assemblies is calculated as:

$$n = 1 - \frac{\sum \frac{4}{3}\pi R^3}{V} \tag{2.2}$$

where V is the total volume of the sample or the container's volume.

The multiplier for all the particles to achieve the target porosity n_0 is defined as:

$$m = \left(\frac{1-n}{1-n_0}\right)^{\frac{1}{3}} \tag{2.3}$$

where n_0 is the target porosity, which in this case is 0.22 for Vosges sandstone.

2.3.2 Servo-Control Mechanism

The aim of the servo-control mechanism is to keep the confining stress constant by adjusting the velocity of the radial wall with specified parameters in every cyle throughout the loading process. The equation for wall velocity is written as:

$$\dot{u}^{(wall)} = G\left(\sigma^{measured} - \sigma^{required}\right) = G\Delta\sigma \tag{2.4}$$

where G is the gain parameter, which is estimated as follows.

The maximum increment of the wall force due to the wall movement within one time-step is

$$\Delta F^{(\text{wall})} = k_n^{(\text{wall})} N_c \dot{u}^{(\text{wall})} \Delta t \tag{2.5}$$

where N_c is the total number of balls in contact with the wall, and $k_n^{(\text{wall})}$ is the average stiffness of these contacts. The change of the average wall stress is:

$$\Delta\sigma^{(\text{wall})} = \frac{k_n^{(\text{wall})} N_c \dot{u}^{(\text{wall})} \Delta t}{A} \tag{2.6}$$

where A is the area of the lateral cylinder wall. To ensure the system stability, the absolute value of the change of the wall stress must be less than the absolute value of difference between the required and measured stresses of the wall. So a relaxation factor α is used to meet the stability requirement, which is expressed as:

$$\left|\Delta\sigma^{(\text{wall})}\right| < \alpha|\Delta\sigma| \tag{2.7}$$

The contant number between balls and each wall is counted every time-step, and the gain parameter for each wall is determined by:

$$G = \frac{\alpha A}{k_n^{(\text{wall})} N_c \Delta t} \tag{2.8}$$

The numerical sampling detail of the gain parameters is listed in APPENDIX A.

2.4 Calculation Cycle in PFC^{3D}

The DEM in PFC^{3D} adopts a time-stepping algorithm, which consists of the repeated applications of the law of motion to each particle, the force displacement law to each contact, and the constant updating of surface and particle positions during every calculation cycle. Contacts are formed and broken during the simulation automatically. The calculation cycle in DEM model is shown in Figure 2.4 with details as following:

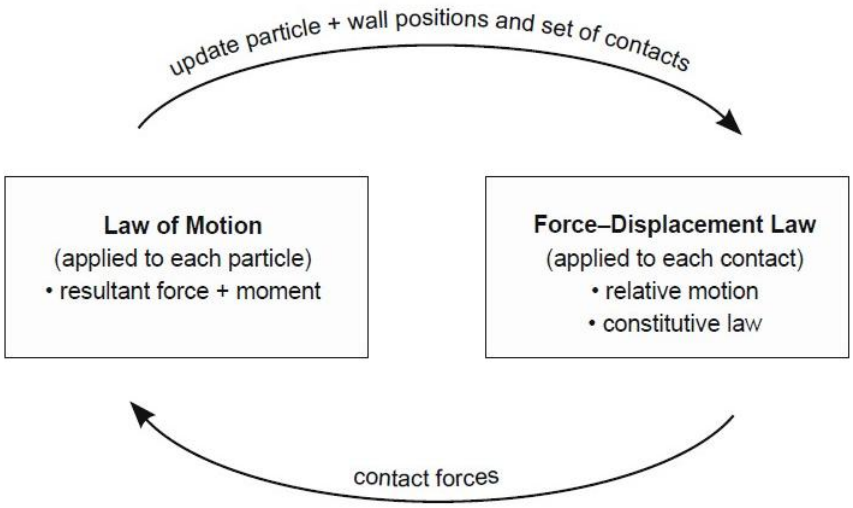

Figure 2.4 Calculation cycle in PFC^{3D} [15]

STEP 1: At the beginning of each time-step, all the particle positions and contact information are delivered from the previous calculation cycle. This information is applied to determine new contacts and deformations to existing contacts for all particles.

STEP 2: The force-displacement law is applied to each contact to determine the contact force due to relative particle deformation (see section 2.5). The values of the contact forces depend on two things: the relative motion between the particles, and the contact model utilized. The different contact models will be described in section 2.7.

STEP 3: The Newton's Second Law of Motion is used to update the velocity and position for each particle. The forces acting on the particles will include contact forces derived from step 2 and any other external forces.

STEP 4: New particle positions and new surface positions are all updated and then passed to the next calculation cycle.

The time-step between each calculation cycle is very small. Therefore, it can be reasonably assumed that the forces acting on each particle have no change throughout each calculation cycle.

2.5 Contact Force Determination

The force-displacement law is used to compute the relative displacement between two particles at a contact. Ball-to-ball and ball-to-wall contact occur in the particulate system in the PFC^{3D} model as shown in Figure 2.5. Both of these types make contact on a point.

This contact can be described as a contact point $x_i^{[c]}$ with a unit normal vector n_i lying on the contact plane. This normal vector is directly along the line between ball centers for ball-to-ball contact. For ball-to-wall contact, the normal vector is along the line which defines the shortest distance between the ball center and the wall.

The total contact force can be decomposed into shear and normal components. The normal component is acting in the direction of the normal vector to calculate the relative normal displacement via the force-displacement law. The shear component is acting on the contact plane (perpendicular to the normal vector) to compute the incremental force and displacement.

The overlap U^n between the particles is defined as the relative contact displacement in the normal direction. The normal contact force vector is computed by

$$F_i^n = K^n U^n n_i \tag{2.9}$$

where K^n is the normal stiffness at the contact, which is a secant modulus because it relates to the total displacement and force.

The shear contact force is computed in an incremental manner step by step. The total shear contact force is initialized to be zero when the contact is formed. In each time-step, relative shear-displacement increment will cause an increment of elastic shear force. The motion of the contact in the shear direction must be considered:

$$F_i^s \leftarrow F_{i-1}^s + k_s \Delta U_i^s \tag{2.10}$$

where K^s is the shear stiffness at the contact, which is a tangent modulus because it relates to the incremental displacement and force.

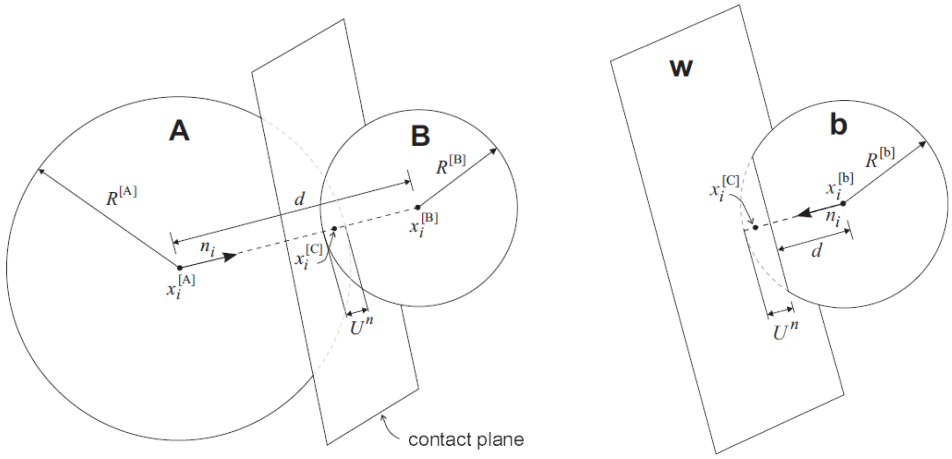

(a) (b)

Figure 2.5 Notation used to describe contacts: (a) Ball-ball, (b) Ball-wall [15]

2.6 Kinematic Implementation

The ordinary differential equations, based on Newton's Laws of Motion, are used to describe the motion of the particles. These equations are integrated numerically by using a step-by-step integration procedure. In this case, the time-step is chosen to be short enough so that the velocities and accelerations of the particles may be assumed to be constant. In order to make the simulation more accurate, the time-step chosen should also be short enough so that, except for its immediate neighbors, other particles cannot directly influence the properties of the particle of interest.

The motions of a single particle, described in terms of the translational motion of a point and the rotational motion of the particle, are determined by the resultant force and moment vectors acting upon it. The position x_i, velocity $\dot{x}_i$ and acceleration $\ddot{x}_i$ are used to represent the translational motion of the center of the particle; the rotational motion of the particle is described in terms of its angular velocity ω_i and angular acceleration $\dot{\omega}_i$ in the same way.

Th translational acceleration $\ddot{x}_i$ can be evaluated as:

$$F_i = m(\ddot{x}_i - g_i) \tag{2.11}$$

where F_i is the resultant force calculated by the sum of all externally applied forces acting on the particle; m is the mass of the particle; and g_i is the body force acceleration vector.

The angular acceleration $\dot{\omega}_i$ can be calculated as:

$$M_i = I\dot{\omega}_i = \left(\frac{2}{5}mR^2\right)\dot{\omega}_i \tag{2.12}$$

where M_i is the resultant moment acting on the particle; and I is the moment of inertia.

The translational and rotational accelerations at time "t" can be expressed in terms of the velocity at mid-intervals as:

$$\ddot{x}_i^{(t)} = \frac{1}{\Delta t}\left(\dot{x}_i^{\left(t+\frac{\Delta t}{2}\right)} - \dot{x}_i^{\left(t-\frac{\Delta t}{2}\right)}\right) \tag{2.13a}$$

$$\dot{\omega}_i^{(t)} = \frac{1}{\Delta t}\left(\omega_i^{\left(t+\frac{\Delta t}{2}\right)} - \omega_i^{\left(t-\frac{\Delta t}{2}\right)}\right) \tag{2.13b}$$

The velocities at time $\left(t + \frac{\Delta t}{2}\right)$ are calculated by:

$$\dot{x}_i^{(t+\Delta t/2)} = \dot{x}_i^{(t-\Delta t/2)} + \left(\frac{F_i^{(t)}}{m} + g_i\right)\Delta t \tag{2.14a}$$

$$\omega_i^{(t+\Delta t/2)} = \omega_i^{(t-\Delta t/2)} + \left(\frac{M_i^{(t)}}{I}\right)\Delta t \tag{2.14b}$$

The new position of the particle is estimated as:

$$x_i^{(t+\Delta t)} = x_i^{(t)} + \dot{x}_i^{(t+\Delta t/2)}\Delta t \tag{2.15}$$

Above all, the force-displacement law can be shortly described as follows. At the beginning of each calculation cycle, the values of $\dot{x}_i^{(t-\Delta t/2)}$, $\omega_i^{(t-\Delta t/2)}$, $x_i^{(t)}$, $F_i^{(t)}$ and $M_i^{(t)}$ are updated, then equation (2.14) is used to obtain the translational velocity $\dot{x}_i^{(t+\Delta t/2)}$ and angular velocity $\omega_i^{(t+\Delta t/2)}$. Then equation (2.15) is used to obtain the displacement $x_i^{(t+\Delta t)}$. The values of the force $F_i^{(t+\Delta t)}$ and moment $M_i^{(t+\Delta t)}$ are obtained by application of the force-displacement law.

2.7 Contact Constitutive Models

Since the Vosges sandstone specimen is a cemented-type material, it is proposed to use the spheres' parallel bond model provided in PFC^{3D} (in addition to the natural contact model). The bonded constitutive model acting at a particle contact consists of three parts: a stiffness model, a slip model, and a bonding model. The stiffness model describes an elastic relation between the contact force and the relative displacement. The slip model relates the normal contact forces and the shear stress so that the two contacting balls can experience relative displacement in the shear direction. The bonding model provides a rolling resistance to restrict the relative rotation of the particle [19].

2.7.1 Contact-Stiffness Models

The normal and shear stiffnesses in the contact model relate the contact forces and the relative displacements in the normal and shear directions.

Since the normal stiffness is a secant stiffness, which associates the total normal force to the total normal displacement. The contact force can be evaluated as:

$$F_i^n = K^n U^n n_i \tag{2.9}$$

The shear stiffness which relates to the incremental shear force and incremental shear displacement is a tangent stiffness, so the shear contact force is computed as:

$$\Delta F_i^s = -k_s \Delta U_i^s \tag{2.16}$$

According to different contact stiffness model, the contact stiffness used in the above equations can take different values. In PFC^{3D}, a linear model and a simplified Hertz-Mindlin model are provided as the contact stiffness model. Because the

Hertz-Mindling model is not defined for tensile forces, a combination of the Hertz-Mindling mode and any other type of bonding model is prohibited.

2.7.1.1 The Linear Contact Model

The linear contact model is charaterized by the normal and shear stiffnesses k_n and k_s of the two contacting particles. By assuming the contact stiffnesses of the two contact particles working together, the contact normal stiffnesses for the linear contact model can be evaluated by

$$K^n = \frac{k_n^{[A]} k_n^{[B]}}{k_n^{[A]} + k_n^{[B]}} \tag{2.17}$$

and the contact shear tangent stiffness is calculated by

$$k^s = \frac{k_s^{[A]} k_s^{[B]}}{k_s^{[A]} + k_s^{[B]}} \tag{2.18}$$

where the superscripts [A] and [B] represent the two particles in contact. The normal secant stiffness k^n is equal to the normal tangent stiffness for the linear model since

$$k^s \equiv \frac{dF^n}{dU^n} = \frac{d(K^n U^n)}{dU^n} = K^n \tag{2.19}$$

2.7.1.2 The Hertz-Mindlin Contact Model

The nonlinear contact formulation of the Hertz-Mindlin contact model is based on an approximation of the theory of Mindlin and Deresiewicz and described in Cundall (1988). This model does not reproduce the continuous nonlinearity in shear and only strictly applicable to the case of spheres in contact. The shear modulus G and Poisson's ratio γ of the two contacting balls are used to define the Hertz-Mindlin contact model.

The contact normal secant stiffness is calculated by:

$$K^n = \left(\frac{2G\sqrt{2\widetilde{R}}}{3(1-\gamma)}\right)\sqrt{U^n} \tag{2.20}$$

and the contact shear tangent stiffness is calculated by:

$$k^s = \left(\frac{2\left(G^2 3\left(1-\gamma\widetilde{R}\right)\right)^{\frac{1}{3}}}{2-\gamma}\right)|F_i^n|^{\frac{1}{3}} \tag{2.21}$$

where U^n is the overlap of the sphere, and $|F_i^n|$ is the magnitude of the normal contact force. The geometric and material properties of the two particles in contact affect the the multipliers to both these equations. For ball-ball contact, the multipliers depend on the average ball radius, the average shear modulous and the average Poisson's ratio.

$$\widetilde{R} = \frac{2R^{[A]}R^{[B]}}{R^{[A]}+R^{[B]}} \tag{2.22a}$$

$$G = \frac{1}{2}\left(G^{[A]}+G^{[B]}\right) \tag{2.22b}$$

$$\gamma = \frac{1}{2}\left(\gamma^{[A]}+\gamma^{[B]}\right) \tag{2.22c}$$

and for ball-wall, the multipliers depend on the following properties of the ball:

$$\widetilde{R} = R^{[ball]} \tag{2.23a}$$

$$G = G^{[ball]} \tag{2.23b}$$

$$\gamma = \gamma^{[ball]} \tag{2.23c}$$

where G is the elastic shear modulus; γ is Poisson's ratio; R is sphere radius. For the Hertz model, the normal secant stiffness and the normal tangent stiffness can be related as:

$$k^s = \frac{dF^n}{dU^n} = \frac{3}{2}K^n \tag{2.24}$$

2.7.2 The Slip Model

The slip model, which is always active, is an intrinsic property of the two particles in contact, where slips can occur by limiting the shear strength. The slip model is compatible with bonding model, combined to represent the cementious materials. The minimum coefficient of friction μ between the contacting balls is used to define the slip model.

The shear strength of the contact force is computed through Mohr-Coulomb failure criteria. The slip condition is checked by calculating the maximum allowable shear contact force:

$$F^s_{max} = \mu|F^n_i| \tag{2.25}$$

If $|F^s_i| > F^s_{max}$, then slip is allowed to occur in the next calculation cycle by setting the magnitude of F^s_i equal to F^s_{max} expressed as:

$$F^s_i \leftarrow F^s_i \left(\frac{F^s_{max}}{|F^s_i|}\right) \tag{2.26}$$

2.7.3 Bonding Models

Particles are allowed to bond together at contacts to simulate the cohesion of the material. Two bonding models are provided in PFC^{3D}. The contact bond model can be envisioned as two particles glued together over a small area only at the contact point. The parallel bond model can be viewed as platen shaped contact of a finite size that act over a circular cross section lying on the contact plane. Only forces can be transmitted through a contact bond model. Both a force and a moment can be transferred through the

parallel bond model. Only particles could be bonded together, while a particle cannot be bonded to a wall. The bonds between particles can never be restored once it is broken.

2.7.3.1 The Contact-Bond Model

A contact bond can be represented by two springs with constant normal and shear stiffness acting on a contact point. The normal spring defines the normal tensile strength, while the shear spring determines the shear strength. The slip is precluded due to the existence of the contact bond. However, the shear contact force and the tensile forces are limited by the bond strength.

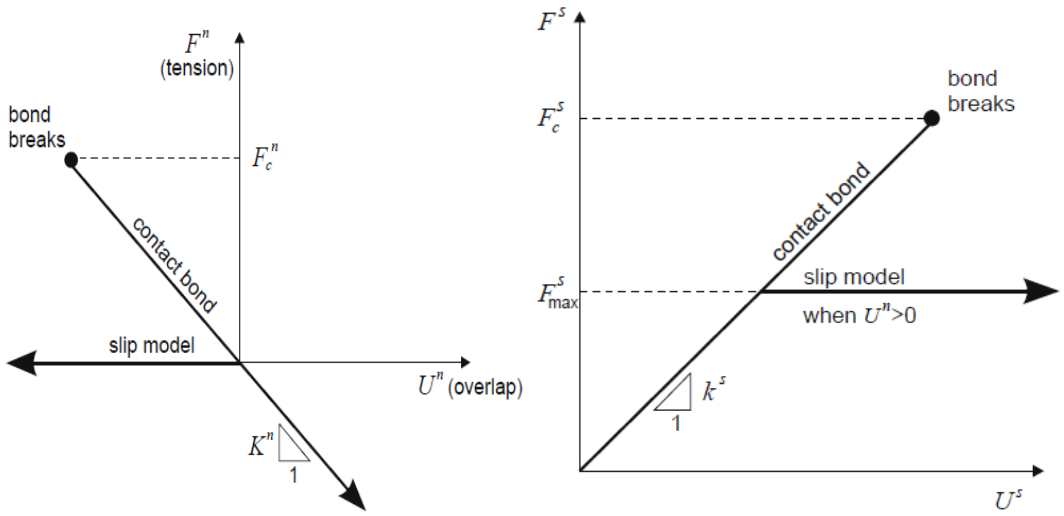

(a) Normal component of contact force (b) Shear component of contact force

Figure 2.6 Constitutive behaviors for point contact [15]

A contact bond is characterized as the normal contact bond strength F_c^n and shear contact bond strength F_c^s. The constitutive behaviors of contact bond model are shown in

Figure 2. 6. The bonds will break when the magnitude of the tensile normal contact force equals or exceeds the normal contact bond strength. After the breakage of the bond, both the normal and shear contact forces are set to zero.

2.7.3.2 The Parallel-Bond Model

In PFC^{3D}, the beam theory is used to calculate the stress within the parallel bond as shown in Figure 2.7. The axial and shear forces (T and V, respectively) along with bending moment (M) and twisting moment (M_t) can be caused by the relative motion of the particles. The maximum normal and shear stresses ($\bar{\sigma}$ and $\bar{\tau}$, respectively) carried by two particles connected by parallel bond can be written as:

$$\sigma_c = \frac{T}{A} + \frac{|M|\bar{R}}{I} \tag{2.27a}$$

$$\tau_c = \frac{|V|}{A} + \frac{|M_t|\bar{R}}{J} \tag{2.27b}$$

where A and I are the area and moment of inertia of the parallel-bond cross-section, J is the polar moment of inertia of the parallel-bond cross-section, and positive T indicates tension.

A parallel bond is defined by the following five parameters: normal and shear stiffnesses, E_{cp} and E_{cps}; normal and shear strengths, σ_c and τ_c; and bond radius, $\bar{R}$. The bond radius is set by specifying $\bar{\lambda}$ such that:

$$\bar{R} = \bar{\lambda}\min\left(R^{[A]}, R^{[B]}\right) \tag{2.28}$$

When either $\bar{\sigma}$ or $\bar{\tau}$ exceeds the corresponding strength, the bond breaks.

The beam cross-sectional area and moment of inertia can be expressed as:

$$A = \pi\bar{R}^2 \tag{2.29}$$

$$I = \frac{1}{12} 3\pi \bar{R}^4 \tag{2.30}$$

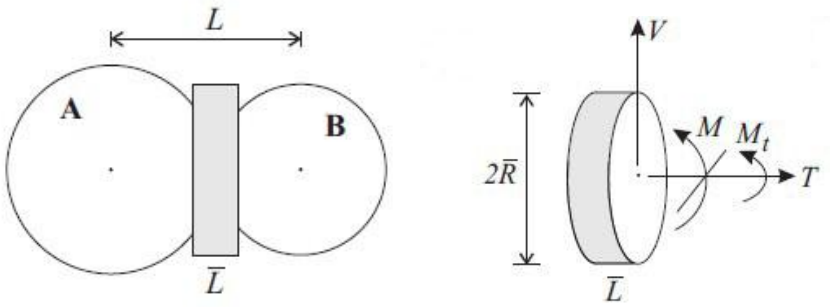

Figure 2.7 Parallel bond idealization and forces carried in 3D bond [15]

2.8 Critical Time-Step Determination

As expressed in Equation (2.13) and (2.14), DEM belongs to a centered finite difference scheme. The stability of the solution is determined by the time-step. The critical time-step relates to the minimum eigenperiod of the total system. The system is stable only if the time-step not exceeding the critical value. Because the DEM model is a constantly changing system, it is impractical to calculate the global eigenvalue of the system.

Therefore, the PFC^{3D} provides a simplified procedure to determine the critical time-step at the start of each calculation cycle. A fraction of this critical value will be used as the actual time-step value, and this fraction can be specified by the user through the command **SET safety_fac**.

To estimate the critical time-step for the solution stability, a one-dimensional mass-spring system, as shown in Figure 2.8(A), is considered first. The critical time-step for this system is defined as:

$$t_{crit} = \frac{T}{\pi} \; ; \qquad T = 2\pi\sqrt{m/k} \tag{2.31}$$

where "k" is the stiffness of the spring, and "m" is the mass of the point, and "T" is the period of the system.

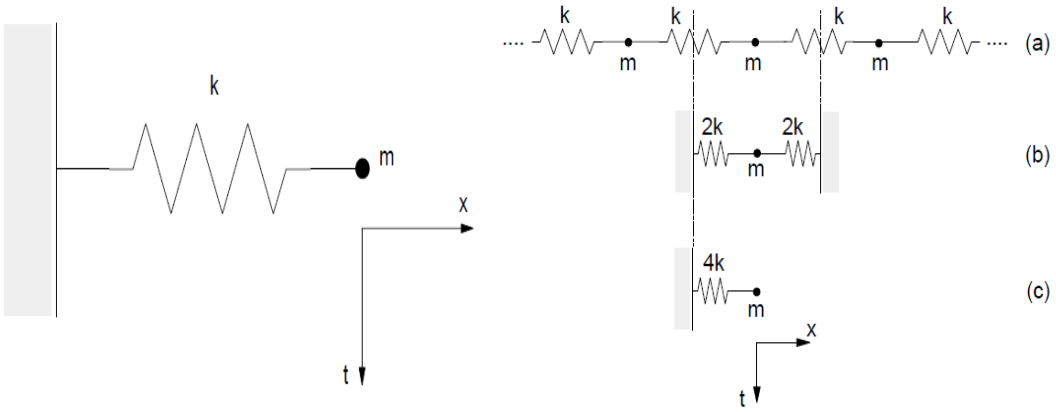

(a) (b)

Figure 2.8 Mass-spring systems: (a) Single mass-spring system; (b) Multi mass-spring system [15]

For a system composed of infinite series of point masses and springs, as shown in Figure 2.8(B), when the masses are moving in synchronized opposing motion, meaning that there is no motion at the center of each spring, the smallest period of this system will occur. Two equivalent systems shown in Figure 2.8(b) and 2.8(c) can be used to

describe the motion of a single point mass. Thus, the critical time-step for this system is given in Equation (2.32).

$$t_{crit} = 2\sqrt{m/(4k)} = \sqrt{m/k} \tag{2.32}$$

where "k" is the stiffness of each spring in the multi-spring system.

The translational motion can be captured by the above two systems. In the same way, the rotational motion can be obtained by replacing mass with moment of inertia and replacing stiffness with rotational stiffness in the previous systems. The critical time-step for the generalized multiple mass-spring system can be expressed as:

$$t_{crit} = \begin{cases} \sqrt{m/k^{tran}} & \text{(translational motion)} \\ \sqrt{I/k^{rot}} & \text{(rotational motion)} \end{cases} \tag{2.33}$$

where k^{tran} and k^{rot} are the translational and rotational stiffnesses and I is the moment of inertia of the particle.

For a system modeled with PFC^{3D}, by applying Equation (2.33), a critical time-step is calculated for each particle separately at each degree of freedom. The final critical time-step is the smallest considering all critical time steps for all particles at all degrees of freedom. For more details about the critical time-step determination in PFC^{3D}, please refer to the User's Guide [15].

2.9 Contact Detection Algorithm

In the calculation cycle of the discrete element model discussed in section 2.4, a key point in the analysis is to define a way to efficiently determine whether two particles are in contact or not, and how many particles are in contact for each time-step in a give

system. Because contact detection is quite time consuming, and can take a considerable portion of the total CPU time that is required to analyze the whole particulate system, an efficient and robust contact detection algorithm is required.

Detection of particles at contacts is an important step in DEM calculations before each calculation cycle begins. In PFC^{3D}, detection of the particles contacts is a simple and quick procedure. By assuming particle A centered at (x_1, y_1) and particle B centered at (x_2, y_2) in a Cartesian coordinate system, they are in contact if the distance *d* between their centers satisfies:

$$d \leq \sqrt{(x_1 - x_2)^2 + (y_1 - y_2)^2} \tag{2.34}$$

In other words, particles are considered to be in contact only if the distance between their centers is less than the sum of their radii. A brief description of the contact detection technique and its implementation in DEM code are presented by Cundall (1988).

CHAPTER III

EXPERIMENTAL DESCRIPTION

In this chapter, the triaxial lab tests performed at the laboratory L3S-R in Grenoble France are introduced [3]. Most of this chapter is referred to the papers on the Vosges sandstone published by Besuelle et al. [3]. The original tests cover the compression test, the extension test with different confining stresses and strain localization observations by X-ray devices. For the calibration purpose of this research, only the compression test sample (H/D=2) under 10MPa confining stress is discussed in detail. Finally, the loading simulation test performed in the PFC^{3D} environment is introduced.

3.1 Experimental Device

The scheme of the triaxial cells used in the lab test is shown in Figure 3.1. The triaxial cells integrated with the axial load device are designed to be autonomous. The confining pressure sustained by the loading cell can be added up to 60 MPa and the deviatoric pressure as high as 270 MPa.

The loading part of the lab experimental apparatus in Figure 3.1 consists of a lower cell (1), an upper cell (3), axial load self-compensated piston (4), top chamber (5), and lower load caps (8). The lower cell can apply a confining pressure and a back pressure to the specimen (2), and the upper cell hosts the axial load piston which can be pushed from the top chamber by oil pressure. The pressure transmitted to the specimen is enlarged by 4.5 times due to the surface ratio of the piston. The lower and upper cells are

connected by eight bolts (6). In order to avoid oil penetration, a neoprene membrane (thickness of 0.7mm) (7) is placed around the specimen in the lower cell. Through the caps, different pore pressure can be added to the specimen. Drainage lines are also connected to the caps, which allow fluid to flow through the specimen for the measurement of the rock permeability. The intermediate smooth enlarged hardened plates (9) are placed between the specimen and the laod caps to ensure a frictionless surface and to avoid edge effects. Two internal tight connectors (10) each with 12 signal conductors are used for the internal instrumentation. The steel sheath (11) is used to protect a thermo-couple for monitoring the oil temperature.

Four identical independent generators are used to generate the deviatoric stress, the top cell pressure, the bottom cell pressure and the pore pressure, which are all generated by a piston moving in a pressure chamber. The pressure generator is guided by an electronic regulator programmed by a PC computer receiving an analogical signal from an external transducer. An angular transducer on the motors is used to measure the volume of the water injected into the cell by the two pore pressure generators. A LVDT measuring the axial displacement of the cell piston regulates the deviatoric pressure of the specimen. The displacement control is to capture the post peak portion of the specimen response.

The scheme of the internatal instrumentation is shown in Figure 3.2. Three axial transducers and four radial transducers regularly spaced around the specimen are used to measure the axial and lateral strain.

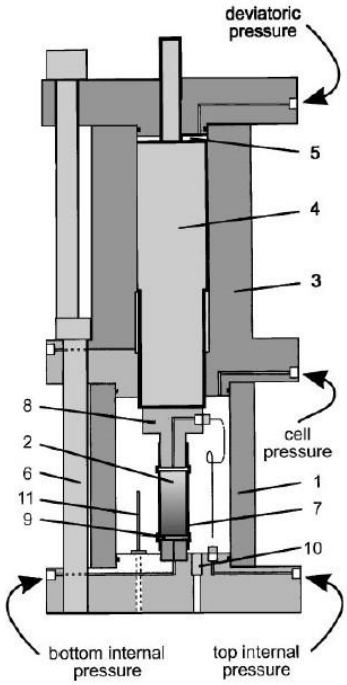

Figure 3.1 Schematic of the triaxial cell [3]. (1) lower cell, (2) specimen, (3) upper cell, (4) self-compensated load piston, (5) deviatoric pressure chamber, (6) bolts, (7) neoprene membrane, (8) load caps, (9) enlarged plated, (10) internal tight connectors, (11) steel sheath.

An axial strain can be deduced from the shortening divided by the initial distance between two marked points on the membrane measured by an axial transducer. These two points relate to the middle of the pseudo-hinged attachment glued to the membrane. By the average of the three measurements from the three axial transducers, the mean of the axial strain can be obtained.

The lateral displacement of the contact point between the transducer and the membrane is measured by a radial transducer at the mid-height of the specimen. The radial strain is measured in two orthogonal directions. The opposite transducers measure

the relative displacement in the radial direction and the axial strain can be computed from the relative displacement divided by the initial diameter of the specimen.

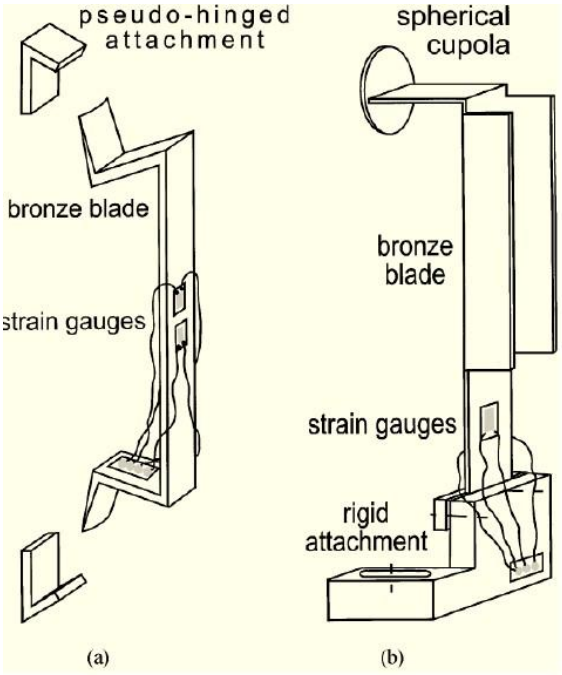

Figure 3.2 Schematic of the internal instrumentation for the (a) axial and (b) radial strain measurement [3]

3.2 Rock Specimen

The rock used in the lab test is natural sandstone obtained from the Woustviller quarry in the Vosges Mountains, France [3]. The pink quartz content in the sandstone is 93%, with a few percent of feldspar and white mica. The Vosges sandstone is poorly cemented material and the cohesion developed is caused by the interpenetration between particle grains under large pressure. The measured porosity of the specimen is about

22%. Under the observation of optical microscopes, the size of a single grain is measured between 0.1 to 0.3mm. The statistical factor of 3/2 can be used to estimate the true size of the grains in three dimensions for spherical grains. The dimension of grains fluctuates between 0.15 and 0.45 mm with average value of about 0.3 mm. Dry specimens are used in the test, so the specimens are exposed to a temperature of 100℃ for a few days.

3.3 Compression Test

The ends of sandstone specimen used in the compression test are adjusted to have a good parallelism, better than ± 0.04 mm. A mixture of Vaseline and stearic acid is used to produce frictionless boundary at the ends. Specimens are loaded at a strain rate of $10^{-5}s^{-1}$, as to slow to avoid any rate effect by the loading cell. During the compression test, the lateral stress is kept constant while the axial stress increased. The deviatoric stress is computed as the axial stress minus the confining stress in triaxial compression test. Specimens are tested from a specified isotropic stress state up to failure state.

The stress and strain can be accurately recorded during the triaxial test. The results can be used as feasible objectives for the discrete particle model. The deviatoric stress and axial strain with confining pressure 10MPa of Vosges sandstone specimen with height/diameter ratio H/D=2 is shown in Figure 3.3, which is used in the following chapters for calibrating the DEM model.

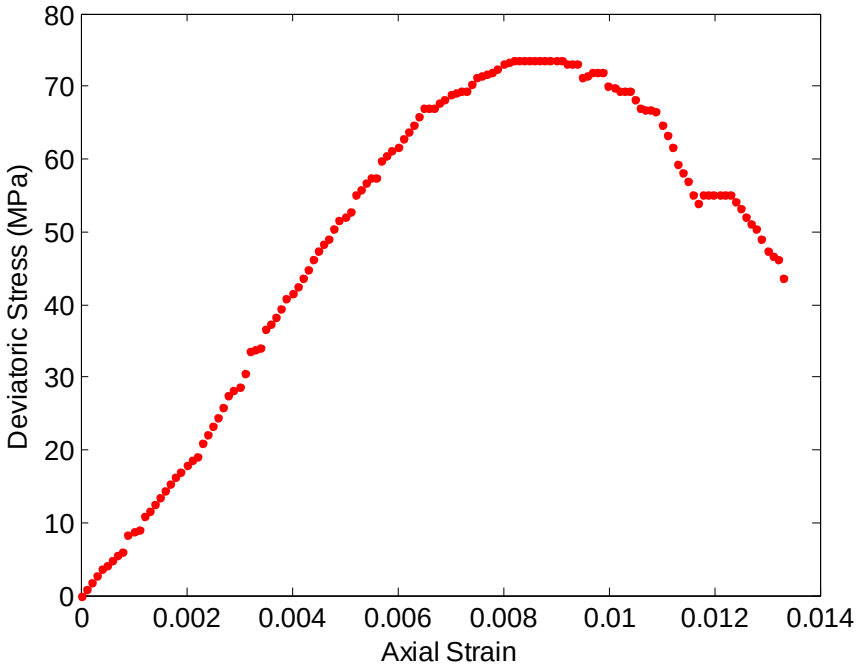

Figure 3.3 Stress strain curve of triaxial compression test with confining pressure 10 MPa [3]

3.4 Loading Simulation in PFC^{3D}

The parameters specifying the loading test simulation in PFC^{3D} are included in APPENDIX C [15]. Key assumptions about the numerical modeling are discussed below.

The stiffness ratio for the cylinder wall (**et3_knrfac**) is set to be 0.005 times of the average particle stiffness, which is designly small to simulate the low stiffness of the water boundary; and the stiffness of the loading platens (**et3_knyfac**) is chosen to be the same as the average particle stiffness to avoid ball penetration through the loading platens.

The confining pressure (**et3_wsrr_req**) is set to be 10MPa to simulate the confining pressure; however, a tolerance ratio (**et3_ws_tol**) of 0.01 is needed in PFC^{3D} to achieve the target values. The loading speed of the platen (**p_vel**) is set to be 0.2, which will be achieved by 1000 cycles (**p_cyc**) over 20 stages (**p_stages**).If the velocity is applied in a single step, the large acceleration will produce inertial forces within the specimen that may result in damage. According to the prescribed lab test data, the final strain of the sample is set to 0.0133 (**et3_strain**).

The top and bottom walls act as loading platens, and the velocities of the lateral walls are controlled by a servo-mechanism that maintains a specified confining stress. After the specified values of confining stress have been applied to the specimen, the specimen dimensions at this stage are taken as the reference dimensions to be used in the wall-based computation of stresses and strains during the subsequent loading phase.

During the triaxial test, the specimen behavior is monitored by using the PFC history mechanism in order to record the relevant quantities.

CHAPTER IV

FAILURE MECHANISMS

This chapter primarily introduces the experimental characterization of the localization phenomenon inside a Vosges sandstone specimen in a triaxial cell performed in the laboratory L3S-R in Grenoble France [3]. Subsequently, the failure mechanism of the discrete particle model is developed to reproduce the experimental strain localization, following with the discussion on micro-crack types.

4.1 Experimental Observation

One or several shear bands are observed throughout the specimen in all the lab compression triaxial tests. To illustrate the effect of confining pressures, the observed shear band patterns are shown in Figure 4.1.

For the long specimen (height diameter ratio H/D=2), when the confining pressure is zero, the sample fails with a combination of axial splitting and inclined failure surfaces. With the increase of the confining pressure, shear bands are observed on the lateral surfaces of the specimen represented by the white inclined lines (Figure 4.2). It is also observed that multi failure surfaces develop with the increasing confining pressure. There is only one or two parallel failure surfaces inclined to the loading direction when the confining pressures are between 10 and 30 MPa.When the confining pressure increases up to 40 MPa, conjugate shear bands are visible throughout the specimen. Compared the failure surfaces of 40MPa, 50MPa and 60 MPa, the distance between the

bands decrease with increasing pressure while the number of failure surfaces increases. Also, the failure regions are more restricted to the top platen with the increasing pressure. The increased confining stress also causes an increasing inclination of the shear band with respect to the loading axis.

For the short specimen (H/D=1), similar failure patterns are observed, but the number of the shear bands has a smaller value for the same confining pressure.

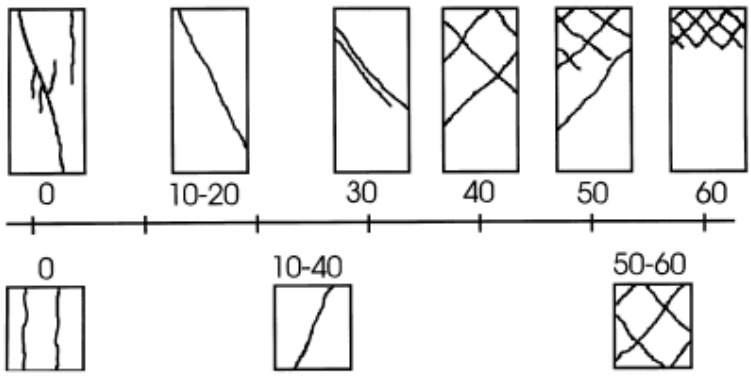

Figure 4.1 Observed shear band patterns for compression test [3]

When the triaxial compression specimen is at failure, the inclined angle between the shear band and the loading direction is measured from the trace appearing on the membrane [3]. Results show that the inclined angle is very sensitive to the confining pressure. This angle for the long specimen almost increases linearly from 35° at 10 MPa confining pressure to 55° at 60 MPa, with a slope of about $0.29°/\text{MPa}$ of the mean

stress. This angle for the short specimen is much smaller than that in the long specimen, with the same slope of evolution of the angle with respect to the mean stress.

Figure 4.2 Sandstone specimen failed at different confining pressure from low (right) to high (left) [3]

The laboratory triaxial compression with confining pressure 10 MPa is used to for the failure mechanism simulation in the discrete particle model. The picture of the specimen at failure of the Vosges sandstone shows a clear shear band (white lines) with 35° inclination to the loading direction (major principal stress) as shown in Figure 4.3.

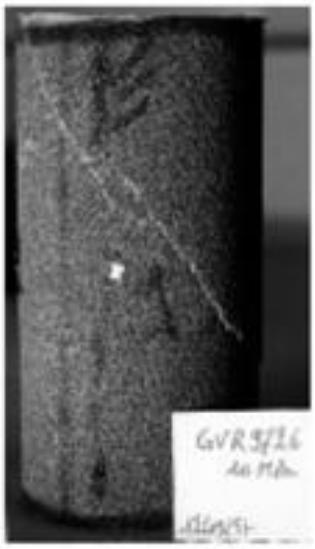

Figure 4.3 Failure damage under laboratory triaxial compression test with confining pressure 10MPa [3]

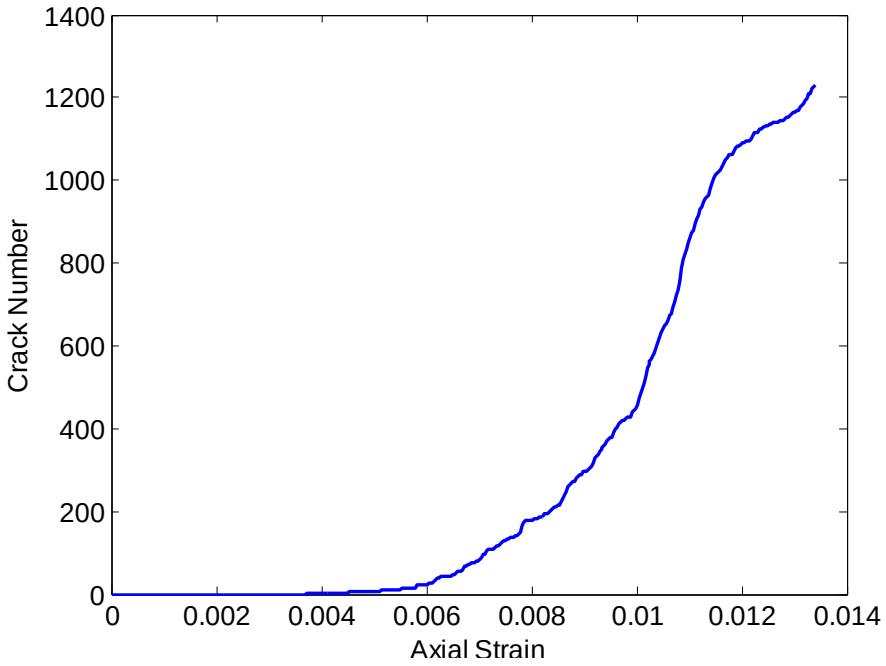

Figure 4.4 Total number of micro-cracks versus axial strain

4.2 Failure Mechanism through DEM Simulation

To observe the failure mechanism, the micro-parameters in the table on p.52 are adopted, which could reproduce the global stress strain behavior (the figure on p.54) of the lab test for Vosges sandstone. The number of the cracks is monitored with respect to axial strain as shown in Figure 4.4. The total number of 1231 micro-cracks occurs at the critical state, close to the end of the loading.

The development of the micro-cracks during the triaxial compression loading is also traced in the PFC^{3D} and presented in Figure 4.5, offering a view of the failure process mechanism of the DEM sample during the compression test. From these two figures (Figure 4.4 and 4.5) it can be observed that a few micro-cracks initiate at pre-peak state; and that with the increasing of the load up to the peak stress, the cracks concentrate close to the platens and particularly close to the upper platen. The post-peak behavior shows an inclined zone, which indicates the presence of a shear banding effect.

For the proposed DEM model, the parallel normal strength is set equal to the parallel shear strength. Figure 4.5 shows the evolution of cracks formation during shearing, with most cracks of the tensile type, indicating that the normal stress of the parallel bond dominates the failure mechanism. For this particular condition ($\sigma_c = \tau_c$), few shearing cracks developed during the triaxial compressive loading. The arrangement of these cracks shows a shearing plane close to $\varepsilon_a = 0.013$.

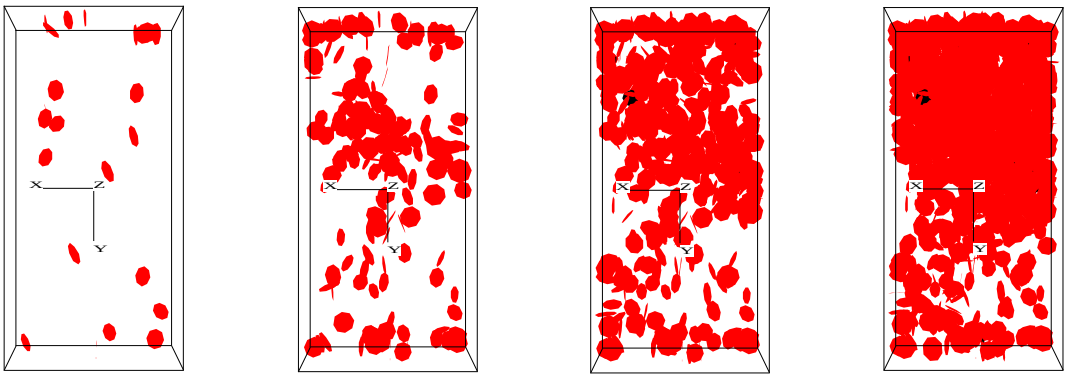

Pre-peak	Peak	Post-Peak	Failure
$\varepsilon_a = 0.006$	$\varepsilon_a = 0.008$	$\varepsilon_a = 0.010$	$\varepsilon_a = 0.013$

Figure 4.5 Micro-cracks development for $\sigma_c = \tau_c$.
Tensile (red) and shear (black) cracks

4.3 Discussion on Crack Type

To explore the influence on the ratio between the bond's maximum normal strength σ_c and shear strength τ_c with respect to different failure mechanisms, a set of PFC^{3D} compression tests were performed by keeping the normal strength constant for increasing combinations of shear strength, while other values of the micro-parameters were kept constant. The crack fields at about the starting of the critical state for these combinations are shown in Figure 4.6, including the displacement field and the contact force field. There representations of cracks alone are not enough as to describe particular type of localization. However, by plotting the displacements induced during the triaxial test, it is observed that various failure planes appear to have formed within the specimen. Displacement fields also indicate trends of shear bands with different inclinations.

Consequently, it can be concluded that the relation between the parallel tensile and shear strength have a determinant impact on the formation of the micro-cracks and the failure mechanisms. Based on the three configurations discussed in Figure 4.6, it can be concluded that the lesser the shear bond is the greater the shear micro-cracks are compared to an equal tensile and shear bond strength condition where the tensile cracks significantly dominate. Therefore, to reproduce the failure mechanism behavior of the lab test of the sandstone specimen, it is necessary to try different combinations of tensile to shear strength ratios, along with the other micro-parameters.

Strength	$\tau_c = \frac{1}{3}\sigma_c = 20\text{MPa}$	$\tau_c = \frac{1}{2}\sigma_c = 30\text{MPa}$	$\tau_c = \sigma_c = 60\text{MPa}$
Displacement Field	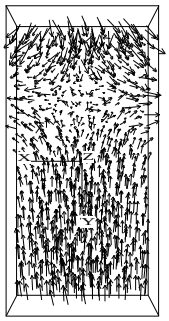	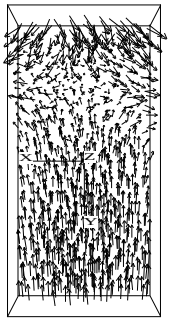	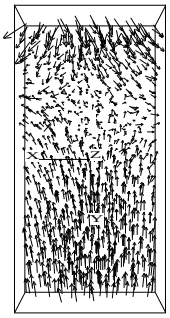
Crack Field			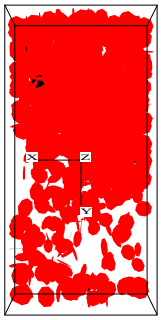
Contact Force	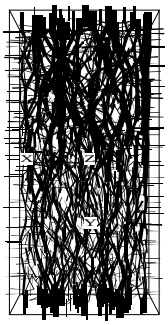	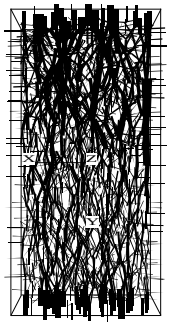	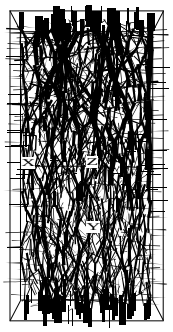

Figure 4.6 Failure mechanism analysis for varying normal to shear bond strengths. Tensile (red) and shear (black) cracks

CHAPTER V

PARAMETRIC ANALYSIS

In this chapter, all the parameters presented in the DEM are firstly divided into two categories: one describing the macro material properties, and the other controlling the micro particle behavior. The macro material properties, such as density, porosity and particle radius, are assumed as constant values for the Vosges's sandstone specimen. Then, a set of micro-parameters referred as 'final sample' is derived by trial and error method to reproduce results from the reference lab test. Based on the final sample, a parametric analysis is performed to analyze the sensitivities of each micro-parameter by changing only one variable at the time, while all others are kept constant.

5.1 Lab Test Simulation in PFC^{3D}

A triaxial model built in PFC^{3D} was introduced in Chapter II with the aim of reproducing the experimental observations from the reference test. Triaxial compression tests can be performed on the specimen and then the reponse can be extracted from the simulation results, i.e. via the stress-strain curve, volumetric change, crack evolution, and boundary of full displacement fields. Once the triaxial testing environment in PFC^{3D} is created, only a few set of parameters will fully control the sample mechanistic behavior.

All the parameters in PFC^{3D} model can be divided into two main groups: the ones describing the main physical properties, such as density, particle diameters, and porosity;

and the ones depicting the particle contact characterization, such as particle-particle friction coefficient, particle contact stiffness and parallel tensile strength. The former are referred as meso-parameters and the latter as micro-parameters. The meso-parameters control the physical constitution of the model. The closer the PFC^{3D} sample's physical constitution to the real experimental sandstone is, the better the micro-parameters will be. The proposed values of the meso-parameters are shown in Table 5.1.

Table 5.1 Meso-parameters for the Vosges sandstone specimen

Meso-parameter	Symbol	Unit	Final Sample
Sample height	h	mm	80
Sample diameter	d	mm	40
Minimum ball radius	r_{min}	mm	3.3
Maximum ball radius	r_{max}	mm	2.0
Porosity	n	-	0.22
Density	ρ	kg/m^3	1960
Locked-in isotropic stress	σ_c	MPa	1
Wall normal stiffness multiplier	β	-	1.1
Minimum number of contacts to be a non-floater	N_f	-	3
Remaining floaters ratio	n_f/N	-	0

To get the similar stress-strain behavior with the lab test, the PFC^{3D} model is performed by adjusting the micro-parameters using trial and error method to get the rough optimization values (reffered as 'final sample'), which make the deviation between lab data and simulation results relatively small. Notice that this is only one likely combination of parameters that fit the observations. The proposed micro-parameters for 'final sample' are shown in Table 5.2.

Table 5.2 Micro-parameters for the Vosges sandstone specimen

Micro-parameter	Symbol	Unit	Final Sample
Contact Young's modulus	$\theta_1 = E_c$	GPa	12.1
Ratio of contact normal to shear stiffness	$\theta_2 = E_s/E_{cs}$	-	6
Inter-particle friction coefficient	$\theta_3 = \mu$	-	3.0
Parallel bond Young's modulus	$\theta_4 = E_{cp}$	GPa	12.1
Ratio of bond normal to shear stiffness	$\theta_5 = E_{cp}/E_{cps}$	-	8
Average bond tensile strength	$\theta_6 = \sigma_c$	MPa	60
Standard deviation in bond tensile strengths	$\theta_7 = \sigma_d$	MPa	6.0
Average bond shear strength	$\theta_8 = \tau_c$	MPa	60
Standard deviation in bond shear strength	$\theta_9 = \tau_d$	MPa	6.0

In Table 5.1, the wall normal stiffness multiplier is the ratio between the stiffness of the wall and the averaged stiffness of the particles which have contacts with the wall, expressed as:

$$\beta = \frac{E^{c\_wall}}{E_{average\ \_particle}} = \frac{E^{c\_wall}}{\sum_{i=1}^{k} E_i^{c\_particle}} \tag{4.1}$$

where k is the number of particles contact with the wall. The parameters $\beta = 1.1$ means the wall stiffness is a little higher than particles, which could prevent the particles penetrating the walls.

The minimum number of contacts to be a non-floater is defined as a 'floater' (see section 2.2) in the sample genesis procedure. A particle needs at least 3 contact points to reach the equilibrium state, so the floaters should be eliminated when no particle in real sanstone exists.

The deviatoric stress versus axial strain curve of the 'final sample' with confining pressure 10MPa is shown in Figure 5.1.

To evaluate the simulation results, the deviation and normalized deviation between the lab test and 'final sample' are shown in Figure 5.2 and Figure 5.3, respectively.

$$\text{Deviation} = \mathbf{d_{prep}} - \mathbf{d_{obs}} \tag{4.2}$$

$$\text{Normalized Deviation} = \frac{\mathbf{d_{prep}} - \mathbf{d_{obs}}}{\mathbf{d_{obs}}} \tag{4.3}$$

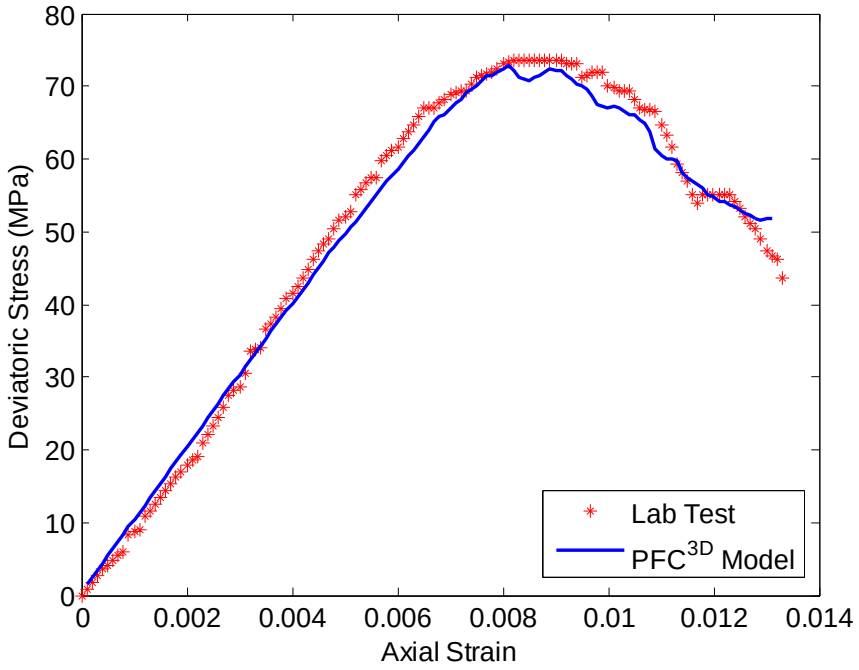

Figure 5.1 Final sample for parametric analysis

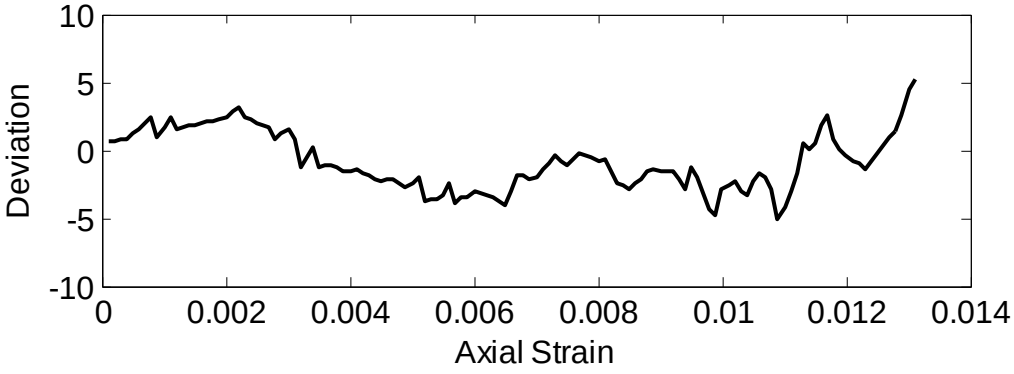

Figure 5.2 Deviation between lab test and final simulation sample

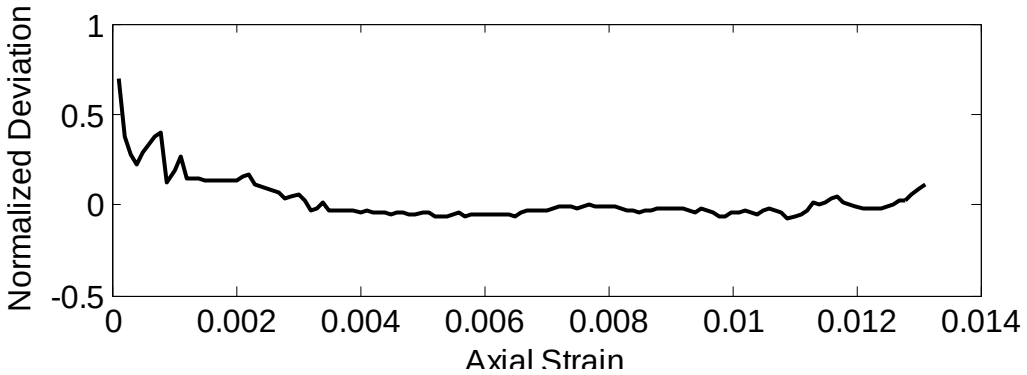

Figure 5.3 Normalized deviation between lab test and final sample

The normalized deviation is very large due to the small value of deviatoric stress at a small strain level ($\varepsilon_a < 0.002$), which is hard to capture at the beginning. When the strain $\varepsilon_a > 0.002$, the results are more accurate, the deviation is much smaller than 5MPa, compared to 70MPa deviatoric stress at peak. The simulation fits the lab test well when $\varepsilon_a < 0.012$. The behavior at large strain is also difficult to reproduce. In general, considering the relatively small normalized deviation, the 'final sample' serves as a very good fit for the triaxial lab test.

5.2 Influence of Micro-Parameters on Macro-Behaviors

The method for parametric analysis is introduced first. Then, the range of each micro-parameter for calibration is listed one by one. Finally several figures showing the sensitivities of the micro-parameters are derived by running the DEM model, followed with a short summary of the parametric study results.

5.2.1 Methods for Parametric Analysis

The parametric analysis aims to develop the influence of each micro-parameter on the macro-response of the specimen. Based on the 'final sample', it is an effective way to conduct the model's sensitivity by changing one parameter while others are kept constant. Since only one parameter is changing at the time, recognizing how the parameter controls the behavior of the sample is straightforward, including initial linear response, the peak strength, and the post peak response. The ranges of the micro-parameters are chosen in varying order to make the results more comparable (Table 5.3), even though the physical meaning of the value may sometimes be out of reasonable range.

Table 5.3 Simulations conducted for parametric analysis

Particle normal stiffness:

Parameter	Final Sample	RUN1	RUN2	RUN3	RUN4
$\boldsymbol{\theta_1 = E_c}$	12.1GPa	10GPa	14GPa	16GPa	18GPa

Particle normal to shear stiffness ratio:

Parameter	Final Sample	RUN1	RUN2	RUN3	RUN4
$\boldsymbol{\theta_2 = E_c/E_{cs}}$	6	1	3	8	10

Table 5.3 Continued

Particle friction coefficient:

Parameter	Final Sample	RUN1	RUN2	RUN3	RUN4
$\theta_3 = \mu$	3	0.5	1	2	3

Parallel bond normal stiffness:

Parameter	Final Sample	RUN1	RUN2	RUN3	RUN4
$\theta_4 = E_{cp}$	12.1GPa	10GPa	14GPa	16GPa	18GPa

Parallel bond normal to shear stiffness ratio:

Parameter	Final Sample	RUN1	RUN2	RUN3	RUN4
$\theta_5 = E_{cp}/E_{cps}$	8	1	3	6	10

Parallel bond tensile strength (Mean):

Parameter	Final Sample	RUN1	RUN2	RUN3	RUN4
$\theta_6 = \sigma_c$	60MPa	50MPa	55MPa	60MPa	65MPa

Parallel bond tensile strength (Standard deviation):

Parameter	Final Sample	RUN1	RUN2	RUN3	RUN4
$\theta_7 = \sigma_d$	6MPa	0MPa	10MPa	15MPa	20MPa

Table 5.3 Continued

Parallel bond shear strength (Mean):

Parameter	Final Sample	RUN1	RUN2	RUN3	RUN4
$\boldsymbol{\theta_8 = \tau_c}$	60MPa	10MPa	20MPa	40MPa	80MPa

Parallel bond shear strength (Standard deviation):

Parameter	Final Sample	RUN1	RUN2	RUN3	RUN4
$\boldsymbol{\theta_9 = \tau_d}$	6MPa	0MPa	10MPa	15MPa	20MPa

5.2.2 Effect of Particle to Particle Normal Stiffness

The particle to particle normal stiffness ($\theta_1 = E_c$) is the normal Young's modulus at each particle-particle contact. In Figure 5.4, the normal Young's modulus controls the initial elastic behavior of the sample in triaxial test. With the increase of the contact normal Young's modulus, the initial elastic linear line moves upwards.

The peak strength is reached at a smaller axial strain with higher contact normal in Young's modulus. When E_c equals to 10GPa, the deviatoric stress reaches a maximum value with ε_a around 0.009, ε_a about 0.008 for E_c 12.1GPa, ε_a about 0.0075 for E_c 14GPa, ε_a about 0.007 for E_c 16GPa, and ε_a about 0.0055 for E_c 18GPa. The influence of the particle to particle normal stiffness on the peak strength and the post peak behavior is hard to draw from Figure 5.4. The peak strength seems to be of the same stress level, except for E_c 14GPa.Therefore, the particle normal stiffness mainly controls the initial linear response of the sample by changing the Young's modulus of the materials.

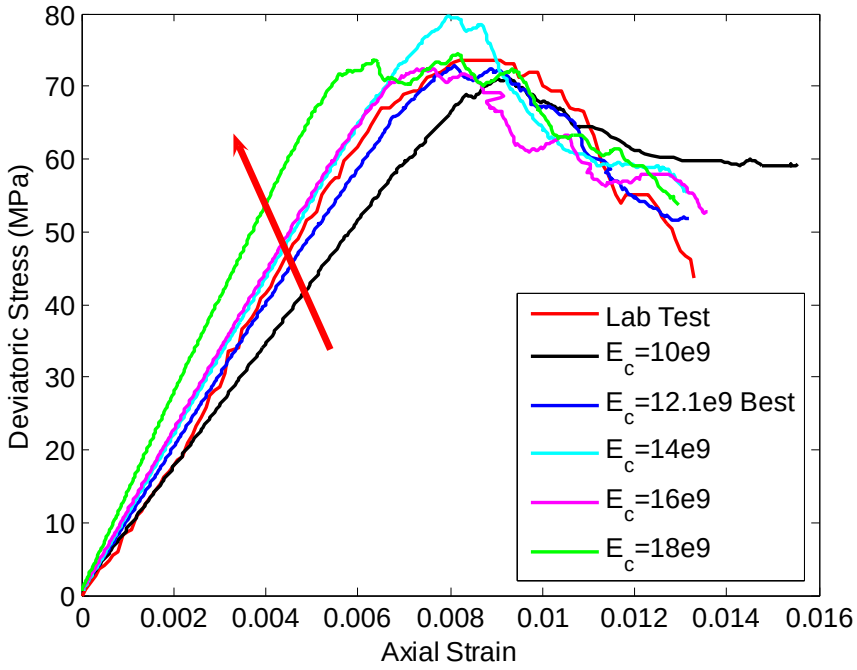

Figure 5.4 Effect of particle to particle normal stiffness

5.2.3 Effect of Particle Normal to Shear Stiffness Ratio

The particle normal to shear stiffness ratio ($\theta_2 = E_c/E_{cs}$) is the ratio of the normal and shear contact Young's modulus. This ratio represents the particle contact shear stiffness when the particle contact normal stiffness is known. Once the normal stiffness is constant, changing this ratio means adjusting the shear Young's modulus of the contact model.

The shear particle stiffness is decreasing with the increase of this ratio. In Figure 5.5, the sample is more deformable with the decreasing of the particle contact shear stiffness, which means that the sample can develop more strain with the same deviatoric stress.

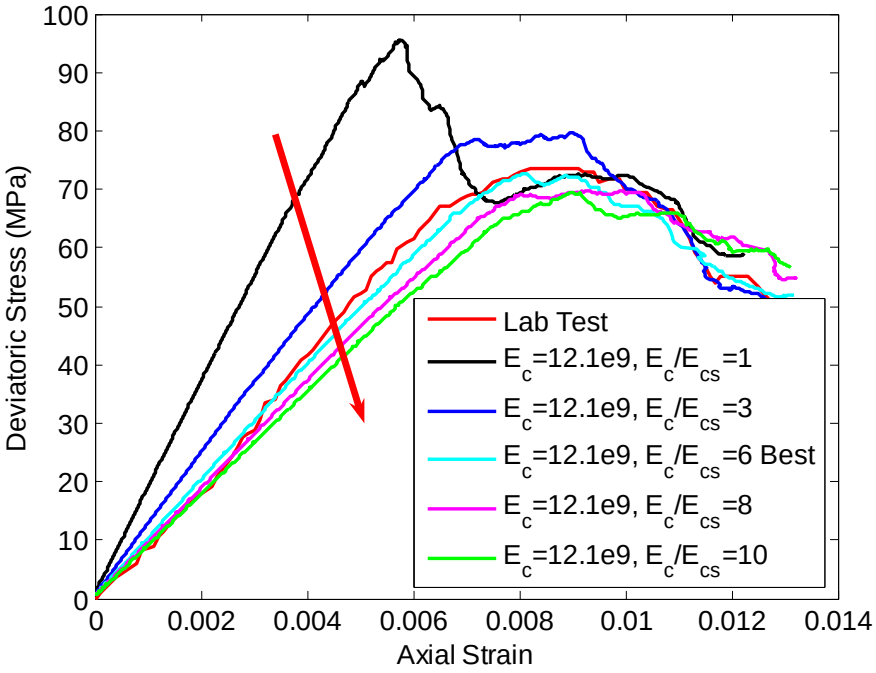

Figure 5.5 Effect of particle normal to shear stiffness ratio

The decreasing of particle shear stiffness also postpones the state of the peak strength, with ε_a about 0.006 for the ratio as 1, ε_a about 0.007 for the ratio as 3, ε_a about 0.008 for the ratio as 6, ε_a about 0.009 for the ratio as 8 and ε_a about 0.0095 for the ratio as 10. The peak strength also slightly decreases with the decrease of the particle shear stiffness when the ratio is greater than 3.

5.2.4 Effect of Particle to Particle Friction Coefficient

The particle to particle friction coefficient ($\theta_3 = \mu$) is added to each contact in the DEM model. The friction coefficient is set to be 3 in the final sample considering the particle interpenetration of the real standstone specimen due to high pressure, also

considering the angular charateristics with different shapes of the sandstone grains. The particle roughness could increase the particle friction up to much greater than 1.

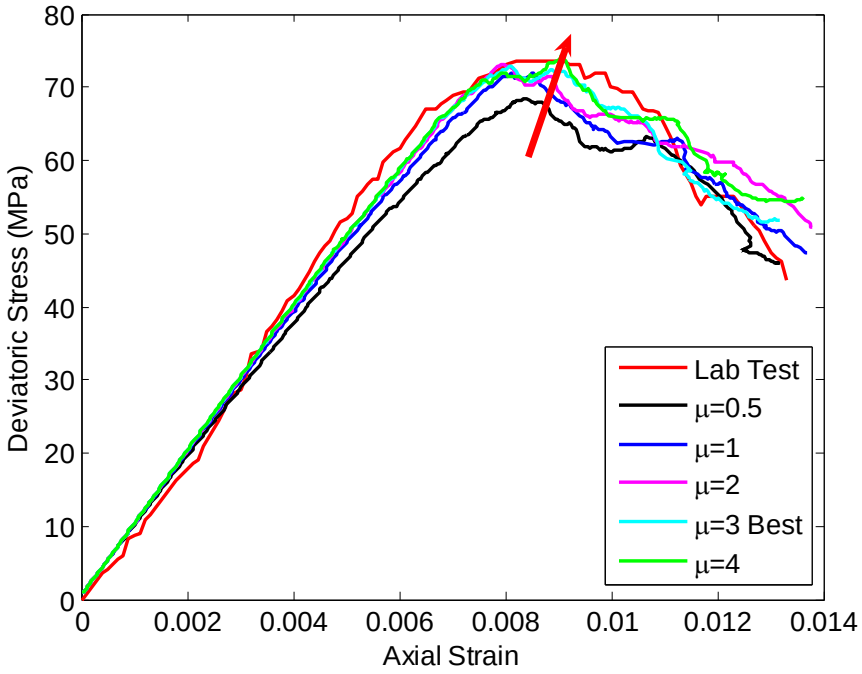

Figure 5.6 Effect of particle to particle friction coefficient

In Figure 5.6, the particle friction coefficient only has slight influence on the behavior of the sample. When $\mu > 1$, the elastic behaviors of the four samples are almost coincident within the elastic range. The post peak behavior shows little change when altering the particle friction coefficient.

The friction coefficient has little influence on the stress strain response to the parallel bonded materials. However, the friction will control the response of granular materials, where bonds and cohesion are excluded.

5.2.5 Effect of Parallel Bond Normal Stiffness

The parallel bond normal stiffness ($\theta_4 = E_{cp}$) is the normal Young's modulus at each parallel bond contact. From Figure 5.7, it is observed that this micro-parameter also controls the initial elastic response of the sample. With the increasing of this micro-parameter, the initial elastic linear line moves upwards, making the sample harder to deform.

With higher parallel normal stiffness, the peak strength state occurs at lower axial strain, which is smaller when compared with contact normal stiffness (Figure 5.4). The peak strength of the sample slightly decreases with the increase of parallel normal stiffness. The parallel bond would break at smaller strain for higher bond stiffness. So the peak strength is decreasing and the post peak behavior reaches lower stress level.

5.2.6 Effect of Parallel Bond Normal to Shear Stiffness Ratio

The parallel bond normal to shear stiffness ratio ($\theta_5 = E_{cp}/E_{cps}$) is the ratio of the normal to shear bond Young's modulus, which indirectly reflects the level of the parallel bond shear stiffness.

In Figure 5.8, decreasing the parallel shear stiffness by increasing this ratio would decrease the initial elastic slope, which implies that this micro-parameter has a relationship with the material Young's modulus. The decreasing parallel shear stiffness also postpones the state of the peak strength and slightly decreases the peak strength.

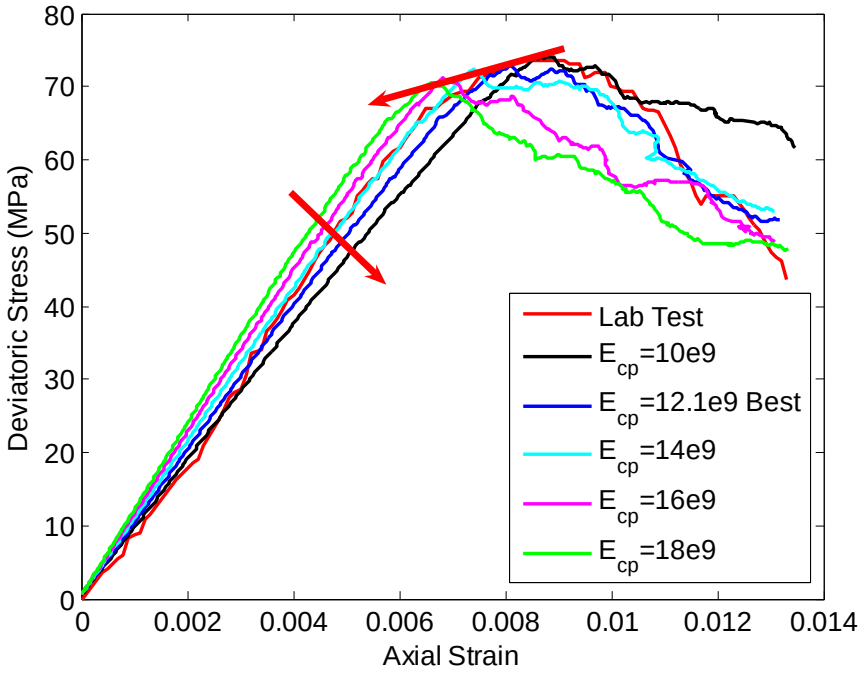

Figure 5.7 Effect of parallel bond normal stiffness

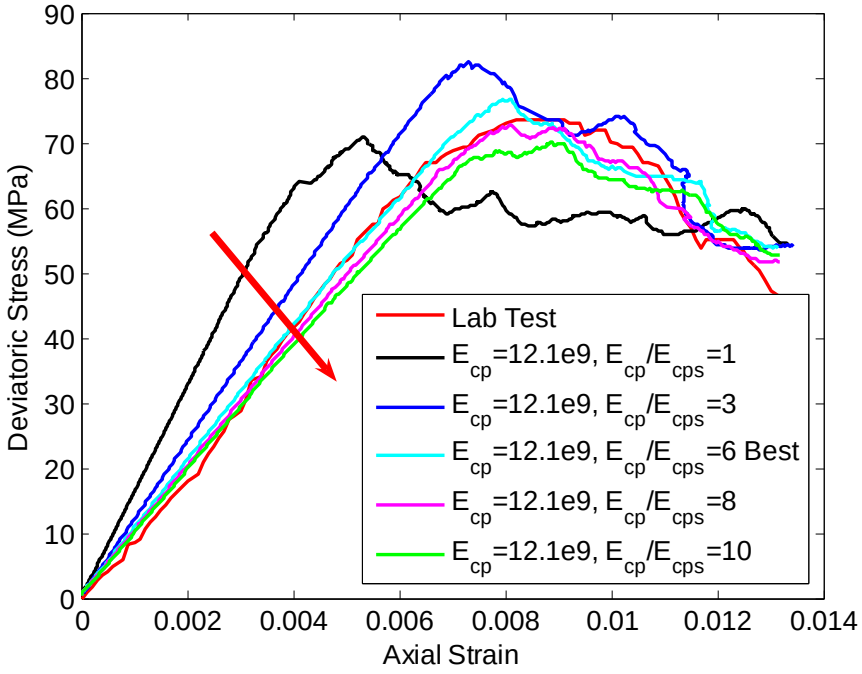

Figure 5.8 Effect of parallel bond normal to shear stiffness ratio

5.2.7 Effect of Parallel Bond Tensile Strength: Mean

The parallel bond tensile strength is the normal strength of the cement-like material represented by parallel bond model. The normal strength among all the parallel bonds follows a Gaussian distribution with the mean value σ_c and standard deviation σ_d. The effect of the parallel bond mean tensile strength $(\theta_6 = \sigma_c)$ is shown in Figure 5.9.

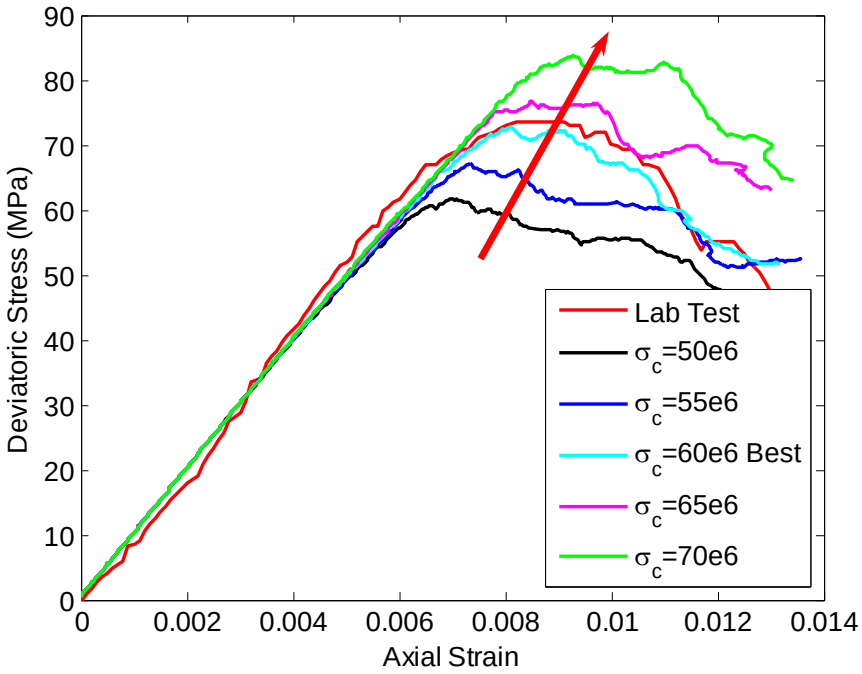

Figure 5.9 Effect of parallel bond mean of tensile strength

The mean value of the parallel tensile strength has little effect on the initial linear elastic behavior of the sample, but significantly increases the peak strength of the sample

with the increase of this micro-parameter. The post-peak behavior becomes more brittle when augmenting the stress level.

5.2.8 Effect of Parallel Bond Tensile Strength: Standard Deviation

The effect of the standard deviation ($\theta_7 = \sigma_d$) of the tensile strength is shown in Figure 5.10. The initial linear response of the sample has almost no changes, which implies that the parallel bond tensile strength deviation has little effect on the Young's modulus of the materials. Also, the post peak behavior of the samples becomes more ductile when increasing the standard deviation. The post peak strength is also greater at large deviation values because the bonds with higher strengths play very significant roles in the development of the strength. Yet this difference is very small compared to the actual value of the corresponding data point.

It is important to note that this effect is not as important as the mean value of the tensile strength. When the mean value is kept unchanged, the influence of the deviation parameter is negligible. In the 'final sample', the standard deviation is 10% of the mean value of 60MPa in the final sample.

5.2.9 Effect of Parallel Bond Shear Strength: Mean

Similar with the parallel normal tensile strength, the parallel shear strength also follows the Gaussian distribution with the mean value ($\theta_8 = \tau_c$) and the standard deviation ($\theta_9 = \tau_d$).

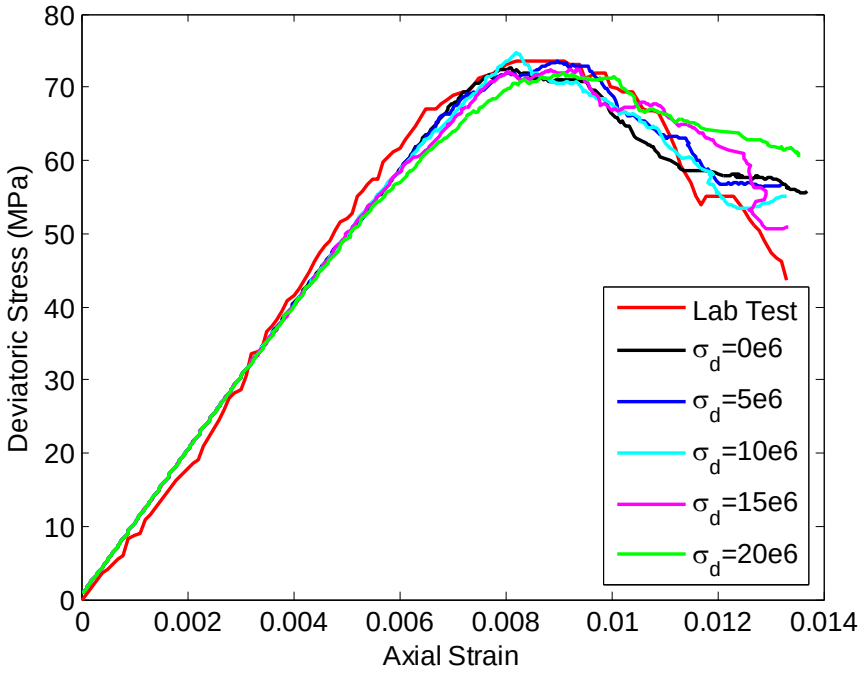

Figure 5.10 Effect of parallel bond standard deviation of tensile strength

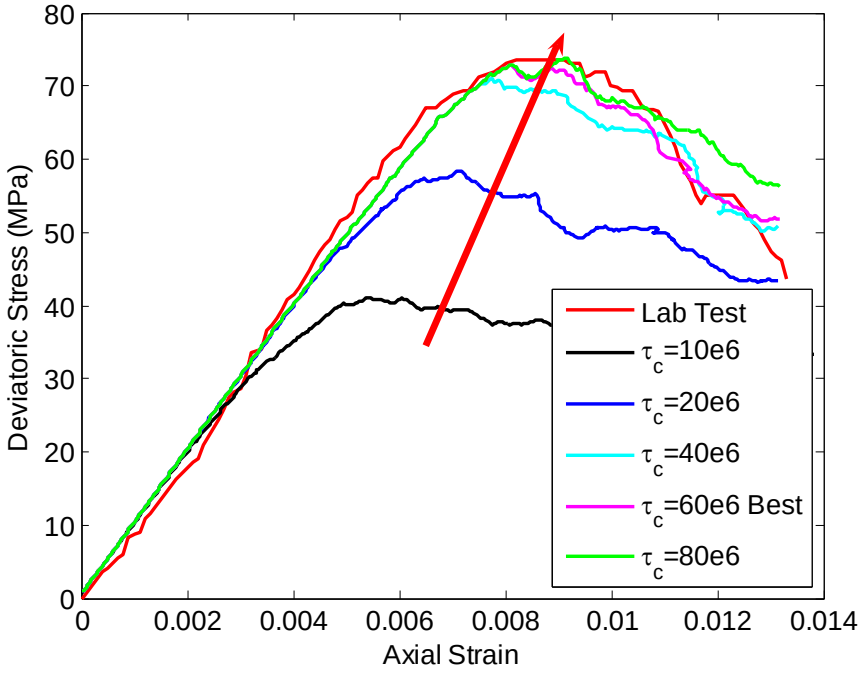

Figure 5.11 Effect of parallel bond mean of shear strength

In Figure 5.11, the increase of the mean shear strength increases the peak strength of the sample significantly. It is relevant to point out that a converging state may be reached as this parameter is increased shown in Figure 5.11 (40MPa, 60MPa, and 80MPa).

When the shear strength is at a lower stress level, the shear stress reaches the maximum shear stress first and then causes the breakage of the parallel bond. Thus, it is the parallel shear strength that controls the stress-strain behavior of the sample. The peak strength increases with the increasing of the parallel shear strength. The parallel normal stress reaches the maximum value first, and then causes a breakage of the parallel bond. Instead, the parallel normal tensile strength controls the peak strength when the parallel shear strength is relative large.

By the increasing parallel shear strength, the stress-strain response must reach some convergence state when the parallel normal tensile strength is kept constant. The relative relationship between parallel tensile strength and shear strength reflects the failure mechanism in the parallel bond model by controlling the crack types as discussed in section 4.3.

5.2.10 Effect of Parallel Bond Shear Strength: Standard Deviation

The effect of the standard deviation ($\theta_9 = \tau_d$) of the parallel bond shear strength is shown in Figure 5.12. The initial slope of the curve has almost no changes, while the post peak behavior of the samples becomes more brittle when increasing the standard deviation. The post peak stress at a larger deviation is smaller because the shear bonds with lower stress are broken in this state.

The standard deviations of the parallel bond tensile and shear strengths control the tensile or shear crack initiation stress respectively. A large value of deviation causes a small value of strength that would be generated within the parallel bond. When the specimen is under loading, the initial crack usually occurs at the weakest plane, which has a relatively small value of tensile or shear strength.

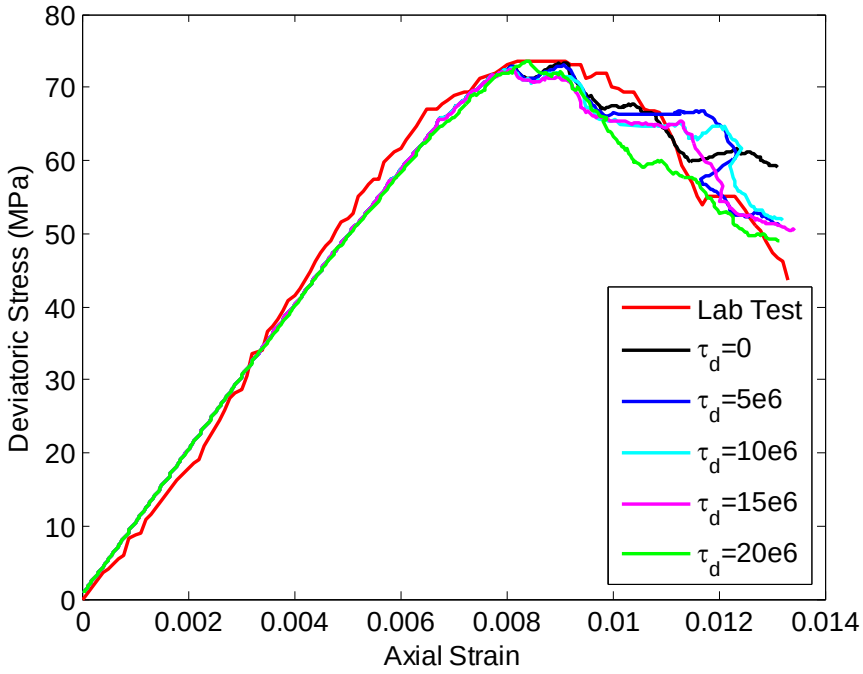

Figure 5.12 Effect of parallel bond standard deviation of shear strength

5.3 Summary

A simple sensitivity analysis is conducted to understand the cross-influence of the micro-parameters on the global mechanistic behavior of the DEM. This is achieved by

changing one micro-parameter at the time. From this exercise, it is possible to characterize the DEM's mechanical response including the initial linear response, the peak behavior, and the post peak behavior. The ranges of the micro-parameters are chosen so as to show a significant specimen's response.

From the figures presented above, it is observed that both particle-particle stiffness and parallel bond stiffness relate to the initial linear behavior of the stress-strain curve. The parallel bond stiffness also controls the peak strength behavior of the sample, which inherently affects the breakage of the parallel bonds. The friction coefficient present in the contact bond has little influence on the behavior of the sample, which implies that the behavior for the sandstone is most controlled by the parallel bond rather than by friction at the contact bond. From the influence of the remaining parameters, it is observed that the Young's modulus and the peak strength are not controlled by only a single parameter. The Young's modulus is related to both the particle normal shear stiffness and the parallel bond normal shear stiffness. The fluctuation of the peak strength seems to be related to all the nine parameters.

CHAPTER VI

PROBABILISTIC CALIBRATION

In this chapter, the Bayesian solution to the inverse problem is introduced first and serves as the fundamental theory of the probabilistic calibration. Then, the numerical integration of the Bayesian posterior is formulated based on Markov Chain Monte Carlo (MCMC) method. This makes the posterior convergent to the target joint probability density and the sampling to the stationary condition as the sample grows, and Metropolis-Hastings (M-H) algorithm, which is the decision rule that selects the sampling points. After introduction of the calibration procedures in detail, the influences of the selection parameter and the coefficient of variation are discussed to investigate the influences of the assumed parameters in the calibration theory.

6.1 Bayesian Solution to Inverse Problem

The Bayesian theorem is a useful method to directly formulate the complete solution to an inverse problem, which is expressed in the form of probability density functions and the covariance matrix among the model parameters. The prior and the likelihood are the two main information sources to makes inferences of the parameters through Bayesian approach. Our previous knowledge of the parameters is the sources of the prior, and the predictive model performance is measured by the likelihood. The priori and the likelihood are always expressed in the form of probability density functions, following statistical distributions as Gaussian distribution, Log-Nomral distribution and Chi

distribution. The integration combined the prior and the likelihood is called the posterior, which is the solution to the inverse problem expressed by a conditional joint probability function.

By capturing the random model behavior introduced by the parameters, the Bayesian paradigm naturally gives the solution to the inverse problem [23], which could be expressed as:

$$\pi(\boldsymbol{\theta}|\mathbf{d_{obs}}) = \frac{f(\mathbf{d_{obs}}|\boldsymbol{\theta})\pi(\boldsymbol{\theta})}{\int f(\mathbf{d_{obs}}|\boldsymbol{\theta})\pi(\boldsymbol{\theta})d\boldsymbol{\theta}} \tag{6.1}$$

where $\pi(\boldsymbol{\theta})$ is the prior; $f(\mathbf{d_{obs}}|\boldsymbol{\theta})$ is the likelihood; and $\pi(\boldsymbol{\theta}|\mathbf{d_{obs}})$ is the posterior. The main concept and application of each component of the Bayesian solution in this research are discussed below.

6.1.1 Prior

The prior $\boldsymbol{\pi(\theta)}$ represents our previous knowledge of the constitutive parameters $\boldsymbol{\theta}$ by defining the proper probability density function. The priori can take any form, but is often selected based on the properties of the parameters, such as a normal stiffness that must be positive. In this research, the vector of the micro-parameters is $\boldsymbol{\theta} = \{\theta_i\}$ with i=1 … 9 according to Table 5.2.

Two types of priori are commonly used in scientific research, the subjective prior and the objective prior [28]. Objective prior is commonly used to represent the parameters whose properties are little known. When we have enough evidence about the distribution of the parameters, the subjective prior can be implemented to reflect this distribution.

In this work, it is proposed to explore the representation of the prior information by using log-normal distribution for the normal modulus E_c and shear modulus E_{cs} and the other parameters as non-informative priori, which can be expressed as:

$$\pi(\boldsymbol{\theta}) \propto \frac{1}{E_c \cdot E_{cs} \cdot \mu \cdot \sigma_c \cdot \sigma_d \cdot \tau_c \cdot \tau_d} \exp\left(-\frac{1}{2}\left(\frac{\log E_c - (\mu_1)_{\log}}{(\sigma_1)_{\log}}\right)^2 * \left(\frac{\log E_{cs} - (\mu_2)_{\log}}{(\sigma_2)_{\log}}\right)^2\right) \quad (6.2)$$

where μ_i and σ_i can be evaluated at each data point by:

$$(\mu_i)_{\log} = \ln(E[X_i] - \frac{1}{2}\ln\left(1 + \frac{Var[X_i]}{E[X_i]^2}\right) \quad (6.3)$$

$$(\sigma_i)_{\log}{}^2 = \ln(1 + \frac{Var[X_i]}{E[X_i]^2}) \quad (6.4)$$

6.1.2 Likelihood

The likelihood $f(\mathbf{d_{obs}}|\boldsymbol{\theta})$ measures the quality of the predictive model performance according to the corresponding parameter $\boldsymbol{\theta}$. Theoretically, the likelihood can take any particular shape based on the difference between the experimental observations and the simulation predictions. However, to better evaluate the model performance, the model should have little error by following a simple and consistent response.

When the global error between the observation and the prediction follows the Gaussian distribution, the sample is called an unbiased sample. In order to calculate the likelihood, the observations at each data point from the experiment are assumed to be independent of each other, and the errors at each data point also follow an independent Gaussian distribution $N(d_{obs}, \sigma_{obs})$, where d_{obs} is the value of the data point, and σ_{obs} is the value of the standard deviation. This definition indicates an uncertainty band with a standard deviation σ_{obs} proportional to the deviatoric stress in the axial strain domain.

The standard deviation of each data point is taken as 30% of the experimental deviatoric stress for different levels of axial strain. This measure introduces a measure of uncertainty for the sampling of the likelihood in the calibration procedure. Further details on the assumptions for selecting this standard deviation measure for the likelihood is discussed in section 6.3.

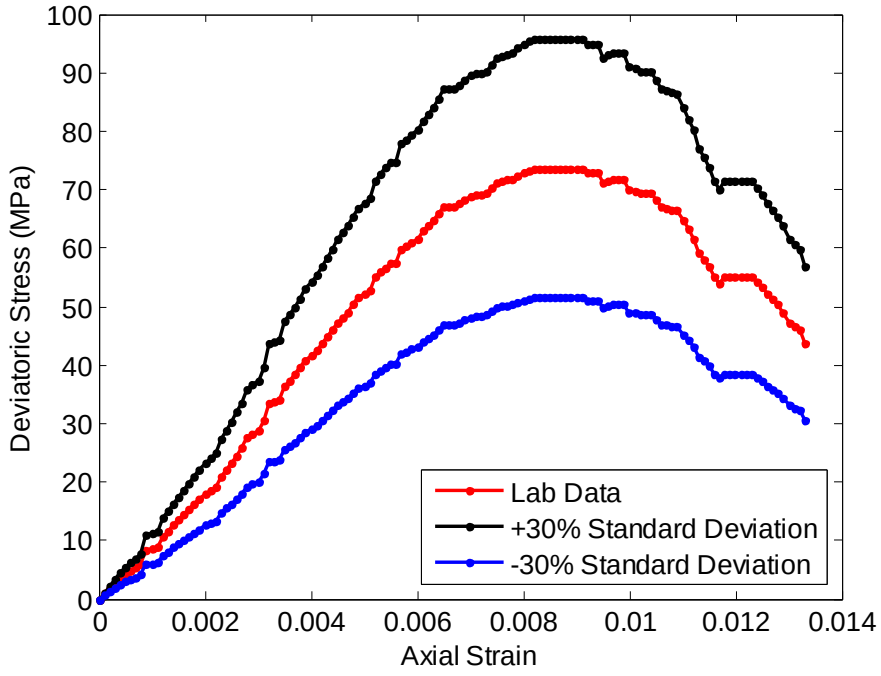

Figure 6.1 Uncertainty measures for observations

The likelihood $f(\mathbf{d_{obs}}|\boldsymbol{\theta})$ is defined as:

$$f(d_{obs}|\theta) = \prod N_i\left(d_{obs}, \sigma(\varepsilon_{a_i})\right) = \left(\mathbf{d_{obs}} - \mathbf{d_{prep}}\right)^T C(\mathbf{d_{obs}} - \mathbf{d_{prep}}) \qquad (6.5)$$

where C is the covariance matrix and only the diagonal elements are non-zero following the independent assumption of each data point.

In the sampling process of the calibration, the likelihood can be evaluated from each data point with respect to the axial strain domain as:

$$f(d_{obs}\,|\theta) \propto \sum_{i=2}^{n-1} \left(\frac{\mathbf{d_{obs}}(\varepsilon_{a_i}) - \mathbf{d_{prep}}(\varepsilon_{a_i})}{\sigma(\varepsilon_{a_i})}\right)^2 \tag{6.6}$$

6.1.3 Posterior

The posterior $\boldsymbol{\pi(\theta|d_{obs})}$ is the joint probability function conditioned on both the prior and the likelihood, which itself is the solution to the inverse problem. The posterior of a single parameter can be expressed as the probability density function indicating the distribution of the parameter. For this study, the posterior for multi-parameters is the joint probability density function between the proposed prior (Eq. 6.2) and Gaussian type likelihood.

6.2 Probabilistic Calibration Procedure

The posterior integration is calculated with respect to the parameter domain to estimate the statistical characteristics of each parameter. This integral is numerically solved by combining Markov Chain Monte Carlo and Metropolis-Hastings algorithms [29] to obtain a full description of the uncertainty corresponding to the model parameters based on the experimental data.

6.2.1 Markov Chain Monte Carlo

The Markov Chain Monte Carlo method is a numerical procedure for the sampling of the posterior. It is important to mention that a key property of the MCMC chain is that the sampling converges to the target joint density of $\boldsymbol{\theta}$ as the sample number grows.

The Metropolis-Hastings is a generalized form of the Metropolis & Gibbs Method, which serves as the decision rule that determines the rejection or acceptance of the candidate point. The M-H criterion is measured by a decision parameter α, which is derived from the model behavior between current and previous simulation steps.

The probabilistic calibration algorithm to solve the solution to the inverse problem is based on the specimen response of the experimental observation and the predictions obtained from the discrete particle model. The MCMC and M-H sampling techniques form the basis for the development of this calibration procedure. The objective of the proposed algorithm is to sample a set of micro-parameters $\boldsymbol{\theta}$ based on a proposed distribution $q(\cdot\,|\widehat{\boldsymbol{\theta}}_{\boldsymbol{s}})$ at each step of the MCMC chain, and to estimate the likelihood and posterior by evaluating their statistics.

The candidate point **Y** is based on the previous set of parameters $\widehat{\boldsymbol{\theta}}_{\boldsymbol{s}}$ by using the previous mean value and the constant standard deviation assumed at the begining at the calibration.The candidate point **Y** is rejected or accepted by the selection parameter evaluated by probability between the current point and the previous, which can be evaluated as following:

$$\alpha\left(\hat{\theta}_s, d_{obs}\right) = \min\left\{1, \frac{\pi_{Proposed}}{\pi_{Previous}}\right\} = \min\left\{1, \frac{\pi(Y|d_{obs})q(\hat{\theta}_s|Y)}{\pi(\hat{\theta}_s|d_{obs})q(Y|\hat{\theta}_s)}\right\} \qquad (6.7)$$

For Gaussian likelihood, the posterior could be evaluated by

$$\frac{\pi_{\text{Proposed}}}{\pi_{\text{Previous}}} = \frac{\pi(Y|d_{obs})}{\pi(\hat{\theta}_s|d_{obs})} \exp\left(-\frac{1}{2}(f(Y|\hat{\theta}_s) - f(\hat{\theta}_s|Y))\right) \quad (6.8)$$

This calculation procedure is repeated until the MCMC sampling reaches the stationary condition. A reasonable probability measure can be obtained in the stationary phase as the random model predictions close to the actural experimental observations. The threshold of the stationary state is defined as the burn-in point [24], which can be viewed as a small range of the calibration chain. The mean value of the sampling points would be convergent in the stationary condition.

6.2.2 Calibration Procedure

The flowchart for the calibration procedure is shown in Figure 6.2. The details of the proposed algorithms programmed combining both MATLAB (MCMC) [22] and PFC^{3D} (DEM) are described as following:

i) Initialize the chain with $\hat{\theta}_0 = \theta_{BESTFIT}$ at s = 0, where $\theta_{BESTFIT}$ is the parameters obtained in Chapter V as the 'final sample' and s counts for iteration. The reason for choosing $\theta_{BESTFIT}$ to initiate the chain is to expedite the simulation convergence.

   a. Load the interpolated data from the lab test

   b. Load the initial guess parameters $\hat{\theta}_0 = \theta_{BESTFIT}$ as the mean value μ_i of each parameter and make the mean vector $\boldsymbol{\mu}$.

   c. Transform the normal stiffness E_c and the shear stiffness E_{cs} into log-normal distribution by Eq. (6.3) and Eq. (6.4.)

d. Load the uncertainty measures for observations

e. Load assumed coefficient of variation (See 6.4) and compute the standard deviation of the parameters to make the covariance matrix

ii) Generate a random candidate point Y from $q(\cdot\,|\hat{\theta}_s)$, which follows multi variant distribution.

a. If the products of the parameters are negative and the ratio $E_c/E_{cs} < 1$, the proposed point Y would be abandoned

b. Define the current step of the chain $\boldsymbol{\mu}$

c. Run the physical model at step 'i' in the chain to get the proposed behavior of the model

d. Evaluate the posterior components for the candidate point on the chain $\pi(Y|d_{obs})$ by Eq. (6.2) and $q(\hat{\theta}_s|Y)$ by Eq. (6.6)

e. Evaluate the posterior components for the current point on the chain $\pi(\hat{\theta}_s|d_{obs})$ by Eq. (6.2) and $q(Y|\hat{\theta}_s)$ by Eq. (6.6)

f. Evaluate the ratio $\frac{\pi_{Proposed}}{\pi_{Previous}}$

g. Evaluate $\alpha(\hat{\theta}_s, d_{obs})$ by Eq. (6.7)

iii) Generate U from a uniform (0,1) distribution

iv) If $U \leq \alpha(\hat{\theta}_s, Y)$, the candidate point is accepted, then set $\hat{\theta}_{s+1} = Y$; if not, Y is rejected by setting $\hat{\theta}_{s+1} = \hat{\theta}_s$. This step implies that the forward should be solved by comparing the previous the selection point $\hat{\theta}_s$ and the current sampling point Y

v) Set s=s+1 and repeat steps 2 through 8.

The previous procedure introduces the hierarchy of the MCMC and M-H sampling used in the probabilistic calibration process. Once the stationary state is reached, it is possible to generate the statistical inferences about the posterior after the burn-in point.

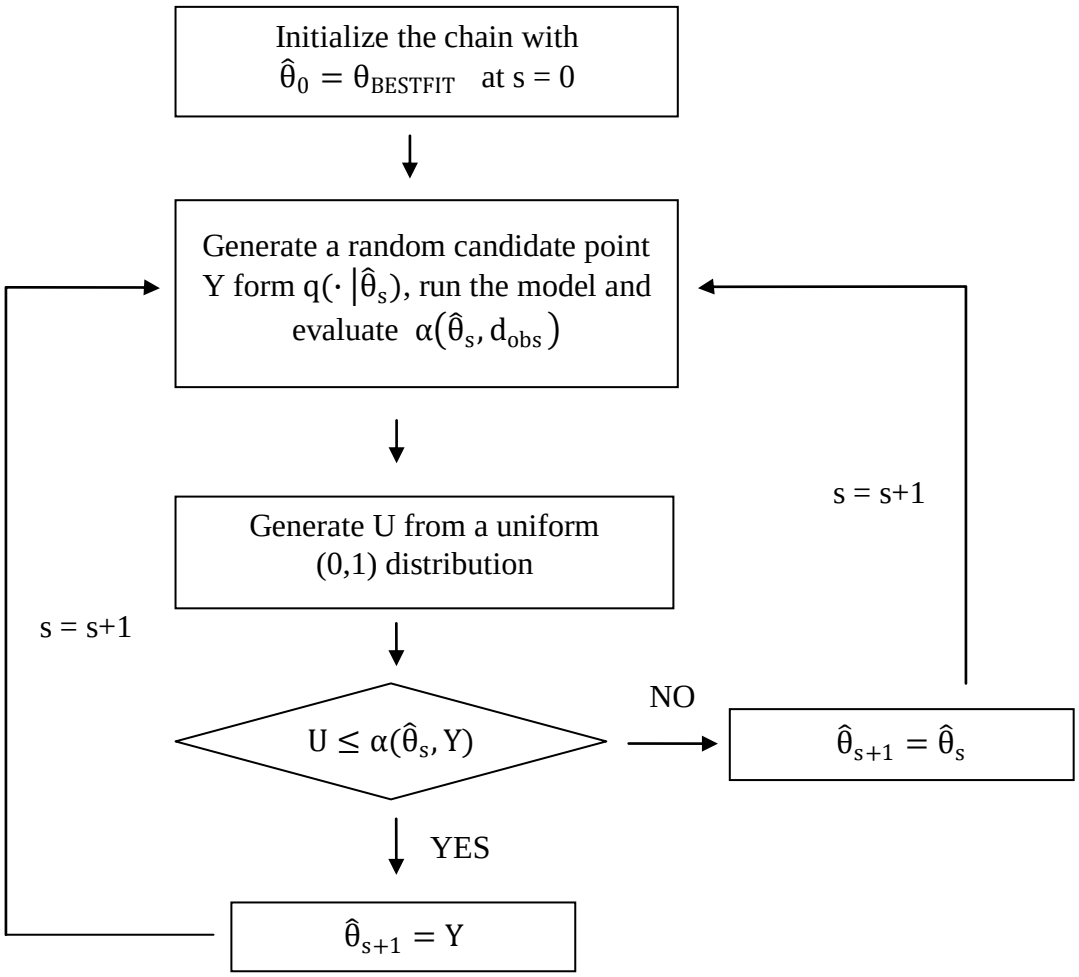

Figure 6.2 Flowchart of the inverse problem for probabilistic calibration

6.3 Influence of Standard Deviation on Selection Parameter

The selection parameter $\alpha(\hat{\theta}_s, d_{obs})$ is used to evaluate the ratio of the possibility between the candidate point and the current point, and then to select the sampling point during the calibration process. This selection parameter is affected significantly by the introduced uncertainty (standard deviation) when sampling the likelihood. The value of the uncertainty not only affects the value of $\alpha(\hat{\theta}_s, d_{obs})$, but also determines the shape of the histogram, which could be evaluated for searching stage or converging stage.

The $\alpha(\hat{\theta}_s, d_{obs})$ can be evaluated by Eq. (6.8), where the likelihood $f(\hat{\theta}_s|Y)$ and $f(Y|\hat{\theta}_s)$ could be estimated by Eq. (6.6). The $\alpha(\hat{\theta}_s, d_{obs})$ is the combination of two ratios: the prior ratio and the likelihood ratio. The prior ratio between the candidate point and the current selection point is almost equal to 1 for each sampling, which means the prior calculated by Eq. (6.2) has little change.

Therefore, the $\alpha(\hat{\theta}_s, d_{obs})$ is directly determined by the likelihood ratio, which is governed by the value of standard deviation introduced at the beginning of the simulation for sampling the likelihood. The absolute value of likelihood evaluated by Eq. (6.6) depends on the value of standard deviation $\sigma(\varepsilon_{a_i})$, which itself is the introduced uncertainty.

The calibration chain is carried out 100 times for standard deviation 10%, 30% and 50% (Figure 6.3, 6.4 and 6.5 respectively) to investigate its influence on $\alpha(\hat{\theta}_s, d_{obs})$ on the selection of the sampling points during probabilistic calibration. The $\alpha(\hat{\theta}_s, d_{obs})$ measures how close the candidate point is to the previous selection point. When the

$\alpha(\hat{\theta}_s, d_{obs})$ is close to 1, the candidate point will be selected, while the $\alpha(\hat{\theta}_s, d_{obs})$ close to 0, the candidate point will be abandoned. The histogram $\alpha(\hat{\theta}_s, d_{obs})$, which directly shows the distribution of all the $\alpha(\hat{\theta}_s, d_{obs})$, is the symbol of the convergent phase of the calibration. The standard deviation is chosen based on its influence on the $\alpha(\hat{\theta}_s, d_{obs})$ at the beginning steps of simulation.

In Figure 6.3, 6.4 and 6.5, the three cases start at the same conditions ('final sample' in Chapter V), only differing in the value of the introduced standard deviation. In Figure 6.3, the shape of the histogram for 10% standard deviation shows the 'stationary state', and almost all the candidate points are rejected, which means the previous point is the best fit to the lab data in the calibration process. The **U** shape of the histogram for 30% standard deviation shown in Figure 6.4 provides a relatively reasonable description of the sampling process since there is more flexibility to explore the parameter space. In Figure 6.5, the histogram for 50% standard deviation shows most sampling points are selected, since the large standard deviation reduces the probability difference between the candidate and the current point, and most of the proposed combinations of parameters are accepted.

A standard deviation of 30% is used in sampling the likelihood in the following research work.

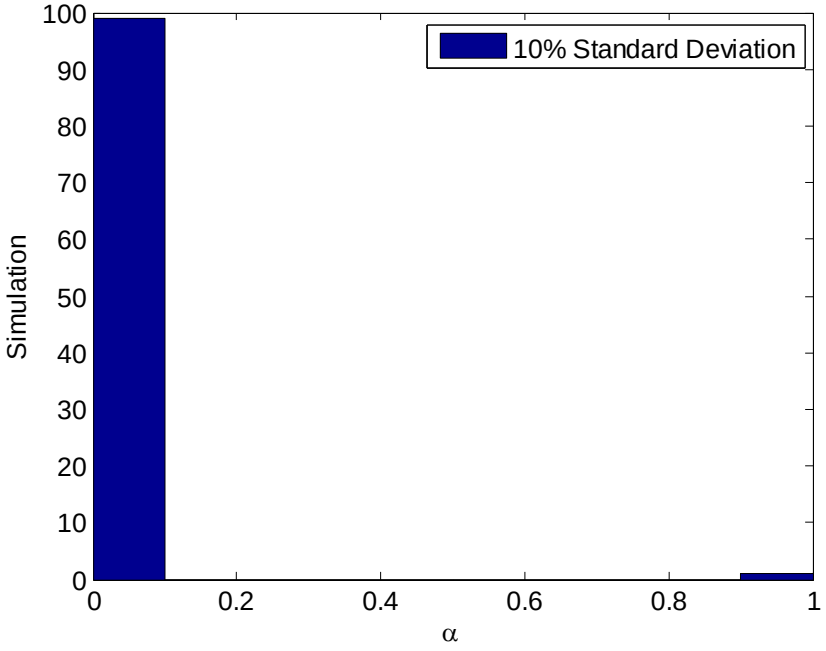

Figure 6.3 Histogram of $\alpha(\hat{\theta}_s, \mathbf{d_{obs}})$ for 10% uncertainty

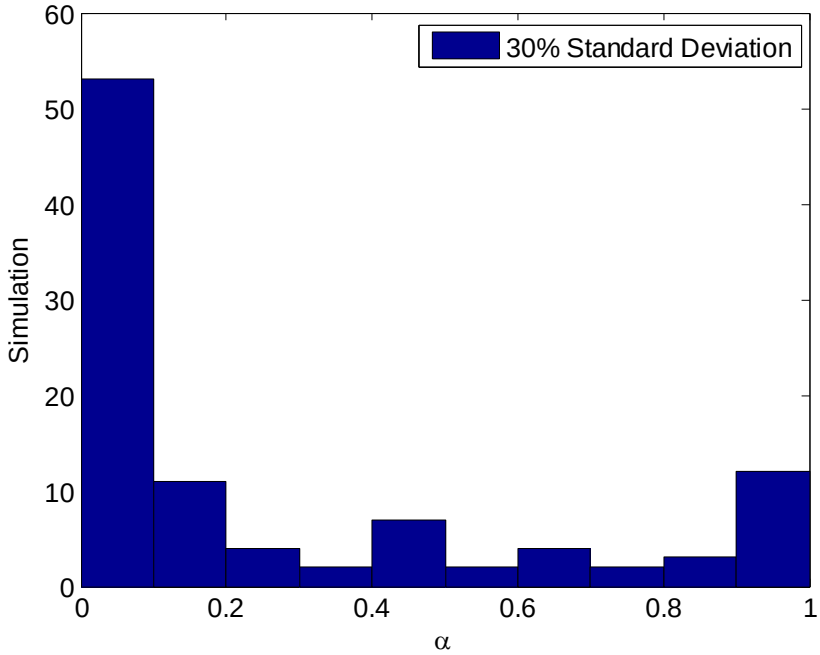

Figure 6.4 Histogram of $\alpha(\hat{\theta}_s, \mathbf{d_{obs}})$ for 30% uncertainty

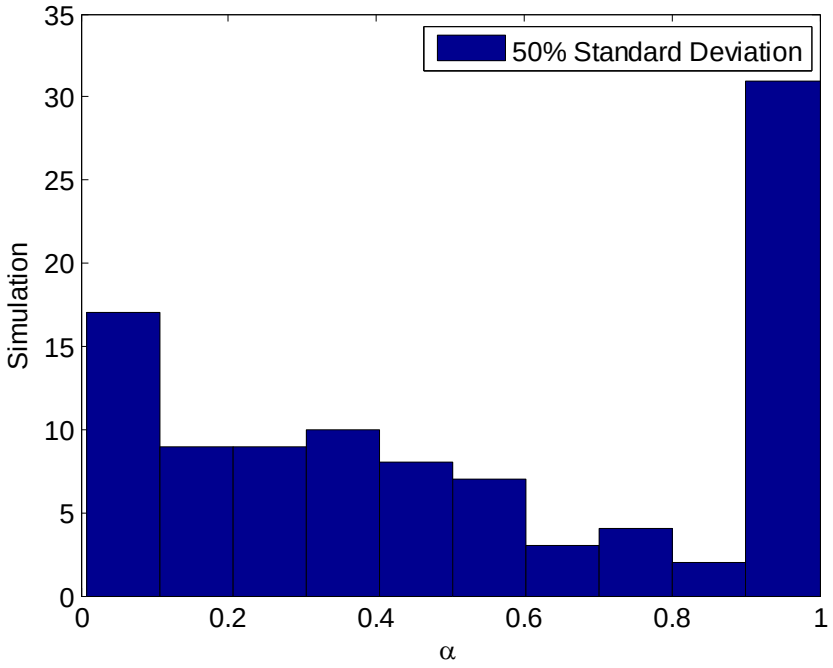

Figure 6.5 Histogram of $\alpha(\hat{\theta}_s, d_{obs})$ for 50% uncertainty

6.4 Influence of Coefficient of Variation on Convergence

The coefficient of variation (CV) is a normalized measure of the probability distribution of the parameter. The coefficient of variation for each parameter is assumed at the beginning of the calibration process to evaluate the standard deviation of the proposed distributions in a uniform way across all possible magnitudes of the micro-parameters. Since the search of the candidate point is assumed to be non-correlated between the micro-parameters. It is then used to build the diagonal of the proposal distribution covariance matrix. At each point of the calibration chain, the candidate point Y is generated by using multi-variate normal distribution function (**mvnrnd**) in MATLAB. The covariance matrix is not changed during the sampling

process, but the mean value for each step is updated as the previous selection point is updated. Herein, the key role of the coefficient of variation is to control the convergent rate of the calibration process

The influences of the coefficient of variation on the selection process for the three main micro-parameters normal stiffness, parallel normal strength and parallel shear strength are shown in Figure 6.6 to Figure 6.14 with CV equal to 0.001, 0.01and 0.05 respectively. To guarantee the consistency and comparability, all the cases start from the same initial state. Because the sampling change is relatively small, the pictures are drawn to scale to compare the influence of CV.

The comparisons for CV as 0.001, 0.05 and 0.01 show the same effect on the prescribed parameters. From these figures, it is observed that the larger CV results in a higher sampling rate.

Another way to exemplify the effect of the CV on the MCMC sampling search is illustrated by changing it from 0.001 to 0.05 after a series of over 8000 simulations. The selection behavior of the normal stiffness, the parallel normal strength and the parallel shear strength are shown in Figure 6.15, 6.16 and 6.17 respectively. Compared with smaller CV of 0.001, the sampling range of the parameters for CV as 0.05 is much larger and the influences of changes are better illustrated.

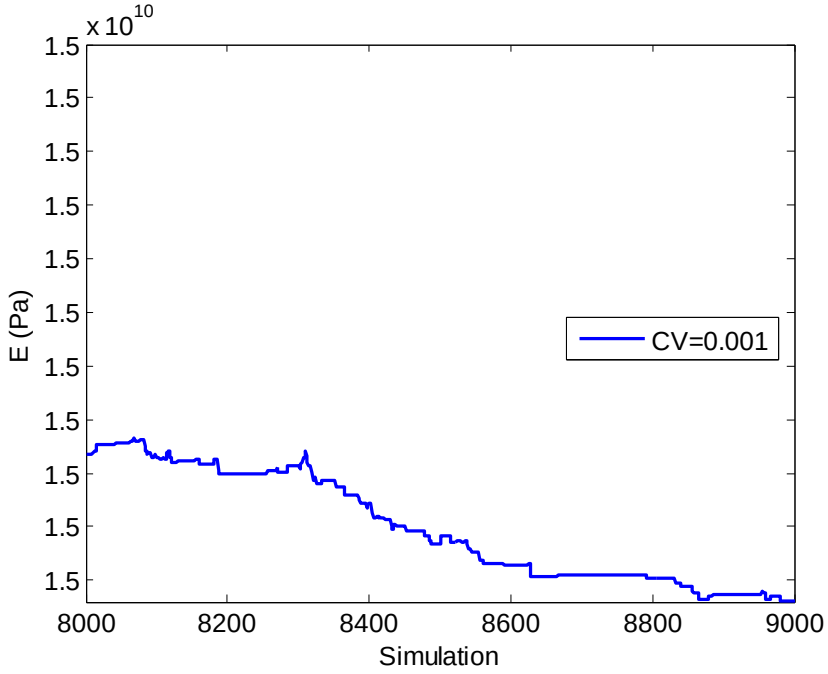

Figure 6.6 Selection process of normal stiffness at CV=0.001

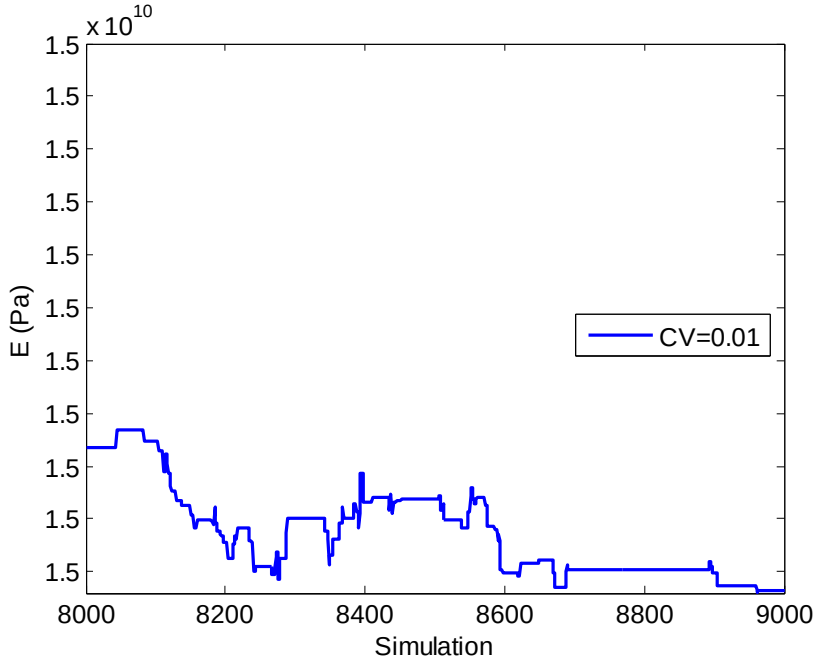

Figure 6.7 Selection process of normal stiffness at CV=0.01

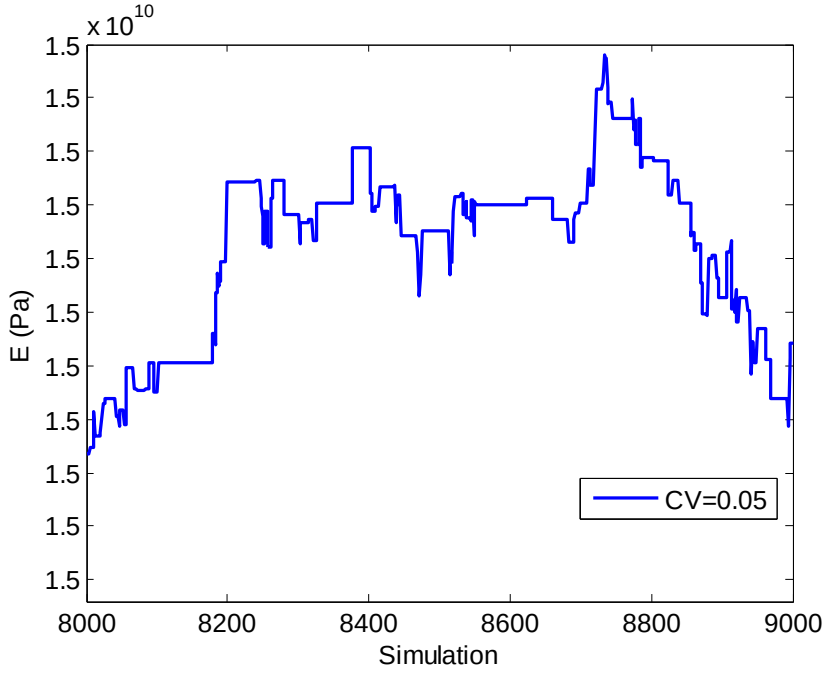

Figure 6.8 Selection process of normal stiffness at CV=0.05

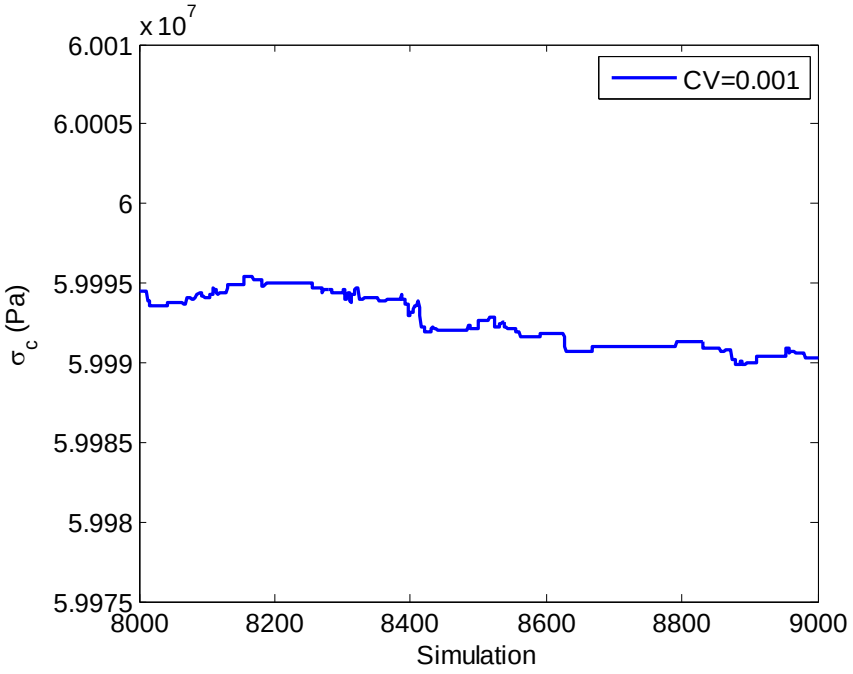

Figure 6.9 Selection process of parallel normal strength at CV=0.001

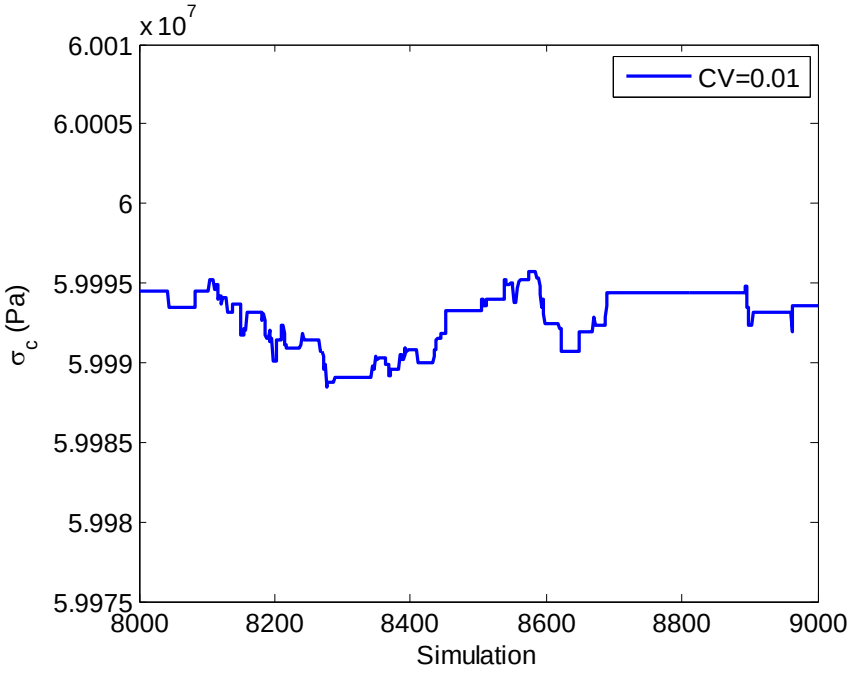

Figure 6.10 Selection process of parallel normal strength at CV=0.01

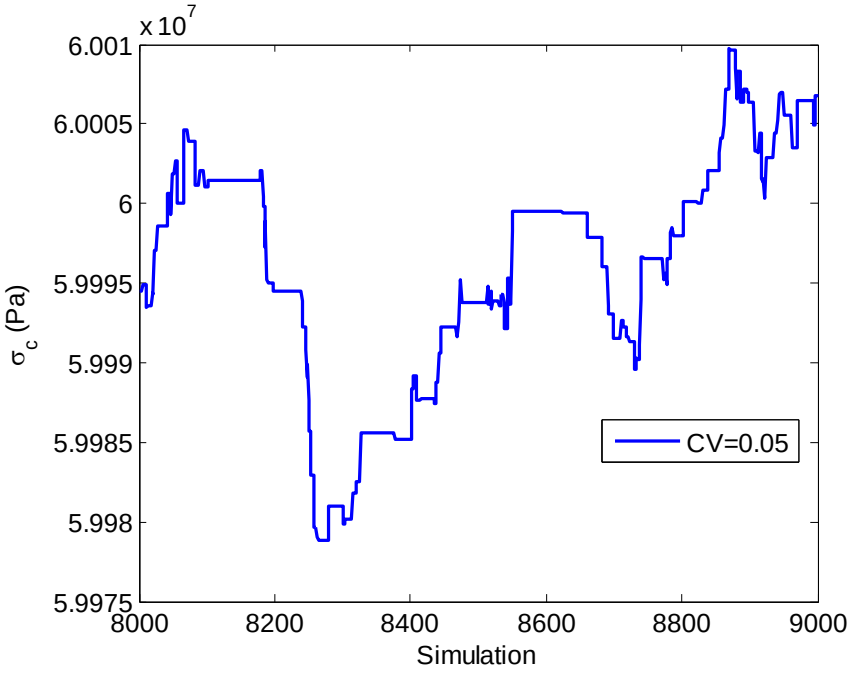

Figure 6.11 Selection process of parallel normal strength at CV=0.05

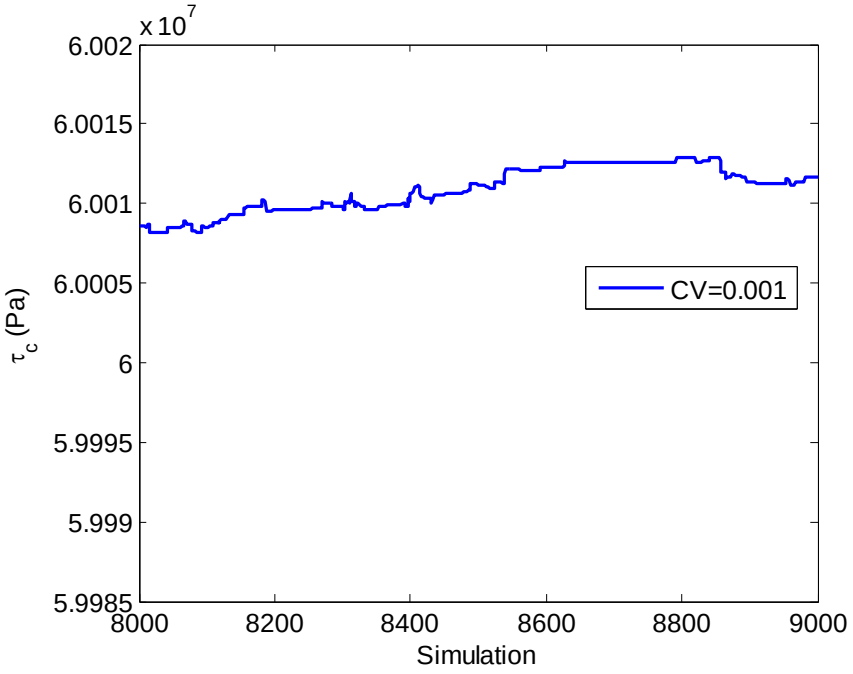

Figure 6.12 Selection process of parallel shear strength at CV=0.001

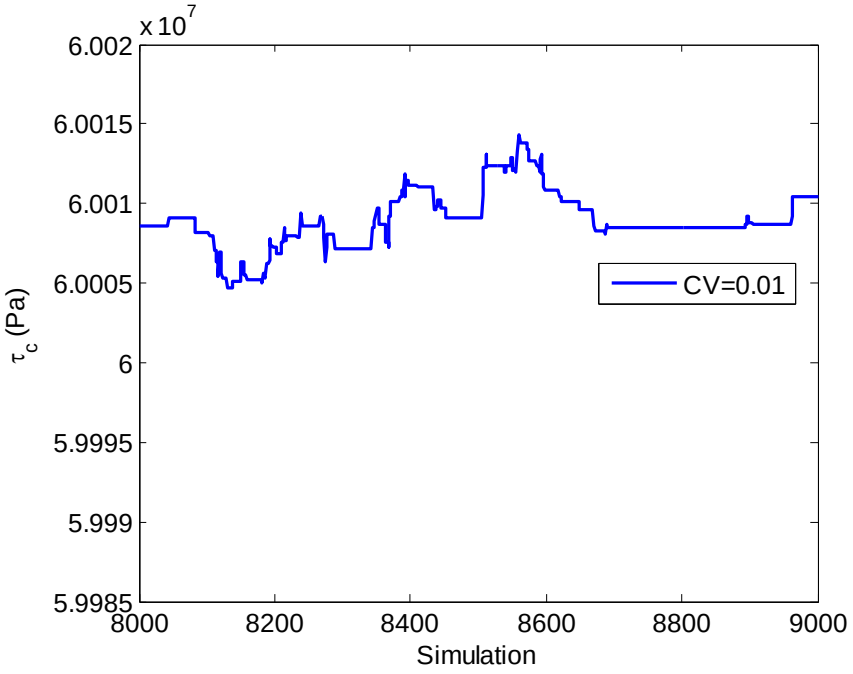

Figure 6.13 Selection process of parallel shear strength at CV=0.01

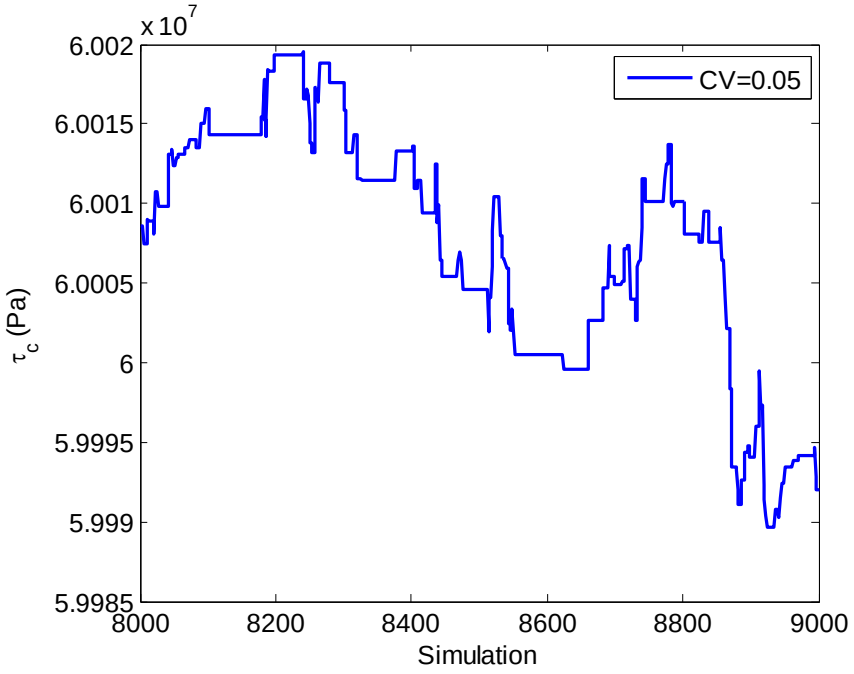

Figure 6.14 Selection process of parallel shear strength at CV=0.05

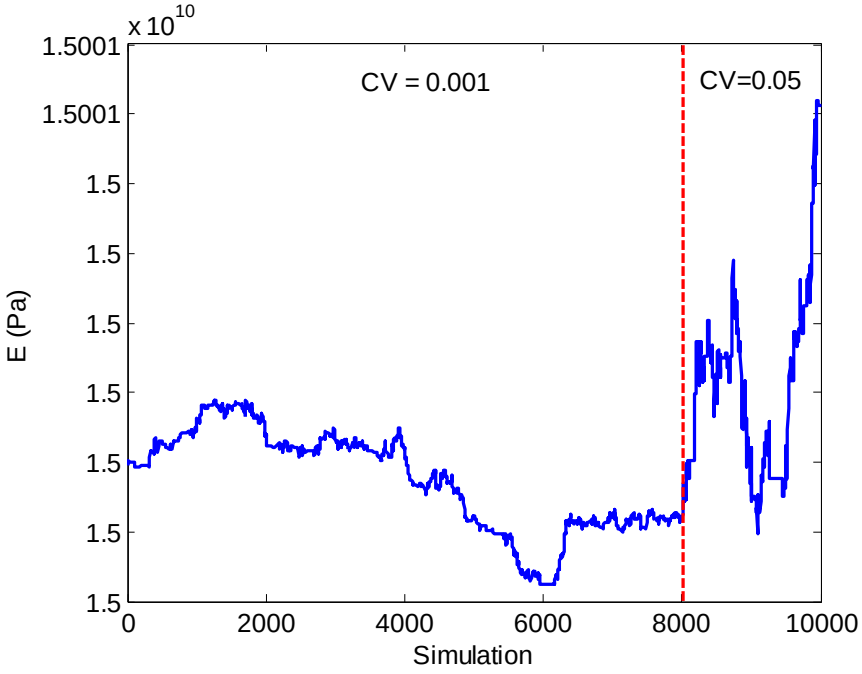

Figure 6.15 Selected normal stiffness due to CV change

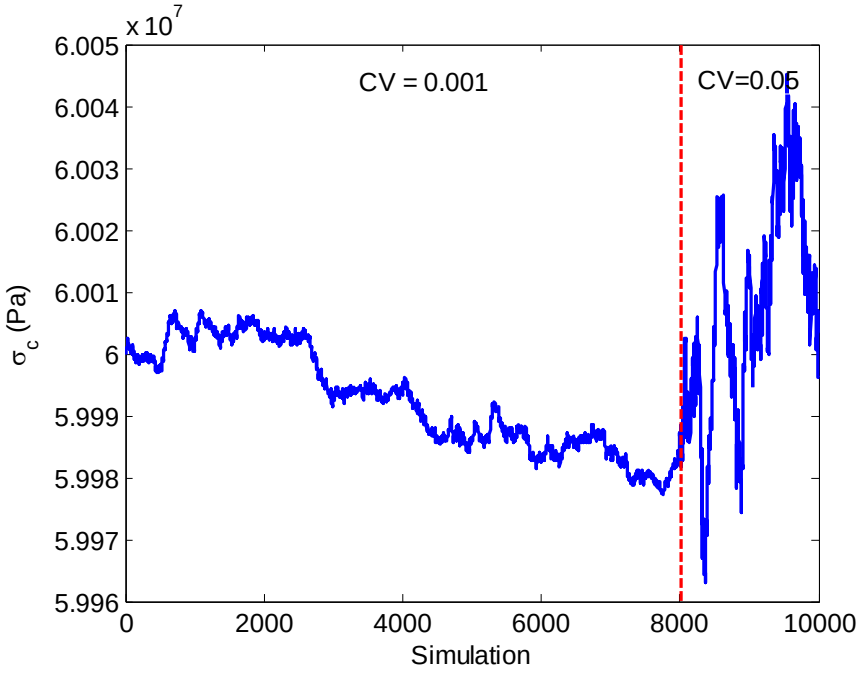

Figure 6.16 Selected parallel normal strength due to CV change

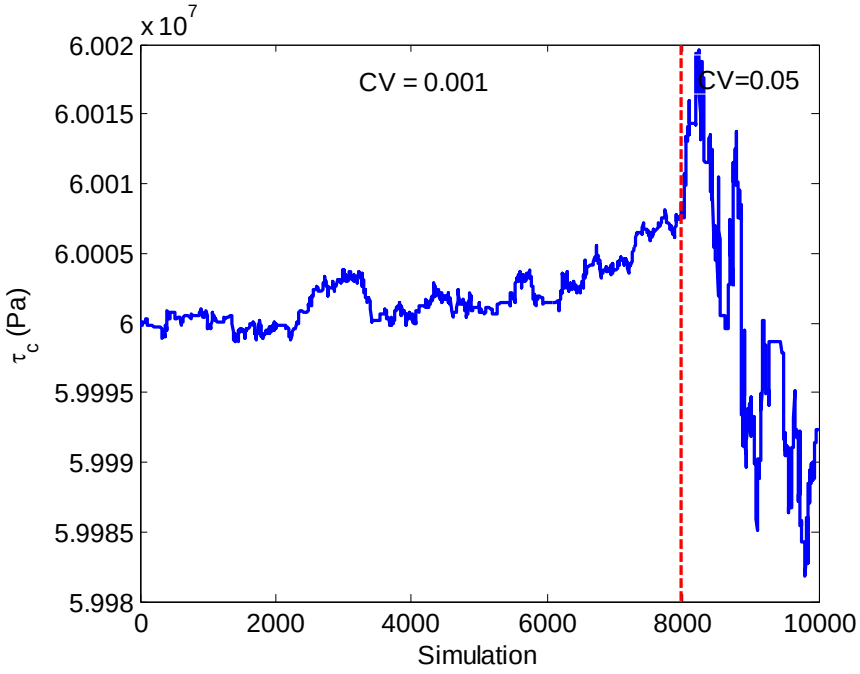

Figure 6.17 Selected parallel shear strength due to CV change

CHAPTER VII

CASE STUDY

This chapter illustrates the applicability of the probabilistic calibration approach to DEM model for the references Vosges sandstone rock specimen. The proposed discrete particle model was introduced in Chapter II. The description of the experiment was discussed in Chapter III. A simple analysis on the DEM failure mechanism was presented in Chapter IV. Also, a simple parametric analysis of the micro-parameters was discussed in Chapter V. The corresponding statistical inferences required for the Bayesian formulation were presented in Chapter VI. It is important to note that although the case study is limited to triaxial test simulation, the calibration method can be implemented for more complex discrete particle models. The following introduces two case studies: one-parameter case and three-parameters case.

7.1 One-Parameter Case

This case study introduces the application of probabilistic calibration for only one parameter based on the experiment data of stress strain behavior for Vosges sandstone with 10MPa confining pressure. As listed in Table 7.1, only the strength parameters are calibrated. The strength parameter is the combination of the parallel normal and shear strengths, which are set to be equal and acting as one parameter during calibration. The elements for the formulation of the posterior as defined by Eq. (6.1) are the same as those discussed in Chapter VI. They consist of a non-informative prior and

Gaussian-type likelihood. The integration of the posterior is performed via MCMC and the M-H algorithms. The coefficient of variation is set be 0.001 initially and then altered to 0.05 for faster convergent speed. The introduced uncertainty (standard deviation) for sampling the likelihood is chosen to be 30%.

Table 7.1 Starting point for one-parameter case

	Micro-parameter	**Symbol**	**Unit**
Calibrated	Paralle bond strength	$\sigma_{c0} = \tau_{c0}$	60 MPa

In Figure 7.1, the calibration process of the strength parameter shows the convergece of the calibration chain. The coefficient of variation changes from 0.001 to 0.05 after 8000 simulations. This change makes the MCMC chain converge more rapidly to the stationary phase. The calibration begins to converge after 17500 simulations. Another 10000 rounds of simulation (Figure 7.2) presents the MCMC stationary phase (Figure 7.5) of the strength parameter, which is the basis of the following discussion. The mean strength (Figure 7.3) better demonstrates the convergence of the calibration chain. The stress strain curve of the stationary phase (Figure 7.6) indicates a large fluctuation in the posk-peak behavior. In Figure 7.7 and 7.8, the mean and the standard deviation of the stress for each data point are plotted with respect to axial strain domain. Compared with the starting point, the MCMC state mean has better captured the stress strain response of the specimen (Figure 7.9). The statistical inferences can be obtained in

the MCMC stationary phase. The relative frequency histogram of the strength is presented in Figure 7.10. The cumulative density function of the strength plotted versus Gaussian distribution is shown in Figure 7.11.

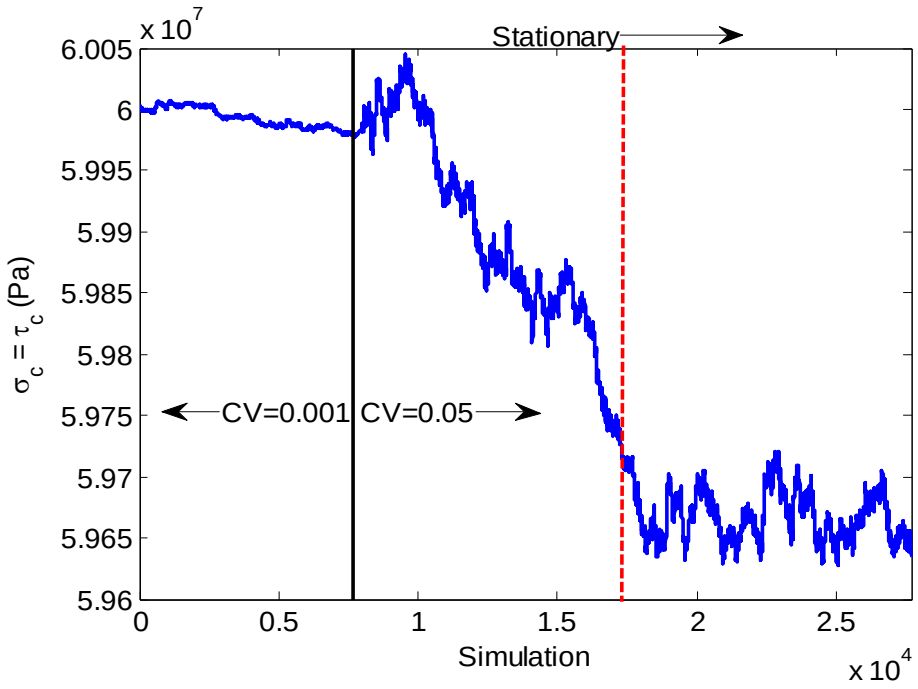

Figure 7.1 Calibration chain of strength

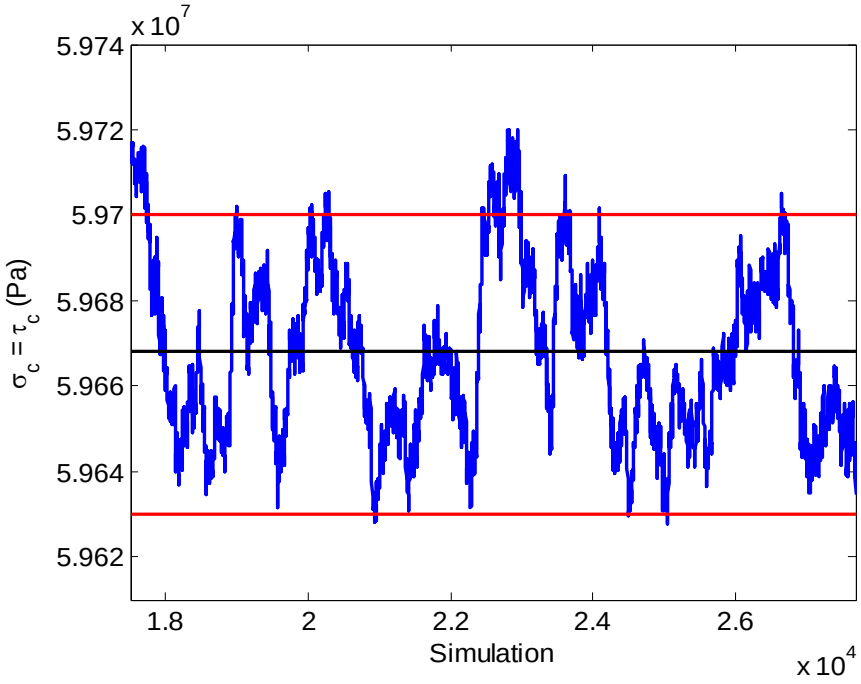

Figure 7.2 MCMC stationary state of strength

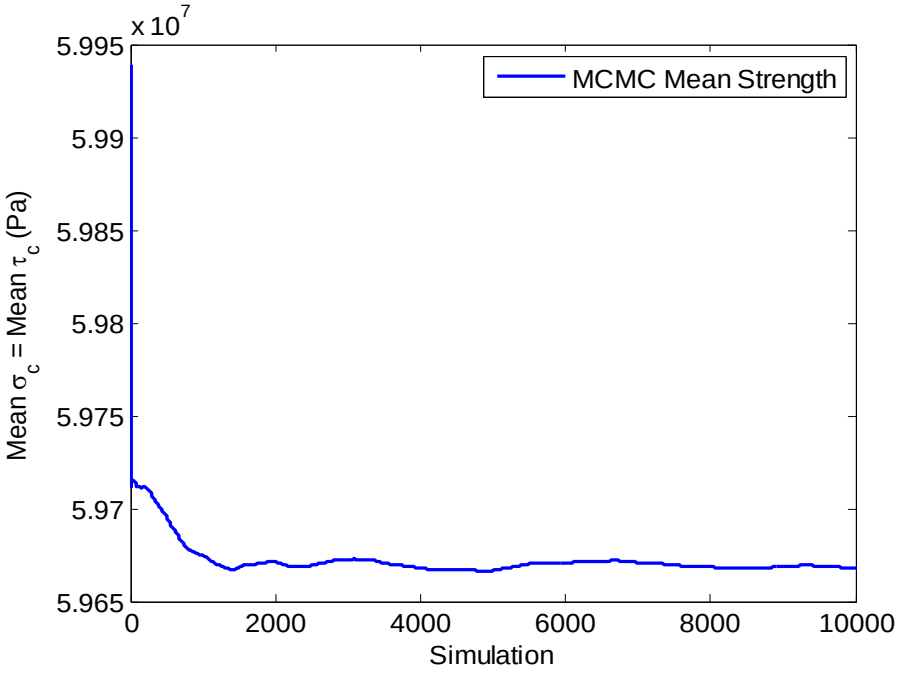

Figure 7.3 Mean strength evolution in MCMC state

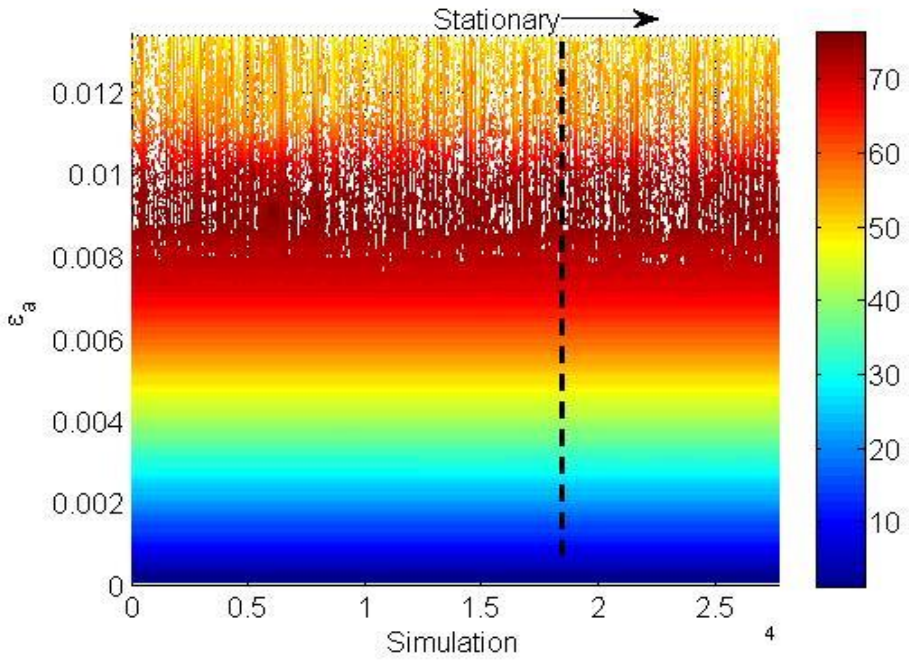

Figure 7.4 Stress strain curves over a series of simulations

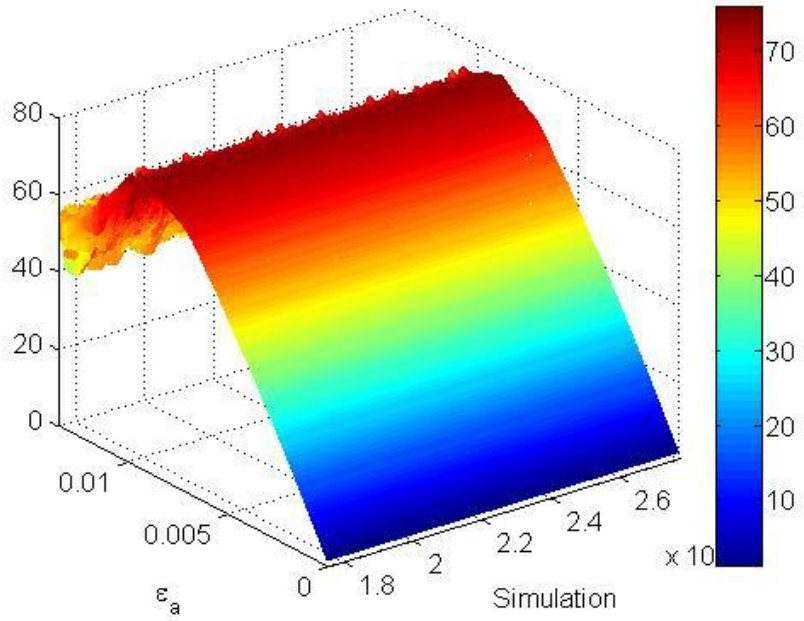

Figure 7.5 3D stress strain curves in MCMC stationary state

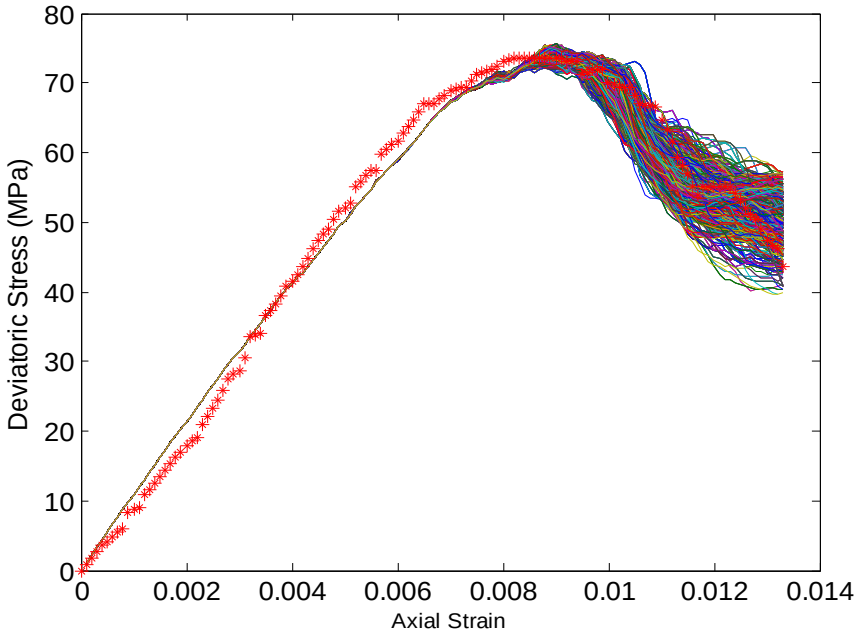

Figure 7.6 Stress strain curves in MCMC stationary state

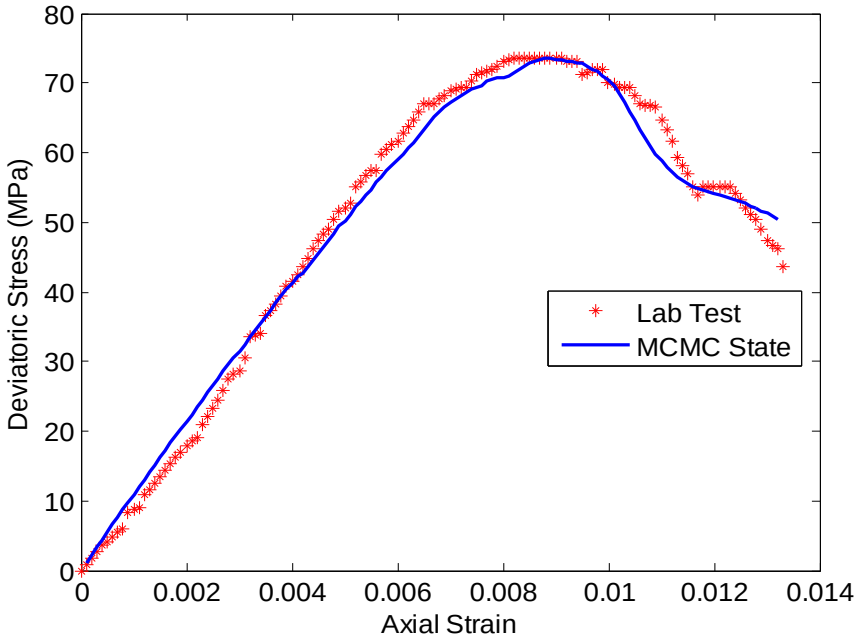

Figure 7.7 MCMC stationary analysis of mean stress strain curve

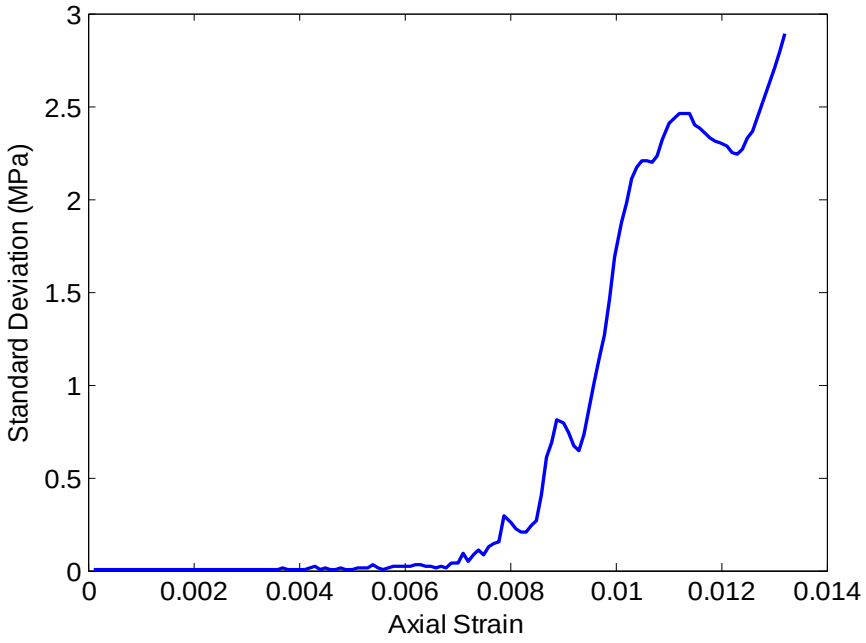

Figure 7.8 MCMC stationary analysis of standard deviation

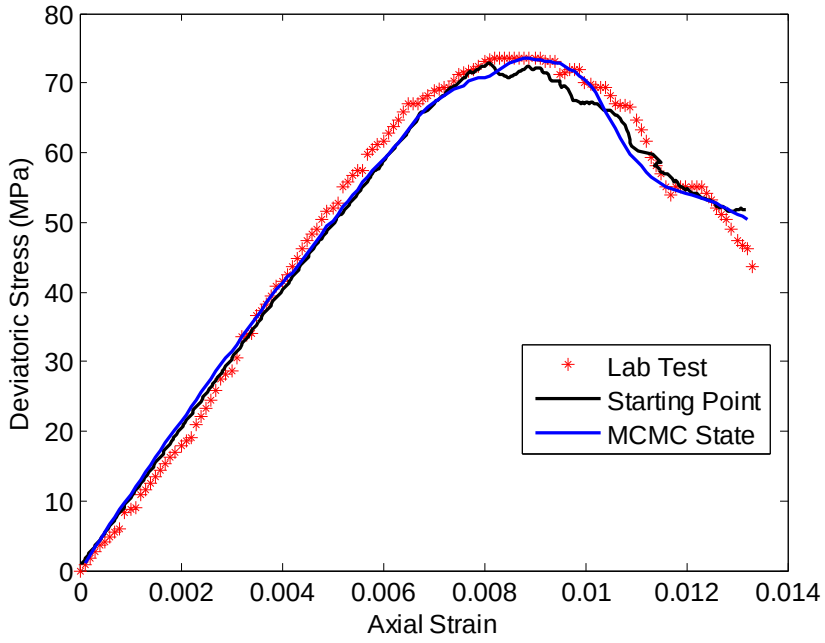

Figure 7.9 Comparison between starting point and MCMC state

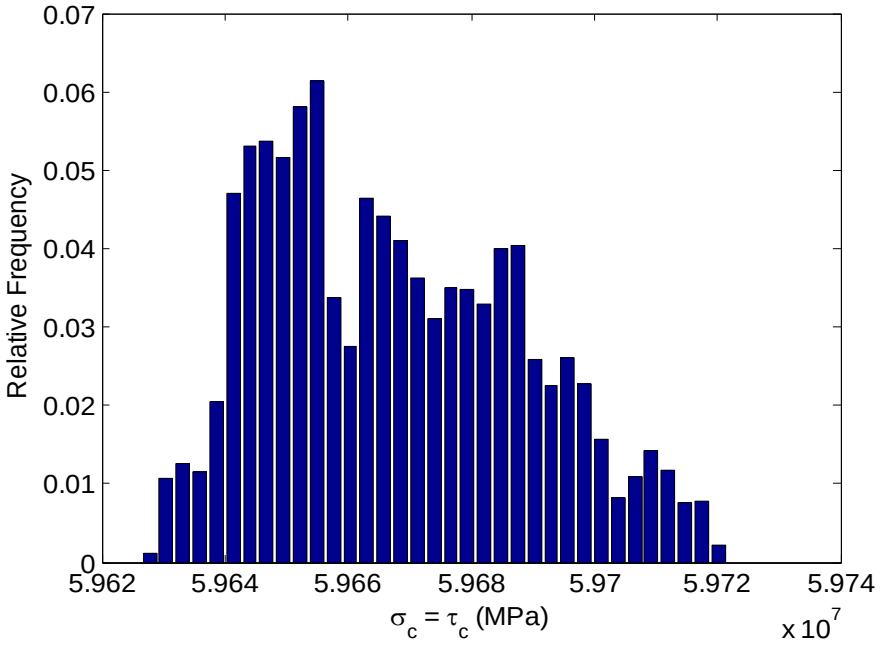

Figure 7.10 Relative frequency histogram of strength

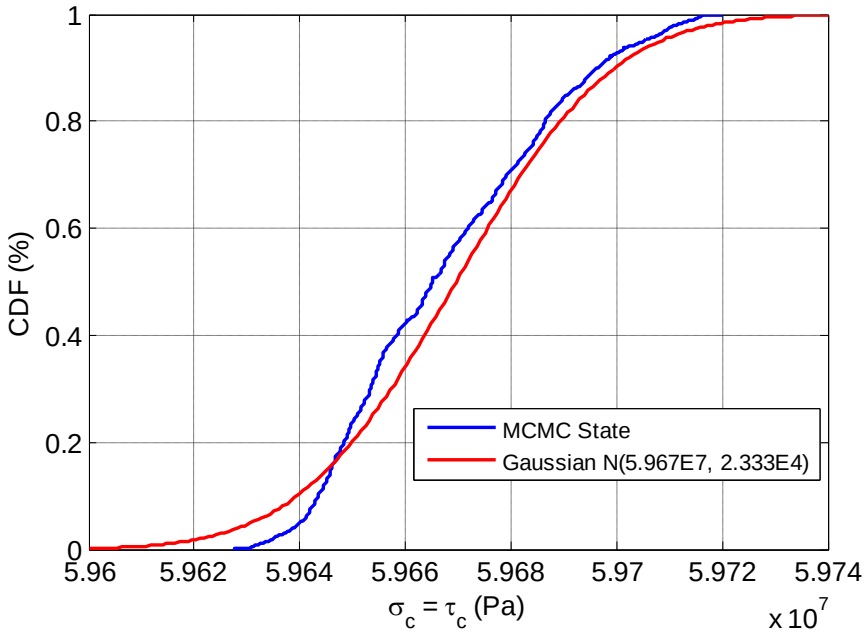

Figure 7.11 Cumulative density function of strength

7.2 Three-Parameters Case

In this case (Table 7.2), the contact normal Young's modulus is set to be equal to the parallel bond normal Young's modulus, together reflecting the Young's modulus of the materials. The parallel bond normal strength and shear strength are the other two parameters included in the calibration. All other remaining micro-parameters are kept constant.

Table 7.2 Starting point for three-parameters case

	Micro-parameter	**Symbol**	**Unit**
Calibrated	Young's modulus	$\theta_1 = \theta_4 = E_0$	15 GPa
	Average bond tensile strength	$\theta_6 = \sigma_{c0}$	60 MPa
	Average bond shear strength	$\theta_8 = \tau_{c0}$	60 MPa

After the stationary condition is researched on the MCMC parameters sampling, the burn in point can be determined, and from this statistical inferences on the parameters and the model response can be formulated. However, at the moment of completing this work, only first order statistics of the model response are discussed since there is no rational prove of convergence of the three parameters.

A sequence of the stress strain curve of deviatoric stress over axial strain is shown in Figure 7.12 indicating the model response achieved on the MCMC sampling so far. The same curve in 3D is presented in Figure 7.13. The elastic behavior of the sample

(represented by the initial slope) has almost no changes in the stationary phase and the peak stress changes little, while the post peak behavior has a relatively large fluctuation.

The mean and standard deviation of the selection sampling points in MCMC state plotted with respect to the axial strain for each data point are shown in Figure 7.14 and 7.15. The mean indicates good agreement with the experimental data, and the standard deviation reflects the variability on the model predictions, which shows a larger variation compared to results obtained for the one-parameter case (Figure 7.8). Further results on the variability and cross-correlation of the micro-parameters will be retrieved as full convergence on the MCMC sampling is achieved. Compared with the starting point, the MCMC state mean has better captured the stress strain response of the specimen (Figure 7.16).

The parallel normal strength, shear strength and normal stiffness sampling analysis obtained so far are plotted in Figures 7.17, 7.18 and 7.19 respectively. The different trends of the curves show the sensitivity of the parameters. The parallel normal strength is convergent in the MCMC stationary condition. The normal stiffness is convergent with small decreasing trend. The shear stiffness still has the decreasing trend. For each trend, it is important to note that the fluctuation is still within 0.1% of the mean value. The relative frequency histogram of the selecting parameter $\alpha(\hat{\theta}_s, d_{obs})$ in the MCMC stationary phase is shown in Figure 7.20. A full 60% of the sampling parameters are within the interval [0, 0.1], and only 10% of the sampling parameters are with the range [0.9, 1.0]. This is a positive indicator of convergence. However, this is not conclusive since the sampling evolution of the three parameters has not been achieved yet.

Preliminary results on the variation of the parameters are presented in Figures 7.21 – 7.23. Figure 7.21 shows the relative frequency histogram of the normal stiffness with a range of [1.4999E10, 1.5001E10] MPa, which shows a 'bell' type curve indicating a normal distribution of the parameter in the stationary condition. Figure 7.22 shows the relative frequency histogram of the parallel normal stiffness with a range of [5.995E7, 6.001E7] MPa. Figure 23 shows a relative frequency histogram for the shear stiffness with a range of [5.995E7, 6.001E7] MPa.

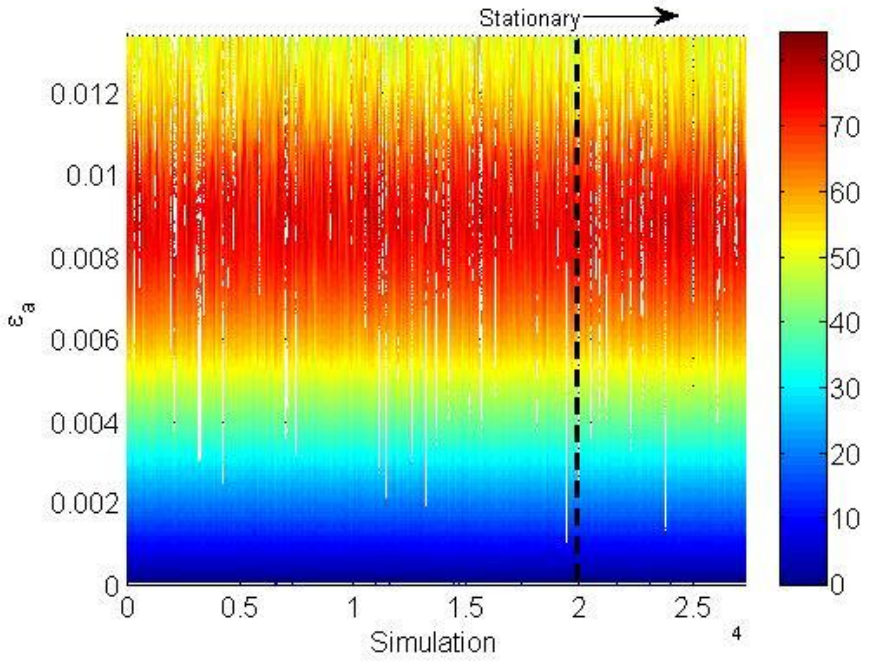

Figure 7.12 Stress strain curves for three-parameters case

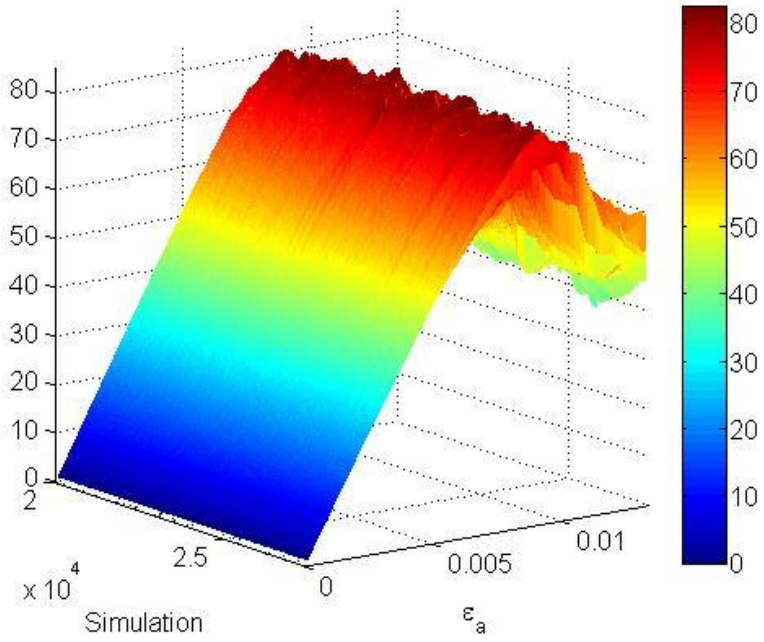

Figure 7.13 3D stress strain curves for three-parameters case

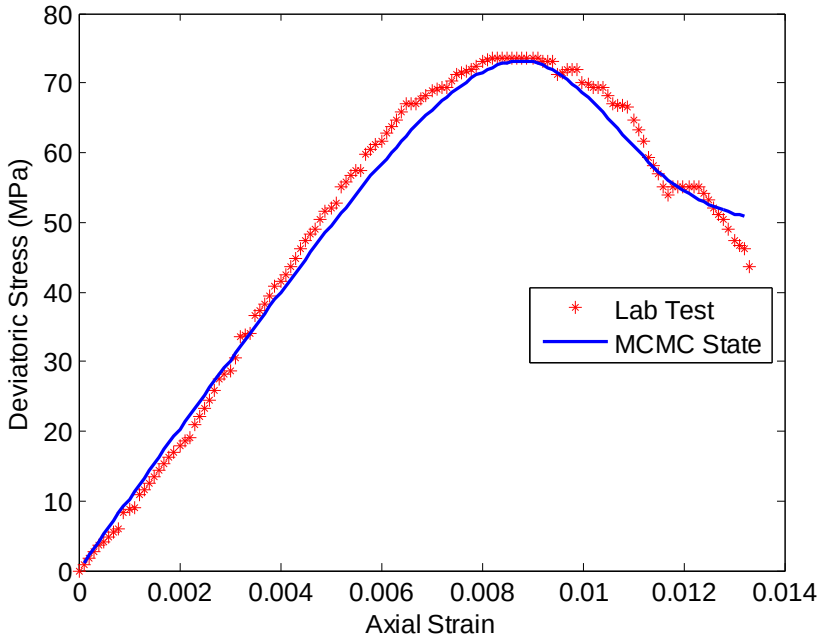

Figure 7.14 Mean stress strain curve for three-parameters case

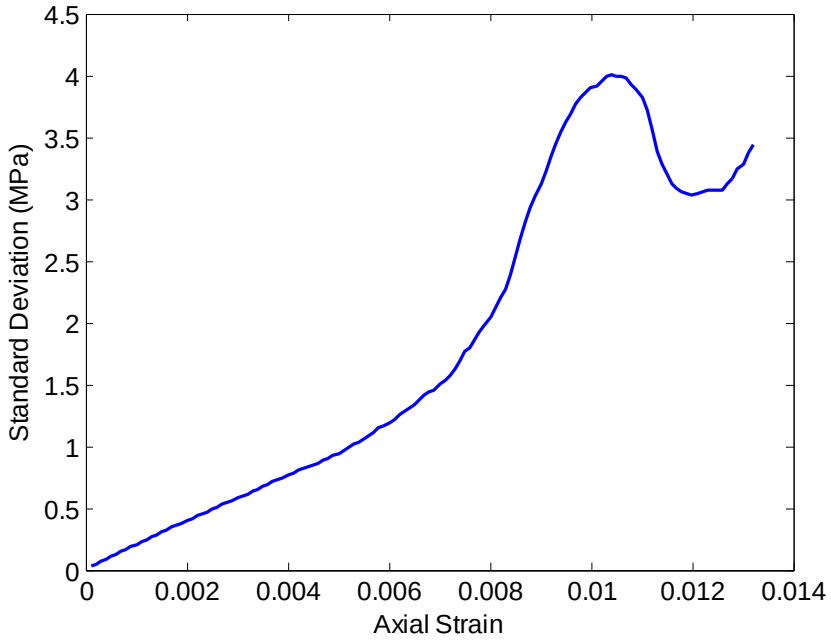

Figure 7.15 Standard deviation versus axial strain for three-parameters case

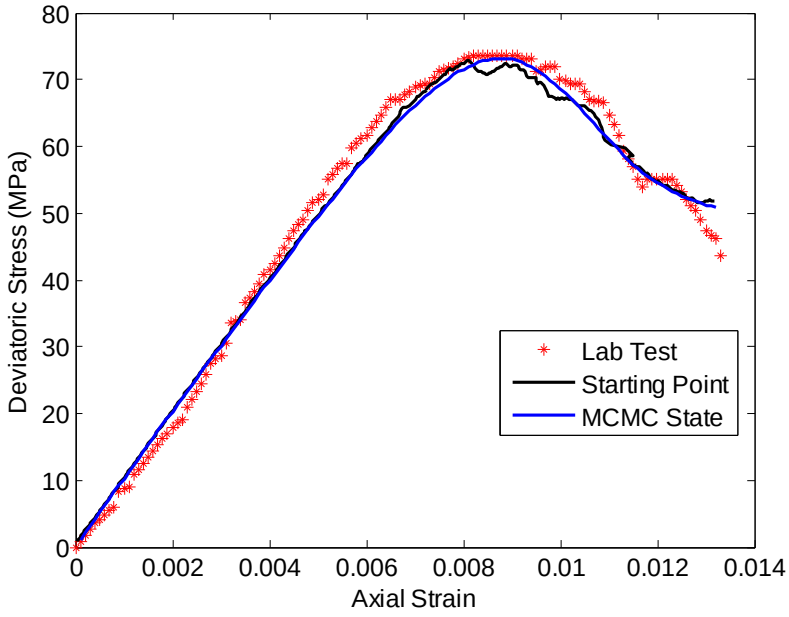

Figure 7.16 Comparison between initial and mean stress strain curves

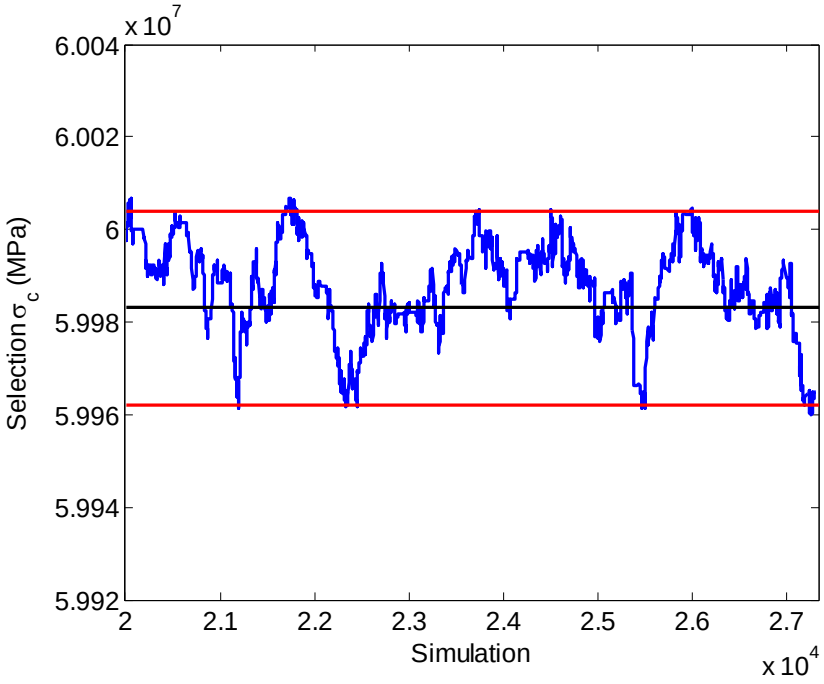

Figure 7.17 MCMC analysis of parallel normal strength

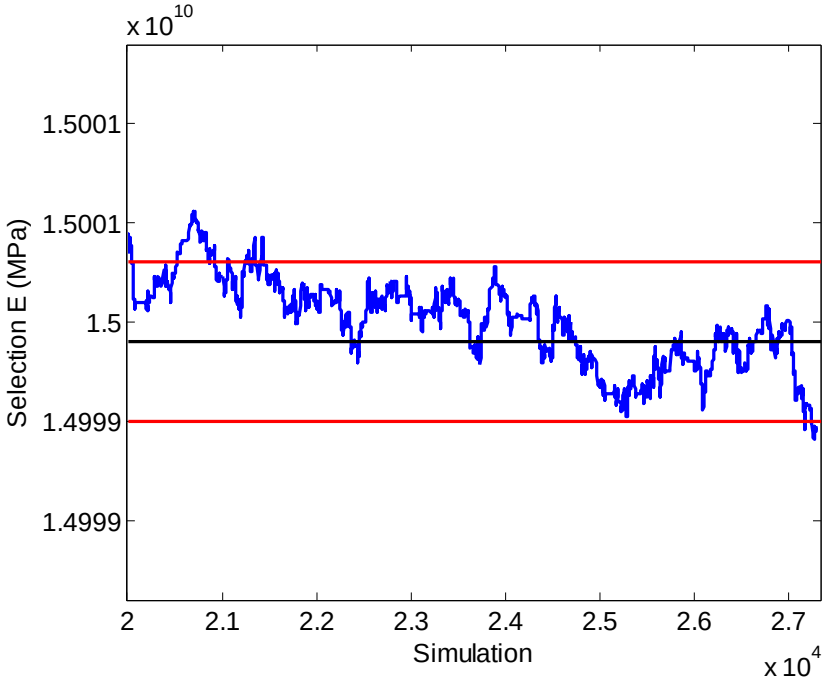

Figure 7.18 MCMC analysis of normal stiffness

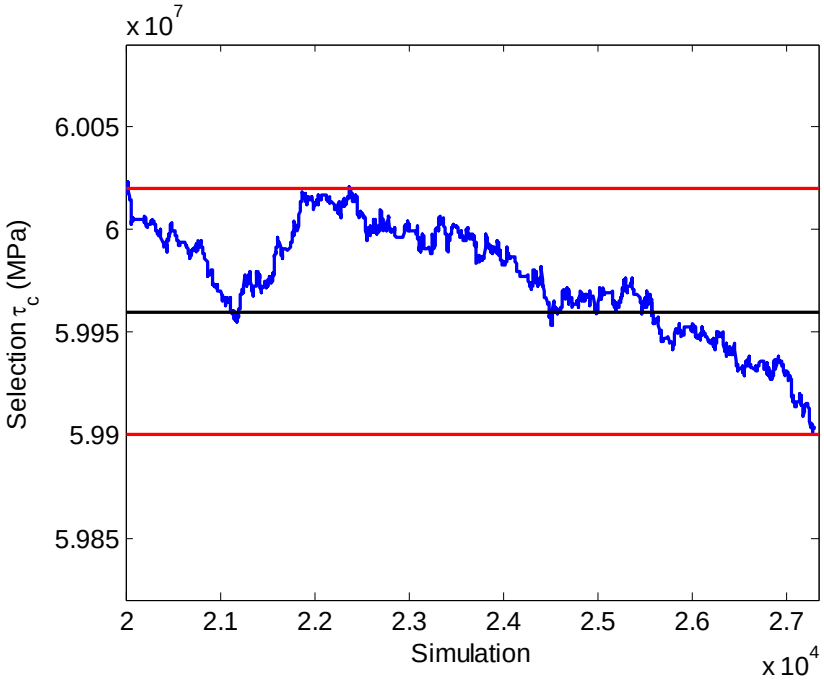

Figure 7.19 MCMC analysis of parallel shear strength

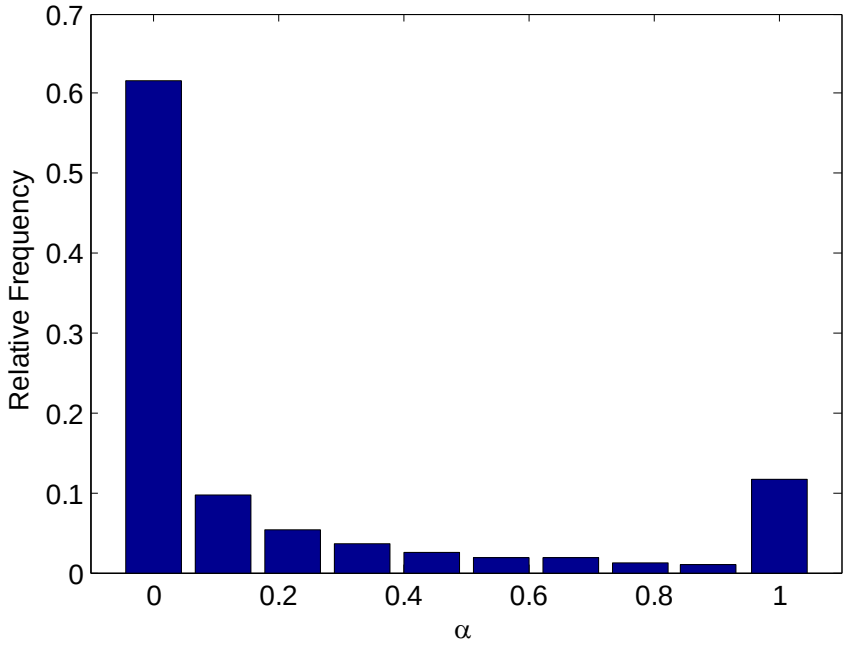

Figure 7.20 Relative frequency histogram of α for the stationary state

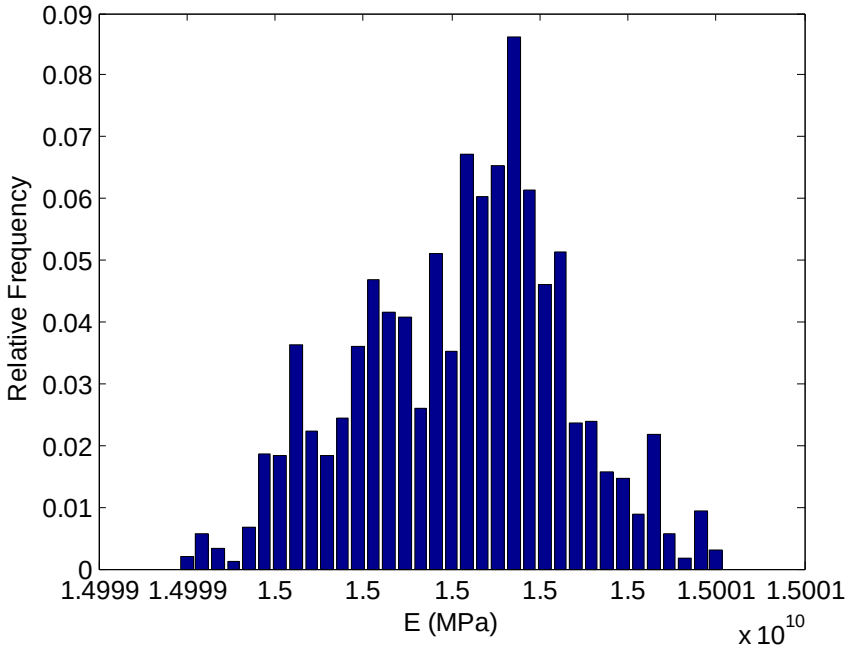

Figure 7.21 Relative frequency histogram of parallel normal stiffness

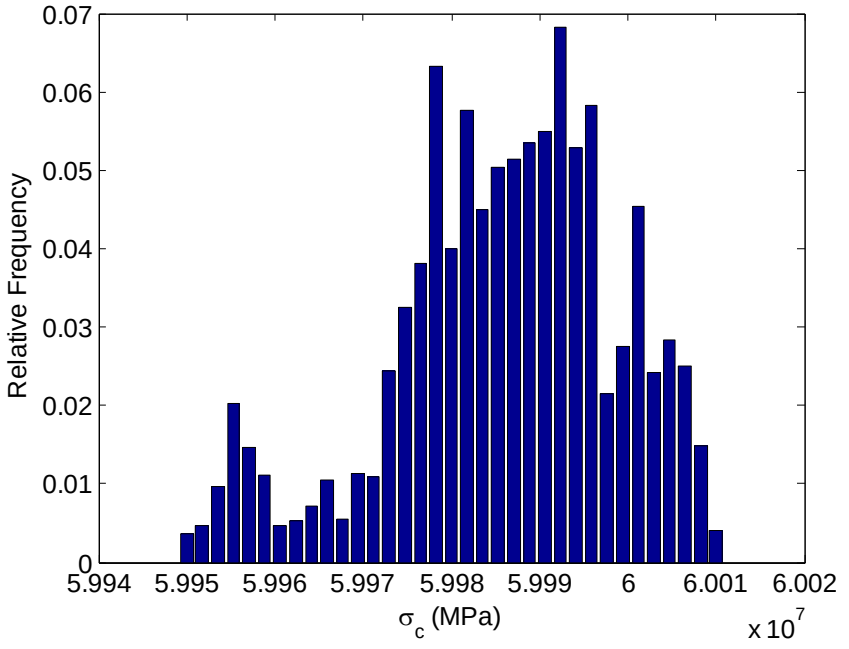

Figure 7.22 Relative frequency histogram of parallel normal strength

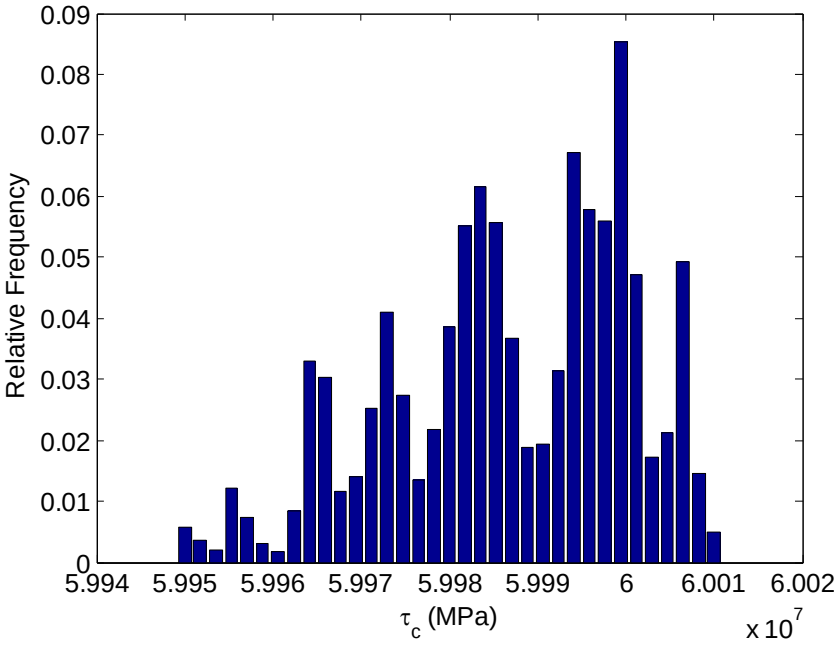

Figure 7.23 Relative frequency histogram of parallel shear strength

CHAPTER VIII

CONCLUSIONS

This paper introduces the use of a probabilistic calibration methodology, a new method getting a complete solution to the inverse problem and for assessing a full description of the micro-parameters in the discrete element model. This chapter first offers the summary of all the results in this thesis. Then, recommendations for the future research work are proposed based on resulting experience.

8.1 Research Summary

The discrete particle model is capable of reproducing the mechanistic behavior of a triaxial compressive test performed on a Vosges sandstone specimen. This is achieved by considering the same experimental testing conditions, and densely packed spherical elements with low lock-in stress. The DEM successfully captures many features of rock behavior, including the global stress-strain and the failure mechanism of the jointed rock. The FISH code developed in this research can be used in simulating the triaxial test environment for sandstone, which can also be used for other materials.

A parametric study is developed to investigate the influence of each micro-parameter on the meso-behavior of the specimen. In the DEM model, the Young's modulus is controlled by both the point contacts properties and the parallel contact properties. The strength of the specimen is affected both by the normal strength and by the shear strength of the parallel bond. The friction coefficient has little effect on the

behaviors of parallel bond materials, but plays an important role for granular materials. The standard deviation of the strength affects the crack initiation stress level of the material.

The Bayesian solution to the inverse problem is introduced including a discussion of all its components when applied to the calibration of a DEM. The theoretical basis for prior, likelihood and posterior is formulated for the proposed discrete particle model, and the interaction between the sampling of the model response set in PFC^{3D} and the uncertainty quantification is implemented in MATLAB following previous efforts of Medina-Cetina and Khoa [24]. The sampling procedures for Markov Chain Monte Carlo method and the Metropolis-Hastings are listed in detail, which are proved to be efficient ways for sampling the posterior.

The goal to develop a probabilistic methodology for the calibration of discrete particle model is reached and validated when applied to the triaxial compression test of Vosges sandstone. A robust computational algorithm is outlined and described when applied to the case study facilitating an understanding of the elements required for the probabilistic calibration. First order statistics on probabilistic results show strong agreement with the lab test, including a measure of the DEM performance for different parameters combinations.

8.2 Future Research

Firstly, more simulations are needed for three-parameters case to get more reasonable results of the MCMC stationary phase and to sample the joint probability

density functions of micro-parameters.

Secondly, only three main parameters (normal stiffness, parallel normal strength and parallel shear strength) of the nine micro-parameters listed in Table 5.2 are calibrated. All the nine parameters can be calibrated together in future research in order to fully define the micro-parameters in the discrete particle model.

Moreover, the failure mechanism discussed in Chapter IV gives an outline of reproducing the evolutionary process of the micro-cracks and the determination of micro-crack types. Probabilistic calibration focusing on micro-cracks is well within the scope of future research.

Finally, parallel bond model presented in section 2.7.3 is difficult to model the post peak behavior of lab triaxial compression test. More realistic constitutive contact models can be developed and implemented within the PFC^{3D} model.

REFERENCES

[1] Asaf Z, Rubinstein D, Shmulevich D. Determination of discrete element model parameters required for soil tillage. Soil Till Res 2007; 92: 227-242.

[2] Belheine N, Plassiard J-P, Donze F-V, Darve F, Seridi A. Numerical simulation of drained triaxial test using discrete element modeling. Comput Geotech 2009; 36: 320-331.

[3] Besuelle P, Desrues J, Raynaud S. Experimental characterization of the localization phenomenon inside a Vosges sandstone in a triaxial cell. Int J Rock Mech Min Sci Geomech 2000; 37: 1223-1237.

[4] Camusso M, Barla M. Microparameters calibration for loose and cemented soil when using particle methods. Int J Geomech 2009; 9(5): 217-229.

[5] Cho N, Martin CD, Sego DC. A clumped particle model for rock. Int J Rock Mech Min Sci Geomech 2007; 44: 997-1010.

[6] Cui L, O'Sullivan C, O'Neill S. An analysis of the triaxial apparatus using a mixed boundary three-dimensional discrete element model. Geotechnique 2007; 57: 831-844.

[7] Cundall PA. A computer models for simulating progressive large scale movements in blocky rock systems. In: Nielen VDM, Grossmann NF, editors. Proceeding of the Symposium of the International Society of Rock Mechanics, Nancy, France; 1971; 1: Paper No. II-8.

[8] Cundall PA. Distinct element models of rock and soil structure. Anal Comput Meth Eng Rock Mech 1987; 4: 129-163.

[9] Cundall PA. Formulation of a three-dimensional distinct element model – Part I. A scheme to detect and represent contacts in a system composed of many polyhedral blocks. Int J Rock Mech Min Sci Geomech 1988; 25(3): 107-116.

[10] Cundall PA, Hart R. Numerical modeling of discontinua. J Eng Comp 1992; 9: 101-113.

[11] Cundall PA, Strack DL. A discrete numerical model for granular assemblies. Geotechnique 1979; 29(1): 47-65.

[12] Fakhimi A, Villegas T. Application of dimensional analysis in calibration of a discrete element model for rock deformation and fracture. Rock Mech Rock Eng 2007; 40(2): 193-211.

[13] Ghaboussi J, Barbosa R. Three-dimensional discrete element method for granular materials. Int J Numer Anal Meth Geomech 1990; 14: 451-472.

[14] Hart R, Cundall PA, Lemos J. Formulation of a three-dimensional distinct element model – Part II. Mechanical calculations for motion and interaction of a system composed of many polyhedral blocks. Int J Rock Mech Min Sci Geomech 1988; 25(3): 117-125.

[15] Itasca Consulting Group, PFC3D (Particle Flow Code in Three-Dimensions) User's manual, Vol. I & II, Version 3.10. Minneapolis, MN, USA; 2005.

[16] Iwashita K, Oda M. Rolling resistance at contacts in simulation of shear band development by DEM. J Eng Mech 1988; 124(3): 285-292.

[17] Jiang MJ, Konrad JM, Leroueil S. An efficient technique for generating homogeneous specimens for DEM studies. Comput Geotech 2003; 30: 579-597.

[18] Jiang MJ, Yan HB. Micro-contact laws of bonded granular materials for DEM numerical analysis. In: Yagawa G, Lu VP, editors. APCOM'07 EPMESC XI conference, Kyoto, Japan; 2007.

[19] Jiang MJ, Yu HS, Harris D. Bonding rolling resistance and its effect on yielding of bonded granulates by DEM analyses. Int J Numer Anal Meth Geomech 2006; 30: 723-761.

[20] Kuhn MR, Mitchelle JK. New perspective on soil creep. J Geotech Eng 1993; 119(3): 506-524.

[21] Lin X, Ng TT. A three dimensional element model using arrays of ellipsoids. Geotechnique 1997; 47(2): 319-329.

[22] Mathworks. http://www.mathworks.com (data accessed on 04/10/10).

[23] Medina-Cetina Z. Probabilistic calibration of a soil model. PHD Dissertation, The Johns Hopkins University, Baltimore, MD, USA; 2006.

[24] Medina-Cetina Z, Khoa HDV. Probabilistic calibration of discrete particle dodels for geomaterials. In: Kusakabe O, Choudhury D, editors. ISSMFE conference, Alexandria, Egypt; 2009.

[25] Ng TT. Numerical simulations of granular soil using elliptical particles, microstructural characterization in constitution modeling of metals and granular media. In: Bhattacharya K, Kyriakides RC, editors. The ASME Summer Mechchanics and Materials Conference, Tempe, AZ; 1992; 95-118.

[26] Plassiard JP, Belheine N. A spherical discrete element model: calibration procedure and incremental response. Gran Mat 2009; 11: 293-306.

[27] Potyondy DO, Cundall PA. A bonded-particle model for rock. Int J Rock Mech Min Sci 2004; 41: 1329-64.

[28] Press J. Subjective and objective Bayesian statistics: principles, models, and applications, 2nd Edition. Wiley-Inter Science; 2003.

[29] Robert CP, Casella G. Monte Carlo statistical methods, Springer; 2005.

[30] Rothenburg L, Bathurst RJ. Analytic study of induced anisotropy in idealized granular materials. Geotechnique 1989; 39(4): 601-614.

[31] Thornton C, Yin KK. Impact of elastic spheres with and without adhesion. Powers Technol 1991; 65: 152-166.

[32] Wang Y, Tonon F. Modeling Lac du Bonnet granite using a discrete element model. Int J Rock Mech Min Sci 2004; 46: 1124-1135.

[33] Wang Y-H, Leung S-C. A particulate-scale investigation of cemented sand behavior. Can Geotech J 2008; 45: 29-44.

APPENDIX A

```
; Filename: et3.FIS
; Purpose: FISH functions comprising the PFC3D element-test environment
; Texas A&M University
; Copyright to Yanbei Zhang (2010)
;=============================================================
def _et3_arrays
   Array et3_vt(8,3)
   Array et3_pt1(3)
   Array et3_pt2(3)
end
;=============================================================
def et3_prep
   et3_setup
   et3_plot_assembly
   if et3_prep_saveall = 1 then
      md_tag_name = '-bal'
      md_save_state
   end_if
   et3_isopack
   if et3_prep_saveall = 1 then
      md_tag_name = '-pck'
      md_save_state
   end_if
   if md_granular # 1 then
      command
         history nstep=50
         his et3_isostr
      end_command
      et3_install_isostr
      if et3_prep_saveall = 1 then
         md_tag_name = '-iso'
         md_save_state
      end_if
      flt_eliminate
      if md_add_pbonds = 1 then
         md_set_balldeform=0
         command
            prop pb_nstr = 1.0 pb_sstr = 1.0
         end_command
         md_pbprops
      end_if
```

```
    end_if
    md_ballfric
    command
       SET dt auto
    end_command
    md_tag_name = '-spc'
    md_save_state
end
;=============================================================
def et3_seattriax
    et3_servo_yon = 1
    et3_servo_ron = 1
    et3_servo_gain_cyc = 100
    et3_servo_vmax = 10000.0 * p_vel
    command
       ini xvel 0.0 yvel 0.0 zvel 0.0 xspin 0.0 yspin 0.0 zspin 0.0
       SET fishcall #FC_CYC_MOT et3_servo
    end_command
    et3_install_ws
    command
       solve
    end_command
    et3_install_ws
    command
       solve
    end_command
    et3_install_ws
end
;=============================================================
def et3_setup
    if tm_numtries = 0 then
       tm_numtries = 125000
    end_if
    w_height = et3_height
    w_width = et3_width
    s_height = et3_height
    s_width = et3_width
    l_ext = 1.5
    et3_makewalls
    _rmax = et3_radius_ratio * et3_rlo
    _rmin = et3_rlo
    _ntries = tm_numtries
    if md_poros # 0 then
         _n = md_poros
```

```
   else
        _n = 0.22
   end_if
   et3_genballs
   et3_install_meas_circles
end
;=============================================================
def et3_genballs
     _rbar = 0.5 * ( _rmin + _rmax )
     rad_cy = 0.5 * w_width
     tot_vol = w_height * pi * rad_cy^2.0
     ;_numballs = 3.0*tot_vol*(1.0 - _n) / (4.0*pi*_rbar^3)-1
     _rlo = 0.5 * _rmin
     _rhi = 0.5 * _rmax
     _xl = -rad_cy
     _xu =    rad_cy
     _yl = -0.5 * w_height
     _yu =    0.5 * w_height
     _zl = -rad_cy
     _zu =    rad_cy
     command
        GENERATE id=(1,@_numballs) &
                     rad=(@_rlo,@_rhi)    &
                     x=(@_xl,@_xu) y=(@_yl,@_yu) z=(@_zl,@_zu) &
               filter ff_cylinder &
                     tries=@_ntries
     end_command
     _et3_poros
     _m = ((1.0 - _n) / (1.0 - _et3_poros)) ^ (1.0/3.0)
     command
        change rad mult @_m
     end_command
end
;=============================================================
def ff_cylinder
   ff_cylinder = 0
   _brad = fc_arg(0)
   _bx      = fc_arg(1)
   _by      = fc_arg(2)
   _bz      = fc_arg(3)
   _rad    = sqrt(_bx^2 + _bz^2)
   if _rad + _brad <= rad_cy then
      ff_cylinder = 0
   else
```

```
      ff_cylinder = 1
   end_if
end
;=============================================================
def et3_makewalls
   _dely = 0.5 * w_height * (l_ext - 1.0)
   _delz = 0.5 * w_width * (l_ext - 1.0)
   _delx = 0.5 * w_width * (l_ext - 1.0)
   rad_cy=0.5 * w_width
   _x1 = 0
   _y1 =          -1 * (0.5 * w_height)-_dely * 0.2
   _z1 = 0
   _x2 = 0
   _y2 =          (0.5 * w_height)+_dely * 0.2
   _z2 = 0
   command
      wall type cylinder id=1 &
                  end1 @_x1 @_y1 @_z1 &
                  end2 @_x2 @_y2 @_z2 &
            rad @rad_cy @rad_cy
   end_command
   wpc = find_wall(1)
;Top platen
   _ptAx =          (0.5 * w_width) + _delz
   _ptAy =          (0.5 * w_height)
   _ptAz =          (0.5 * w_width) + _delz
   _ptBx = -1.0*_ptAx
   _ptBy =           _ptAy
   _ptBz =           _ptAz
   _ptCx = -1.0*_ptAx
   _ptCy =           _ptAy
   _ptCz = -1.0*_ptAz
   _ptDx =           _ptAx
   _ptDy =           _ptAy
   _ptDz = -1.0*_ptAz
   command
      wall id=6 face @_ptAx,@_ptAy,@_ptAz &
                        @_ptBx,@_ptBy,@_ptBz &
                        @_ptCx,@_ptCy,@_ptCz &
                        @_ptDx,@_ptDy,@_ptDz
   end_command
   wpy1 = find_wall(6)
   wy1    = _ptAy
;Bottom platen
```

```
   _ptAx =          (0.5 * w_width) + _delx
   _ptAy = -1.0*(0.5 * w_height)
   _ptAz =          (0.5 * w_width) + _delz
   _ptBx =           _ptAx
   _ptBy =           _ptAy
   _ptBz = -1.0*_ptAz
   _ptCx = -1.0*_ptAx
   _ptCy =           _ptAy
   _ptCz = -1.0*_ptAz
   _ptDx = -1.0*_ptAx
   _ptDy =           _ptAy
   _ptDz =           _ptAz
   command
      wall id=5 face @_ptAx,@_ptAy,@_ptAz &
                           @_ptBx,@_ptBy,@_ptBz &
                           @_ptCx,@_ptCy,@_ptCz &
                           @_ptDx,@_ptDy,@_ptDz
   end_command
   wpy2 = find_wall(5)
   wy2    = _ptAy
end
;=============================================================
def et3_install_meas_circles
   if et3_meas_numr = 0 then
      et3_meas_numr = 1
   end_if
   if et3_meas_numy = 0 then
      et3_meas_numy = 2
   end_if
   md_radii    ; {o: md_ravg}
   meas_rad = 0.5 * (w_width - 2.0 * et3_meas_numr * md_ravg)
   meas_x = 0.0
   meas_y = 0.0
   meas_z = 0.0
   command
      measure x=@meas_x y=@meas_y z=@meas_z rad=@meas_rad id=2
   end_command
   meas_y = et3_meas_numy * md_ravg + meas_rad - 0.5 * w_height
   command
      measure x=@meas_x y=@meas_y z=@meas_z rad=@meas_rad id=3
   end_command
   meas_y = -meas_y
   command
      measure x=@meas_x y=@meas_y z=@meas_z rad=@meas_rad id=1
```

```
    end_command
end
;=============================================================
def et3_isopack
    md_dens = md_dens
    if tm_steps = 0 then
        tm_steps = 5000
    end_if
    md_balldeform
    command
        set dt dscale
        prop dens=@md_dens fric=0.0
    end_command
     md_wid=1
    md_wallkn
     md_wid=5
    md_wallkn
     md_wid=6
    md_wallkn
    command
        wall id=1 ks=0.0 fric=0.0
        wall id=5 ks=0.0 fric=0.0
        wall id=6 ks=0.0 fric=0.0
    end_command
    loop _iter (1,30)
        command
            cycle 5
            prop xvel=0.0 yvel=0.0 zvel=0.0 xspin=0.0 yspin=0.0 zspin=0.0
        end_command
    end_loop
    _nstep = tm_steps - 150
    command
        cycle @_nstep
    end_command
end
;=============================================================
def et3_install_isostr
    _totvol = w_height * pi * rad_cy ^ 2
    loop while 1 # 0
        _iso = et3_isostr
        _diso = tm_req_isostr - _iso
        if abs(_diso/tm_req_isostr) <= tm_req_isostr_tol then
            exit
        end_if
```

```
      oo = out('Current isotropic stress = ' + string(_iso))
      md_expand_radii
      command
         solve
      end_command
   end_loop
end
;=============================================================
def et3_plot_assembly
   command
      plot create assembly
      plot add ball yellow
      plot add wall white
      plot add axes black
   end_command
end
;=============================================================
def et3_wss
      s_w_width = 2 * w_radend1(wpc)
      s_w_height = (wy1 + w_y(wpy1)) - (wy2 + w_y(wpy2))
      et3_werr = (s_w_width - w_width) / w_width
      et3_wsrr = -w_radfob(wpc) / (s_w_height * s_w_width * pi)
      et3_wsyy = 0.5*(w_yfob(wpy2) - w_yfob(wpy1))/(pi * s_w_width^2.0/4)
      et3_weyy    = (s_w_height - w_height) / w_height
      et3_wevol = et3_werr + et3_weyy + et3_werr
      et3_wsm = (et3_wsyy + 2 * et3_wsrr)/3.0
      et3_wsd = et3_wsyy - et3_wsrr
      et3_wsd_max = max( et3_wsd_max, abs(et3_wsd) )
      if _et3_gageset = 1 then
         s_s_width = 0.5 * (((b_x(gbpx1) + b_rad(gbpx1)) - (b_x(gbpx2) -
b_rad(gbpx2)))+((b_z(gbpz1) + b_rad(gbpz1)) - (b_z(gbpz2) - b_rad(gbpz2))))
         s_s_height = (b_y(gbpy1) + b_rad(gbpy1)) - (b_y(gbpy2) - b_rad(gbpy2))
         et3_serr    = (s_s_width - s_width) / s_width
         et3_seyy    = (s_s_height - s_height) / s_height
         et3_sevol = 2 * et3_serr + et3_seyy
      end_if
end
;=============================================================
def et3_wf
   et3_wss
   et3_wfrr = et3_wsrr * (s_w_height * pi * s_w_width)
   et3_wfrr_max = max( et3_wfrr_max, abs(et3_wfrr) )
end
;=============================================================
```

```
def et3_isostr
   et3_wss
   et3_isostr = et3_wsm
end
;
=================================================================
def et3_e_delstrain
   et3_e_delstrain = (e_strain + e_bond) - et3_e_strain0
end
;
=================================================================
def et3_wallstiff
     md_wEcfac = et3_knrfac
     md_wid = 1
     md_wallkn
     md_wEcfac = et3_knyfac
     md_wid = 5
     md_wallkn
     md_wid = 6
end
;=================================================================
def et3_servo
   _vmax = abs(et3_servo_vmax)
   et3_wss
   if et3_ucs = 0 then
      if et3_servo_ron = 1
         _sgn = sgn( et3_wsrr - et3_wsrr_req )
         if et3_wsrr # 0.0 then
            w_radvel(wpc) = et3_servo_gr * (et3_wsrr - et3_wsrr_req)
         else
            w_radvel(wpc) = _sgn * _vmax
         end_if
         if abs(w_radvel(wpc)) > _vmax then
            w_radvel(wpc) = _sgn * _vmax
         end_if
         w_radvel(wpc) = - w_radvel(wpc)
      end_if
   end_if
   if et3_servo_yon = 1
      _sgn = sgn( et3_wsyy - et3_wsyy_req )
      if et3_wsyy # 0.0 then
         w_yvel(wpy2) = et3_servo_gy * (et3_wsyy - et3_wsyy_req)
      else
         w_yvel(wpy2) = _sgn * _vmax
```

```
      end_if
      if abs(w_yvel(wpy2)) > _vmax then
         w_yvel(wpy2) = _sgn * _vmax
      end_if
      w_yvel(wpy1) = -w_yvel(wpy2)
   end_if
end
;============================================================
def et3_servo_gain
   ii=pre_cycle
   if et3_servo_alpha = 0 then
      et3_servo_alpha = 0.5
   end_if
   if et3_ucs = 0 then
       sum_knr = 0.0
       cp = w_clist(wpc)
       loop while cp # null
          if md_virtual = 0 then
             sum_knr = sum_knr + c_kn(cp)
          end_if
          cp = c_b2clist(cp)
       end_loop
       if sum_knr # 0.0 then
          et3_servo_gr = et3_servo_alpha * (s_w_width * s_w_height * pi) / (sum_knr *
tdel)
       else
          et3_servo_gr = 0.0
       end_if
   end_if
   sum_kny = 0.0
   cp = w_clist(wpy1)
   loop while cp # null
      if md_virtual = 0 then
         sum_kny = sum_kny + c_kn(cp)
      end_if
      cp = c_b2clist(cp)
   end_loop
   cp = w_clist(wpy2)
   loop while cp # null
      if md_virtual = 0 then
         sum_kny = sum_kny + c_kn(cp)
      end_if
      cp = c_b2clist(cp)
   end_loop
```

```
   sum_kny = 0.5 * sum_kny    ; take average of both opposing walls
   if sum_kny # 0.0 then
      et3_servo_gy = et3_servo_alpha * (pi * s_w_width^2/4) / (sum_kny * tdel)
   else
      et3_servo_gy = 0.0
   end_if
end
;=============================================================
def et3_install_ws
   et3_servo_gain_cyc = et3_servo_gain_cyc
   loop while 1 # 0
      et3_servo_gain
      _rokay = 0
      _yokay = 0
      if et3_servo_ron = 0 then
         _rokay = 1
      end_if
      if et3_servo_yon = 0 then
         _yokay = 1
      end_if
      if et3_servo_ron = 1 then
         if abs((et3_wsrr - et3_wsrr_req)/et3_wsrr_req) <= et3_ws_tol then
            _rokay = 1
         end_if
      end_if
      if et3_servo_yon = 1 then
         if abs((et3_wsyy - et3_wsyy_req)/et3_wsyy_req) <= et3_ws_tol then
            _yokay = 1
         end_if
      end_if
      if _rokay = 1 then
         if _yokay = 1 then
               exit
         end_if
      end_if
      command
         cycle @et3_servo_gain_cyc
      end_command
   end_loop
end
;=============================================================
def et3_sample_dimensions
   et3_e_strain0 = e_strain + e_bond
   et3_wsd_max = -1.0e20
```

```
   _et3_setgage
   et3_wss
   w_width = s_w_width
   w_height = s_w_height
   s_width = s_s_width
   s_height = s_s_height
   command
      SET fishcall 0 et3_strains
   end_command
   et3_merr = 0.0
   et3_meyy = 0.0
   et3_mevol = 0.0
   et3_werr = 0.0
   et3_weyy = 0.0
   et3_wevol = 0.0
   mp1 = maddr(1)
   mp2 = maddr(2)
   mp3 = maddr(3)
end
;=============================================================
def _et3_setgage
   gbpx1 = ball_near3(    0.5 * et3_width, 0.0, 0.0 )
   gbpx2 = ball_near3( -0.5 * et3_width, 0.0, 0.0 )
   gbpy1 = ball_near3(    0.0,    0.5 * et3_height, 0.0 )
   gbpy2 = ball_near3(    0.0, -0.5 * et3_height, 0.0 )
   gbpz1 = ball_near3(    0.0, 0.0,    0.5 * et3_width )
   gbpz2 = ball_near3(    0.0, 0.0, -0.5 * et3_width )
   _et3_gageset = 1
end
;=============================================================
def et3_strains
   oo = measure(mp1, 2)
   oo = measure(mp2, 2)
   oo = measure(mp3, 2)
   _avg = (m_ed11(mp1) + m_ed11(mp2) + m_ed11(mp3)) / 3.0
   et3_mexx = et3_mexx + _avg * tdel
   _avg = (m_ed22(mp1) + m_ed22(mp2) + m_ed22(mp3)) / 3.0
   et3_meyy = et3_meyy + _avg * tdel
   _avg = (m_ed33(mp1) + m_ed33(mp2) + m_ed33(mp3)) / 3.0
   et3_mezz = et3_mezz + _avg * tdel
   et3_merr = 0.5 * (et3_mexx + et3_mezz)
   et3_mevol = et3_mexx + et3_meyy + et3_mezz
end
;=============================================================
```

```
def et3_msrr
   oo = measure(mp1, 1)
   oo = measure(mp2, 1)
   oo = measure(mp3, 1)
   _msxx = (m_s11(mp1) + m_s11(mp2) + m_s11(mp3)) / 3.0
   et3_msyy = (m_s22(mp1) + m_s22(mp2) + m_s22(mp3)) / 3.0
   et3_mszz = (m_s33(mp1) + m_s33(mp2) + m_s33(mp3)) / 3.0
   et3_msm = (_msxx + et3_msyy + et3_mszz) / 3.0
   et3_msd = et3_msyy - 0.5*(_msxx + et3_mszz)
   et3_msrr = _msxx
end
;=============================================================
def et3_accel_platens
   _delvel = p_vel / p_stages
   _niter = p_cyc / p_stages
   _vel = 0.0
   loop ap_ii (1,p_stages)
      _vel = _vel + _delvel
      if p_close = 1 then
         _fvel = _vel
      else
         _fvel = -_vel
      end_if
         _mfvel = -_fvel
      command
            wall id=5    yvel= @_fvel
            wall id=6    yvel= @_mfvel
            cycle @_niter
      end_command
   end_loop
end
;=============================================================
def et3_viewstriax
   command
      plot create energies
      plot set title text &
         'Incremental total strain energy and boundary work vs. axial strain'
      plot add his 30 35 vs -11 xmin 0.0 ymin 0.0
      plot create axial_stress_strain
      plot set title text &
         'Axial and confining stresses vs. axial strain'
      plot add his -14 -13 -15 vs -11 xmin 0.0 ymin 0.0
   end_command
end
```

```
;=============================================================
def et3_pi_spec
   plot_item
   if et3_pi_cur = 1 then
      _width = s_w_width
      _height = s_w_height
   else
      _width = w_width
      _height = w_height
   end_if
   stat=set_line_width(et3_pi_thick)
   et3_vt(1,1) = -(0.5 * _width)    ; negative-y face: et3_vt(1...4,*)
   et3_vt(1,2) = -(0.5 * _height)
   et3_vt(1,3) =    (0.5 * _width)
   et3_vt(2,1) =    (0.5 * _width)
   et3_vt(2,2) = -(0.5 * _height)
   et3_vt(2,3) =    (0.5 * _width)
   et3_vt(3,1) =    (0.5 * _width)
   et3_vt(3,2) = -(0.5 * _height)
   et3_vt(3,3) = -(0.5 * _width)
   et3_vt(4,1) = -(0.5 * _width)
   et3_vt(4,2) = -(0.5 * _height)
   et3_vt(4,3) = -(0.5 * _width)
   et3_vt(5,1) = -(0.5 * _width)
   et3_vt(5,2) =    (0.5 * _height)
   et3_vt(5,3) =    (0.5 * _width)
   et3_vt(6,1) =    (0.5 * _width)
   et3_vt(6,2) =    (0.5 * _height)
   et3_vt(6,3) =    (0.5 * _width)
   et3_vt(7,1) =    (0.5 * _width)
   et3_vt(7,2) =    (0.5 * _height)
   et3_vt(7,3) = -(0.5 * _width)
   et3_vt(8,1) = -(0.5 * _width)
   et3_vt(8,2) =    (0.5 * _height)
   et3_vt(8,3) = -(0.5 * _width)
     _vi1 = 1
     _vi2 = 2
     _load_et3_ptX    ;{i: _vi1, _vi2}
   stat = draw_line( et3_pt1, et3_pt2 )
     _vi1 = 2
     _vi2 = 3
     _load_et3_ptX    ;{i: _vi1, _vi2}
   stat = draw_line( et3_pt1, et3_pt2 )
     _vi1 = 3
```

```
    _vi2 = 4
    _load_et3_ptX    ;{i: _vi1, _vi2}
  stat = draw_line( et3_pt1, et3_pt2 )
    _vi1 = 4
    _vi2 = 1
    _load_et3_ptX    ;{i: _vi1, _vi2}
  stat = draw_line( et3_pt1, et3_pt2 )
    _vi1 = 5
    _vi2 = 6
    _load_et3_ptX    ;{i: _vi1, _vi2}
  stat = draw_line( et3_pt1, et3_pt2 )
    _vi1 = 6
    _vi2 = 7
    _load_et3_ptX    ;{i: _vi1, _vi2}
  stat = draw_line( et3_pt1, et3_pt2 )
    _vi1 = 7
    _vi2 = 8
    _load_et3_ptX    ;{i: _vi1, _vi2}
  stat = draw_line( et3_pt1, et3_pt2 )
    _vi1 = 8
    _vi2 = 5
    _load_et3_ptX    ;{i: _vi1, _vi2}
  stat = draw_line( et3_pt1, et3_pt2 )
    _vi1 = 1
    _vi2 = 5
    _load_et3_ptX    ;{i: _vi1, _vi2}
  stat = draw_line( et3_pt1, et3_pt2 )
    _vi1 = 2
    _vi2 = 6
    _load_et3_ptX    ;{i: _vi1, _vi2}
  stat = draw_line( et3_pt1, et3_pt2 )
    _vi1 = 3
    _vi2 = 7
    _load_et3_ptX    ;{i: _vi1, _vi2}
  stat = draw_line( et3_pt1, et3_pt2 )
    _vi1 = 4
    _vi2 = 8
    _load_et3_ptX    ;{i: _vi1, _vi2}
  stat = draw_line( et3_pt1, et3_pt2 )
end
;=============================================================
def et3_pi_gage
  plot_item
  stat= set_color( 0 )
```

```
      et3_pt1(1) = b_x(gbpx1)
      et3_pt1(2) = b_y(gbpx1)
      et3_pt1(3) = b_z(gbpx1)
                _rad = b_rad(gbpx1)
    stat = fill_circle( et3_pt1, _rad )
      et3_pt1(1) = b_x(gbpx2)
      et3_pt1(2) = b_y(gbpx2)
      et3_pt1(3) = b_z(gbpx2)
                _rad = b_rad(gbpx2)
    stat = fill_circle( et3_pt1, _rad )
      et3_pt1(1) = b_x(gbpy1)
      et3_pt1(2) = b_y(gbpy1)
      et3_pt1(3) = b_z(gbpy1)
                _rad = b_rad(gbpy1)
    stat = fill_circle( et3_pt1, _rad )
      et3_pt1(1) = b_x(gbpy2)
      et3_pt1(2) = b_y(gbpy2)
      et3_pt1(3) = b_z(gbpy2)
                _rad = b_rad(gbpy2)
    stat = fill_circle( et3_pt1, _rad )
      et3_pt1(1) = b_x(gbpz1)
      et3_pt1(2) = b_y(gbpz1)
      et3_pt1(3) = b_z(gbpz1)
                _rad = b_rad(gbpz1)
    stat = fill_circle( et3_pt1, _rad )
      et3_pt1(1) = b_x(gbpz2)
      et3_pt1(2) = b_y(gbpz2)
      et3_pt1(3) = b_z(gbpz2)
                _rad = b_rad(gbpz2)
    stat = fill_circle( et3_pt1, _rad )
end
;=============================================================
def et3_runtriax
    loop while 1 # 0    ; infinite loop
        command
            cycle 100
        end_command
        if abs(et3_wsd) < (et3_peakfac * et3_wsd_max) then
                exit
        end_if
        if abs(et3_weyy) > et3_strain then
                exit
        end_if
    end_loop
```

```
end
;=============================================================
def et3_gd3_triax
   gd3_test = 0
   gd3_triaxcore
end
;=============================================================
def gd3_triaxcore
   if pk_ci_fac = 0 then
      pk_ci_fac = 0.02
   end_if
   gd3_init    ;{i: gd3w_test}
   gd3_pk_syy
   gd3_pk_emodnu
   gd3_pk_crknum
   gd3_syy_ci
   case_of gd3_test
                ; default case
        ii=out('***** Triaxial-test results follow. . .')
        ii=out('          md_run_name = '+string(md_run_name))
        ii=out('          md_numballs = '+string(md_numballs))
        if et3_ucs = 0 then
           ii=out('          Confinement: et3_wsrr_req = '+string(et3_wsrr_req))
           ii=out('                                et3_wsyy_req = '+string(et3_wsyy_req))
        else
           ii=out('       Fully unconfined test (no side walls).')
        end_if
      case 2 :
        ii=out('***** Core-test results follow. . .')
        ii=out('          (Only valid for unconfined tests!)')
        ii=out('          md_run_name = '+string(md_run_name))
        ii=out('          md_numballs = '+string(md_numballs))
        ii=out('          Confinement: ct3_s11 = '+string(ct3_s11))
        ii=out('          Confinement: ct3_s33 = '+string(ct3_s33))
   end_case
   ii=out('===== Elastic Constants:')
   ii=out('          (Secant values: start of test and when one-half')
   ii=out('            of peak strength has been obtained.')
   ii=out('            Wall-based means stresses from walls and')
   ii=out('                 strains from 4 reference balls.')
   ii=out('            Fully wall-based means stresses from walls and')
   ii=out('                 strains from walls.)')
   ii=out('   ----------------------------')
   ii=out('   E    (fully wall-based) = '+string(pkw_emod))
```

```
   ii=out('    nu (fully wall-based) = '+string(pkw_nu))
   ii=out('    ----------------------------')
   ii=out('    E    (wall-based) = '+string(pk_emod))
   ii=out('    nu (wall-based) = '+string(pk_nu))
   ii=out('    ----------------------------')
   ii=out('    E    (meas-based) = '+string(pkm_emod))
   ii=out('    nu (meas-based) = '+string(pkm_nu))
   ii=out('===== Strengths:')
   ii=out('    peak strength (wall-based) = '+string(pk_syy))
   ii=out('    peak strength (meas-based) = '+string(pkm_syy))
   ii=out('    crack-initiation factor, pk_ci_fac = '+string(pk_ci_fac))
   ii=out('    crack-initiation stress (wall-based) = '+string(pk_syy_ci))
   ii=out('===== Damage at peak stress (wall-based):')
   ii=out('    pk_crk_num = '+string(pk_crk_num))
   ii=out('       pk_crk_num_cnf = '+string(pk_crk_num_cnf))
   ii=out('       pk_crk_num_csf = '+string(pk_crk_num_csf))
   ii=out('       pk_crk_num_pnf = '+string(pk_crk_num_pnf))
   ii=out('       pk_crk_num_psf = '+string(pk_crk_num_psf))
end
;=============================================================
def gd3_init
   case_of gd3_test
                ; default case, Triaxial Test
      command
         history write 18    table 1008    ; et3_wsd
         history write 14    table 1005    ; et3_wsyy
         history write 211 table 1003    ; et3_seyy
         history write 216 table 1009    ; et3_sevol
         history write 11 table 3003     ; et3_weyy
         history write 16 table 3009     ; et3_wevol
         history write 118 table 2008    ; et3_msd
         history write 114 table 2005    ; et3_msyy
         history write 111 table 2003    ; et3_meyy
         history write 116 table 2009    ; et3_mevol
      end_command
    case 1 :    ; Brazilian Test
      command
         history write 204 table 1204    ; et3_wfrr
      end_command
    case 2 :    ; Core Test
      command
         history write    350 table 1008    ; ct3_sdev
         history write    200 table 1005    ; ct3_s22
         history write 1200 table 1003    ; ct3_e22
```

```
            history write 1700 table 1009    ; ct3_evol
         end_command
   end_case
   command
      history write 1 table 1001    ; crk_num
      history write 2 table 1050    ; crk_num_cnf
      history write 3 table 1051    ; crk_num_csf
      history write 4 table 1052    ; crk_num_pnf
      history write 5 table 1053    ; crk_num_psf
   end_command
end
;=============================================================
def gd3_pk_syy
   pk_pos_syy = 0
   pk_syy = 0.0
   _wsd_max = -1.0e20
   loop _i (1, table_size(1008))
      _wsd = abs( ytable(1008, _i) )
      if _wsd > _wsd_max then
         pk_pos_syy = _i
         _wsd_max = _wsd
      end_if
   end_loop
   pk_syy = ytable( 1005, pk_pos_syy )
   pkm_pos_syy = 0
   pkm_syy = 0.0
   _wsd_max = -1.0e20
   loop _i (1, table_size(2008))
      _wsd = abs( ytable(2008, _i) )
      if _wsd > _wsd_max then
         pkm_pos_syy = _i
         _wsd_max = _wsd
      end_if
   end_loop
   pkm_syy = ytable( 2005, pkm_pos_syy )
end
;=============================================================
def gd3_pk_emodnu
   gd3_pk_syy    ; {o:pk_syy, pkm_syy}
   ;
   ; FULLY WALL-BASED values
   _syy_mid = abs(0.5 * (pk_syy+et3_wsrr_req))
   section
      loop _i (1, table_size(1005))
```

```
      _syy = abs( ytable(1005, _i) )
      if _syy > _syy_mid then
         _syy1    = ytable(1005, _i)
         _evol1 = ytable(3009, _i)
         _eyy1    = ytable(3003, _i)
         exit section
      end_if
   end_loop
end_section
_syy0 = ytable(1005, 1)
_evol0 = ytable(3009, 1)
_eyy0 = ytable(3003, 1)
pkw_emod = (_syy1 - _syy0) / (_eyy1 - _eyy0)
pkw_nu = 0.5*( 1.0 - (_evol1 - _evol0)/(_eyy1 - _eyy0))
;
; WALL-BASED values
_syy_mid = abs(0.5 * (pk_syy+et3_wsrr_req))
section
   loop _i (1, table_size(1005))
      _syy = abs( ytable(1005, _i) )
      if _syy > _syy_mid then
         _syy1    = ytable(1005, _i)
         _evol1 = ytable(1009, _i)
         _eyy1    = ytable(1003, _i)
         exit section
      end_if
   end_loop
end_section
_syy0 = ytable(1005, 1)
_evol0 = ytable(1009, 1)
_eyy0 = ytable(1003, 1)
pk_emod = (_syy1 - _syy0) / (_eyy1 - _eyy0)
pk_nu = 0.5*( 1.0 - (_evol1 - _evol0)/(_eyy1 - _eyy0))
;
; MEASURE-BASED values
_syy_mid = abs(0.5 * (pkm_syy+et3_wsrr_req))
section
   loop _i (1, table_size(2005))
      _syy = abs( ytable(2005, _i) )
      if _syy > _syy_mid then
         _syy1    = ytable(2005, _i)
         _evol1 = ytable(2009, _i)
         _eyy1    = ytable(2003, _i)
         exit section
```

```
         end_if
      end_loop
   end_section
   _syy0 = ytable(2005, 1)
   _evol0 = ytable(2009, 1)
   _eyy0 = ytable(2003, 1)
   pkm_emod = (_syy1 - _syy0) / (_eyy1 - _eyy0)
   pkm_nu = 0.5*( 1.0 - (_evol1 - _evol0)/(_eyy1 - _eyy0))
end
;=============================================================
def gd3_pk_fxx
   pk_pos_fxx = 0
   pk_fxx = 0.0
   _fxx_max = -1.0e20
   loop _i (1, table_size(1204))
      _fxx = abs( ytable(1204, _i) )
      if _fxx > _fxx_max then
         pk_pos_fxx = _i
         _fxx_max = _fxx
      end_if
   end_loop
   pk_fxx = ytable( 1204, pk_pos_fxx )
   pk_sigt = pk_fxx / ( pi * bt_rad * et3_bthick )
end
;=============================================================
def gd3_pk_crknum
   if gd3_test = 1 then
      gd3_pk_fxx    ; {o: pk_pos_fxx}
      _pos = pk_pos_fxx
   else
      gd3_pk_syy    ; {o: pk_pos_syy}
      _pos = pk_pos_syy
   end_if
   pk_crk_num         = ytable( 1001, _pos )
   pk_crk_num_cnf = ytable( 1050, _pos )
   pk_crk_num_csf = ytable( 1051, _pos )
   pk_crk_num_pnf = ytable( 1052, _pos )
   pk_crk_num_psf = ytable( 1053, _pos )
end

;=============================================================
def gd3_syy_ci
   gd3_pk_crknum    ; {o: pk_crk_num}
   _crknum_ci = int( pk_ci_fac * pk_crk_num )
```

```
   pk_pos_ci = 0
   section
      loop _i (1, table_size(1001))
         _crknum = ytable( 1001, _i )
         if _crknum >= _crknum_ci then
            pk_pos_ci = _i
            exit section
         end_if
      end_loop
   end_section
   if pk_pos_ci = 0 then
      pk_syy_ci = 0.0
   else
      pk_syy_ci = ytable( 1005, pk_pos_ci )
   end_if
end
;=============================================================
def _load_et3_ptX
   loop _idx (1,3)
      et3_pt1(_idx) = et3_vt(_vi1, _idx)
      et3_pt2(_idx) = et3_vt(_vi2, _idx)
   end_loop
end
; ============================================================
def _et3_poros
   _totvol = 0.0
   bp = ball_head
   loop while bp # null
      _totvol = _totvol + (4.0/3.0)*pi*b_rad(bp)^3
      bp = b_next(bp)
   end_loop
   _specvol = w_width^2 * w_height * pi / 4
   _et3_poros = 1.0 - ( _totvol / _specvol )
end
;============================================================
return
; END OF Filename: et3.FIS
```

APPENDIX B

```
; Filename: sandstone.DVR
; PURPOSE: Create sandstone specimen for triaxial test
; Texas A&M University
; Copyright to Yanbei Zhang (2010)
;=============================================================
new
SET safe_conversion on
SET random      ; for reproducibility
def set_fist_env
   environment('itascaFishTank') = 'C:\\Program Files\\Itasca\\shared\\FisTEnv-3h\\'
end
set_fist_env
SET echo off      ; load support functions
call %itascaFishTank%\md.FIS
call %itascaFishTank%\et3.FIS
call %itascaFishTank%\flt.FIS
SET echo on;
SET md_run_name = 'Sandstone'
Title Sandstone Triaxial Test
SET et3_height=80e-3    et3_width=40e-3
SET et3_radius_ratio=1.66    et3_rlo=2.0e-3
SET md_poros = 0.22 md_wEcfac=1.1
SET tm_req_isostr=-1.0e6    tm_req_isostr_tol=0.50
SET flt_def=3    flt_remain=0.0
SET md_granular=0 md_add_pbonds=1
SET md_fric=3.0
SET md_knoverks=7.0
SET pb_knoverks=7.0
SET pb_sn_sdev=6e6
SET pb_ss_sdev=6e6
SET md_dens=1960.0
SET md_Ec=15e9
SET pb_radmult=1.0
SET pb_Ec=15e9
SET pb_sn_mean=60e6
SET pb_ss_mean=60e6
SET et3_prep_saveall=1
et3_prep
;=============================================================
return
; END OF Filename: sandstone.DVR
```

APPENDIX C

```
; Filename: sandstone_test.DVR
; PURPOSE: Perform triaxial tests upon sandstone specimen at Pc = 10MPa
; Texas A&M University
; Copyright to Yanbei Zhang (2010)
;=========================================================
SET logfile sandstone_test.log
SET log on overwrite
def set_my_env
   environment('itascaFishTank') = 'C:\\Program Files\\Itasca\\shared\\FisTEnv-3h\\'
   environment('WorkingPlace') = 'C:\\ProbabilisticCalibration\\'
end
set_my_env
;=========================================================
SET echo off       ; load support functions
call %WorkingPlace%\Testing-Three\sandstone.DVR     ;=>Sandstone-spc.SAV
SET echo on
;=========================================================
restore Sandstone-spc.SAV
SET safe_conversion on
SET md_run_name='Sandstone_10MPa_00'
title 'Sandstone_10MPa_00'
def my_save_state
   my_path_name = string('C:\\ProbabilisticCalibration\\')
   _fname = my_path_name + md_run_name + md_tag_name + string('.SAV')
   command
      save @_fname
   end_command
end
;=========================================================
SET et3_knrfac=0.005    et3_knyfac=1.0
SET et3_wsrr_req=-10e6 et3_wsyy_req=-10e6 et3_ws_tol=0.01
SET p_vel=2.0e-1    p_cyc=1000    p_stages=20
SET et3_strain = 0.0133 et3_peakfac=0.01    pk_ci_fac=0.01
SET echo off
call %itascaFishTank%\_ttw.DVR    ;=> Sandstone_10MPa_00-{tw0,tw1}.SAV
hist write -18 -11 16 file = %WorkingPlace%\Sandstone_10MPa.his overwrite
SET echo on
SET log off
;=========================================================
return
; END OF Filename: sandstone_test.DVR
```

VITA

Yanbei Zhang was born in February, 1985, Zhengzhou, China. He graduated from Zhengzhou No.1 Senior High School in Zhengzhou, China in 2004. He received a Bachelor of Science in civil engineering from Hohai University in China in 2008 and graduated with the highest honors of the Chinese Civil Engineering Society as the Outstanding Graduate. He took one year of master's courses in geotechnical engineering in Tongji University and then attended Texas A&M University in August 2009, where he earned his master's degree in August 2010. He continues his research on discrete particle modeling under the direction of Dr. Zenon Medina-Cetina.

Mr. Zhang may be reached at The Zachry Department of Civil Engineering, Texas A&M University,College Station, TX 77843-3136. His email address is yanbei_zhang@tamu.edu.